Evaluation of In-Situ Variability of Concrete Pavement Characteristics and Their Effect on Performance

A Dissertation
SUBMITTED TO THE FACULTY OF
UNIVERSITY OF MINNESOTA
BY

Mary Elizabeth Vancura

IN PARTIAL FULFILLMENT OF THE REQUIREMENTS
FOR THE DEGREE OF
DOCTOR OF PHILOSOPHY

Lev Khazanovich
Randal Barnes

December 2013

Acknowledgements

I would like to thank my advisors, Dr. Lev Khazanovich and Dr. Randal Barnes, for their assistance and instruction while researching and writing this dissertation.

I would like to thank my committee members, Dr. Steve Wojtkiewicz, Dr. Alex Fok, Dr. Khazanovich, and Dr. Barnes for reviewing this dissertation.

I would like to thank the Minnesota Department of Transportation for allowing me to take MIRA measurements on their newly placed rigid pavements and sharing the pavements' flexural strength data with me.

Finally, I would like to thank Dr. Kyle Hoegh, Dr. Derek Tompkins, and Rita Lederle for editing and offering constructive criticism of this dissertation.

Abstract

Pavement performance prediction must account for uncertainties in pavement characteristics, climate, traffic loading, etc. Past research identified that concrete thickness and flexural strength were two pavement characteristics that significantly affected transverse cracking in Jointed Plain Concrete Pavements (JPCP). This dissertation concentrated on quantifying the effect of concrete thickness variability and, to a lesser extent, flexural strength variability on the reliability analysis of jointed plain concrete pavement (JPCP) performance.

Concrete thickness is typically assessed by measuring the length of concrete cores, but this procedure limits the amount of information collected. The possibility of using non-destructive testing to assess concrete thickness was evaluated and significant efforts were dedicated to quantification of the variability of constructed pavement concrete thickness and determination of requirements for thickness sampling spacing using autocorrelation concepts.

The Mechanistic Empirical Pavement Design Guide (MEPDG) is a tool used to evaluate the performance of JPCP, which predicts pavement distresses based on a desired reliability of design. MEPDG's current reliability analysis does not allow the MEPDG to quantify the effect of improved material characterization prior to design or the effect of quality control on pavement performance. In this study, a method to account for pavement characteristic variability in the reliability analysis is presented and evaluated the measured variability of rigid pavement concrete thickness and flexural strength.

Table of Contents

LIST OF TABLES

LIST OF FIGURES

1 INTRODUCTION

1.1 Introduction

The Mechanistic-Empirical Pavement Design Guide (MEPDG), recently adopted by the American Association of State Highway and Transportation Officials (AASHTO), is a procedure for the design of new and reconstructed jointed plain concrete pavements (JPCP) (Darter et al., 2005). The MEPDG uses performance prediction models to evaluate the adequacy of a pavement design by comparing the predicted distresses with an acceptable level of distress. Reliability analysis is an important part of the MEPDG used to ensure that pavements perform at a desired level of reliability.

The MEPDG recognizes that pavement performance predictions are uncertain due to uncertainty in estimating traffic loads, fluctuations in climate over many years, variations in layer thicknesses, material properties, subgrade characteristics along the project, differences between the mean as-designed and as-built materials and layer properties, and prediction model limitations and errors (Darter et al., 2005). In the current version of the MEPDG, the prediction uncertainty due to the variability of pavement characteristics is considered at the same time, and uncertainty and variability of individual pavement characteristics are not considered. Because of this limitation, there is little incentive to decrease uncertainty and variability of pavement characteristics during construction in order to improve the reliability of the performance predictions. One of the reasons for this limitation is that it has been difficult to collect accurate in-situ information in sufficient quantity from pavements that would allow the characterization of uncertainty due to individual pavement characteristics.

Recently, non-destructive testing (NDT) device technology has been improved so that rigid pavement concrete layer thickness can be measured accurately and with a greater frequency than is prescribed by most state departments of transportation. As background information for the research presented in this dissertation, non-destructive testing technology was used to characterize concrete layer thickness variability in concrete pavements. The technology allowed a more detailed characterization of concrete layer thickness variability than could have been possible if measuring concrete thickness by taking concrete cores.

Using concrete thickness variability as an example, a methodology is proposed to account for the design uncertainty in the MEPDG contributed by the measureable variability of a single pavement performance characteristic and how to remove a known uncertainty from the total uncertainty that accounts for the error distribution about the mean predicted distress.

1.2 Thesis Organization

Chapter 2 is comprised of the literature review, which focuses on the features, design, and analysis of jointed plain concrete pavement (JPCP), current non-destructive testing (NDT) devices for the evaluation of physical and material concrete properties, and a review of autocorrelation techniques.

Chapter 3 evaluates the accuracy of the ultrasonic tomography device, MIRA, as a tool for measuring concrete thickness.

Chapter 4 investigates the variability of the concrete layer thickness in JPCPs as measured by MIRA and concrete cores and assesses concrete thickness according to the Minnesota Department of Transportation's (MN/DOT) QA/QC protocol.

Chapter 5 presents two methods for estimating appropriate thickness sample spacing based on thickness data autocorrelation.

Chapter 6 evaluates the effect of as-constructed thickness and modulus of rupture (MR) variation on JPCP transverse cracking predictions, and proposes an approach for direct accounting for this variability in the MEPDG.

Chapter 7 summarizes the dissertation's findings and makes suggestions for future research.

2 LITERATURE REVIEW

2.1 Introduction

This literature review will first examine jointed plain concrete pavements (JPCPs), including the layers in the pavement system, joints and reinforcement, the importance of the concrete layer thickness, pavement loads and resulting stresses, and JPCP response to stresses. Next, the literature review will focus on the Mechanistic-Empirical Pavement Design Guide (MEPDG), a procedure that incorporates pavement performance prediction into pavement design and some of the concrete material properties that are used as inputs into the MEPDG JPCP performance prediction models. Then, non-destructive testing (NDT) devices that measure various properties of concrete pavements will be assessed. Finally, the Minnesota Department of Transportation's QA/QC concrete thickness measurement protocol will be summarized and pavement performance prediction specifications will be discussed.

2.2 Jointed Plain Concrete Pavements

Flexible and rigid pavements are the primary pavement types in the United States. This dissertation will focus on rigid pavements. There are several types of rigid pavements, but jointed plain concrete pavements (JPCPs) are the most widely used type of rigid pavement in the United States. The JPCP layers and primary features will be briefly reviewed.

2.2.1 JPCP Layers

A jointed plain concrete pavement consists of multiple layers. The concrete layer is the top layer and the primary load-carrying structure of the pavement. The concrete layer typically ranges in thickness between 6 in. and 12 in. Below the concrete layer is a

base layer. The purpose of the base layer is to provide uniform support to the concrete layer, distribute load, contribute to the concrete's stiffness, and facilitate drainage. Below the base or subbase is the subgrade, which typically consists of the virgin soil (ACPA, 2008). The "side view" in Figure 2.1 shows the layers in a typical JPCP (Pavement Interactive, 2007a).

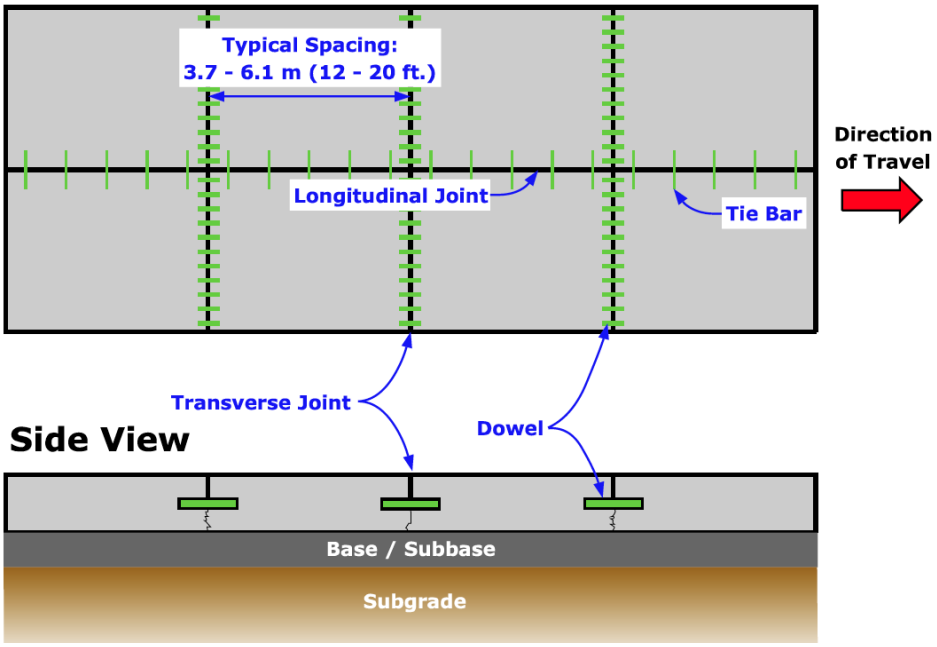

Figure 2.1 Schematic of jointed plain concrete pavement (JPCP) joints and layers (Pavement Interactive, 2007a)

2.2.2 JPCP Joints and Load Transfer Mechanisms

Jointing and reinforcing at the joints is an important design feature of JPCPs. Figure 2.1 presents JPCP transverse and longitudinal joints, dowel bars, and tie bars. Joints are saw-cut into JPCPs within 24 hours of concrete placement, and a typical joint spacing is 15 ft. (ARA, Inc., 2004b). The purpose of the transverse joints is to control the location of transverse cracks caused by shrinkage stresses. An example of a crack

forming below a saw-cut joint is illustrated in Figure 2.2. Without joints, transverse cracks would form randomly.

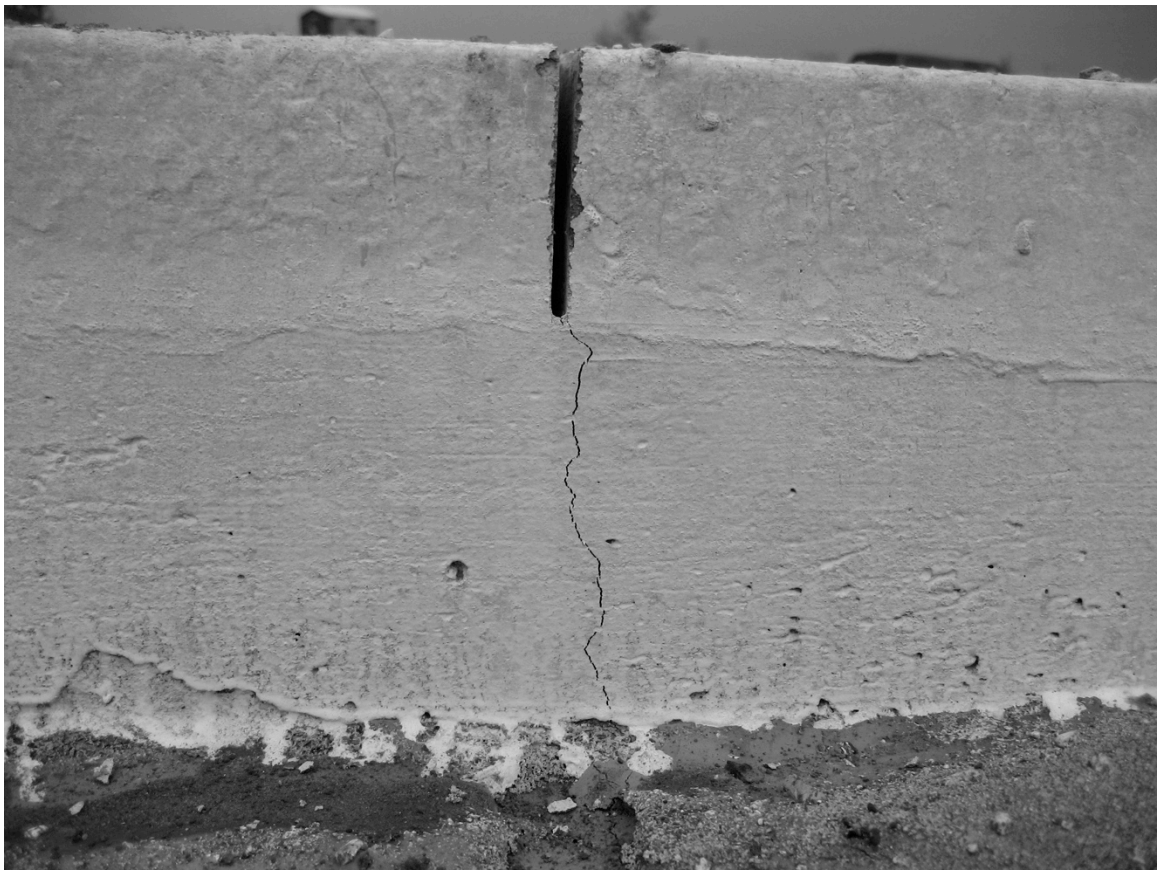

Figure 2.2 JPCP cracked at sawed joint within 24 hours of paving

Dowels positioned across a transverse joint increase the load transfer efficiency across the joint, which helps to distribute wheel loads between adjacent slabs (ARA, Inc., 2004b). Dowels are the primary method for controlling joint faulting and maintaining a smooth pavement surface. Figure 2.3 shows dowels positioned on the base with dowel bar baskets before the JPCP concrete layer is placed.

Figure 2.3 Dowel bars in baskets placed on JPCP base layer prior to placing the concrete layer

Longitudinal joints are cut into rigid pavements to prevent longitudinal cracks from randomly forming. Tie bars are placed across longitudinal joints in order to hold the faces in contact. Tie bars do not act as load transfer devices (Pavement Interactive, 2007b).

2.2.3 Concrete Layer Thickness

In JPCP's, concrete layer thickness is an important rigid pavement design consideration that affects transverse cracking in the concrete layer (Khazanovich et al., 1998). Increasing the concrete thickness decreases the flexural stresses and deflections in the concrete during loading. After a JPCP is constructed, concrete layer thickness is most often verified for quality assurance and quality control (QA/QC) by measuring the

thickness of a concrete core sample drilled from the pavement. This is a destructive process and is illustrated by Figure 2.4.

Figure 2.4 Hole resulting from drilling a concrete core for thickness measurements

There are drawbacks to measuring concrete thickness by the method of measuring drilled cores. The first drawback is that because the process is destructive, the sample spacing is on the order of 500-1000 ft. The Minnesota Department of Transportation's (MN/DOT's) quality control requirement is that a core be taken every 1000 ft. unless a core's measured thickness is more than 0.5 in. less than the design thickness. A second drawback is that although the core hole is filled with a specialized concrete mixture, coring creates a weak point in the pavement surface. Because of the weakness, the safest place to take a core is in the middle of the slab where stresses caused by traffic, temperature, and moisture loads are smallest. Cores in wheel paths and near the pavement's edges are often avoided because these are the areas of the rigid pavement

experience the highest stresses. This results in limited information about thickness variation in the transverse direction.

A study was commissioned by the Federal Highway Administration to evaluate the potential uncertainty and variability of the concrete layer thickness in rigid pavements. To perform the study, the authors used concrete layer thickness data from the Long Term Pavement Performance (LTPP) database, which houses concrete pavement data from almost every state. The concrete pavement thickness study used design concrete layer depth and measured concrete layer depth from the LTPP database to assess the variability of concrete thickness in rigid pavements. One finding of the study was that concrete layer thickness data was normally distributed 86% of the time, so concrete thickness data can be assumed normally distributed. Another finding of the study was that typical values for standard deviation, mean design minus measured thickness, and range of thicknesses for 8 in. and 11 in. concrete layers of rigid pavements. Table 2.1 summarizes the findings from this study (Jiang et al., 2002 and Jiang et al., 2003).

Table 2.1 Summary of the LTPP study on concrete thickness variation

Design Thickness (in)	# of pavements evaluated	Mean Difference Design-measured (in)	Standard Deviation (in)	Min Difference (in)	Max Difference (in)
8	71	0.39	0.55	-0.89	2.06
11	71	0.03	1.12	-3.73	1.25

In accordance with standard practices across the United States, the Minnesota Department of Transportation (MN/DOT) uses concrete cores to measure the in-situ concrete thickness of finished rigid pavements. The primary reasons for measuring in-situ concrete thickness values are QA/QC and assembly of information for the as-built condition of the pavement. In the State of Minnesota, contractor pay for state-funded

concrete pavement projects is partially contingent on the average measured thickness of the pavement (See Table 2.2). The following list outlines the official MN/DOT specifications for collecting QA/QC thickness cores from concrete pavements. The text in the list is taken directly from the MN/DOT specification (Minnesota Department of Transportation, 2005). The reason for presenting these criteria are to illustrate the inadequateness of these procedures to accurately measure post-construction concrete thickness of rigid pavements because the distance between cores is great.

- Each 5,000 foot segment of concrete pavement = 1 section
- One core will be taken within each 1,000 ft. of the section.
- If the section is less than 5,000 feet, the fractional section will be the length of the pavement
- In each fractional section greater than 500 ft., a core will be taken every 1000 ft., but no less than 3 cores must be collected from the fractional section.
- If a core shows a deficiency of more than ½ in., exploratory cores will be taken
- The initial exploratory cores will be 10 ft. on either side of the deficient core location and at the same distance from the centerline as the deficient core. An additional exploratory core will be taken on the adjacent driving lane if that lane was poured integrally with the lane where the deficient core was extracted.
- If the depth of any of the exploratory cores is less than the planned thickness minus 0.5 in., more exploratory cores will be taken at 10-25 ft. spacing until both cores are of adequate depth.

- If the core depth exceeds the design thickness by more than 0.3 in., the core will only be counted as the design thickness + 0.3 in. in determining the average thickness of the cores from each section (or fractional section).
- If the average thickness of the cores taken from a pavement section (or fractional section) is less than the design thickness minus 0.10 in., the contractor will be penalized as shown on Table 2.2 for the area of pavement in that section (or factional section). If the pavement thickness is less than the design thickness minus 0.5 in., the contractor decides if he wants to replace the pavement at no additional charge to the owner or take a payment penalty on the defective area (measured from core to core).
- If the pavement is less than the design thickness minus 1 in., the pavement must be replaced unless an alternate agreement is made between the contractor and engineer.

Table 2.2 MN/DOT contractor compensation deductions for thickness deficiencies in a section (or fractional section) of concrete pavement (Minnesota Department of Transportation, 2005)

Table 2301-14 Deductions for Thickness Deficiencies	
Thickness Deficiency Exceeding Permissible Deviations, *in [mm]*	**Adjusted contract unit price per sq. yd [sq. m] of Payment**
0.00 – ≤ 0.10 [≤ 3]	None (tolerance)
0.10 – ≤ 0.20 [3 – ≤ 5]	$0.20 [$0.25]
0.20 – ≤ 0.30 [5 – ≤ 8]	$0.40 [$0.50]
0.30 – ≤ 0.40 [8 – ≤ 10]	$0.70 [$0.90]
0.40 – ≤ 0.50 [10 – ≤ 13]	$1.00 [$1.25]
0.50 – ≤ 1.00 [13 – ≤ 25]*	$20.00 [$25.00]
* Perform exploratory coring as required by the Engineer.	

To summarize, one core is taken every 1000 ft. per lane to measure concrete layer thickness variation. Other state highway agencies have different but still similar methodologies for measuring concrete layer thickness.

2.2.4 Concrete Flexural Strength

The significant material properties of the concrete layer of JPCPs include flexural strength, modulus of elasticity, Poisson's ratio, drying shrinkage, coefficient of thermal expansion, thermal conductivity, and heat capacity. These properties are important because they govern the response of the JPCP concrete layer to load conditions (ARA, Inc., 2004b). Flexural strength will be highlighted here because, in addition to concrete thickness, concrete flexural strength affects transverse cracking in JPCPs (ARA, Inc., 2003a).

Concrete flexural strength, also called the modulus of rupture (MR), is important in the design and analysis of JPCPs because it is one of the primary parameters effecting fatigue cracking potential for a given magnitude of repeated flexural stress (ARA, Inc., 2004b). The flexural strength of concrete is primarily governed by the water-to-cement (w/c) ratio and the percent hydration of the concrete. For concretes with the same w/c ratio, the flexural strength is determined by (Kosmatka & Wilson, 2011):

- Aggregate size, grading, surface texture, shape, strength, and stiffness
- Differences in types and sources of cementing materials
- Entrained air content
- Use of admixtures
- Length of curing time and temperature

In the United States, measuring the flexural strength of concrete for purposes of pavement construction QA/QC is often accomplished by the concrete flexural strength method ASTM C 78: Standard Method for Flexural Strength of Concrete (Using Simple Beam with Third-Point Bending). This method requires that a concrete beam, typically

20 in. x 6 in. x 6 in. be cast in a form, cured, and broken in 3 point bending. Figure 2.5 shows concrete being formed into a concrete beam mold.

Figure 2.5 Concrete being formed into a 20 in. x 6 in. x 6 in. beam that will be used to test the concrete's flexural strength

While the three-point bending method is widely used to assess concrete flexural strength, the technique produces questionable and varying results and has been the topic of much discussion and research. For example, the American Concrete Pavement Association (APCA) released a position statement encouraging agencies not to use the flexural beam test. According to the ACPA, agencies should specify concrete pavement strength acceptance based on the compressive strength of concrete cores rather than the flexural strength of concrete beams due to the variation of flexural strength results that are obtained with ASTM C 78 (ACPA, 1997). The reasons for this statement include the fact that compression cylinders or cores are easier to manage than flexural beams and they are less prone to measurement error than flexural strength beam samples. In fact, ASTM sensitivity statements show that the variation of the flexural strength test of beams

is almost twice that of cylinders (Morian, 2010). A drawback to using the compressive strength tests to predict flexural strength is that there is not a well-defined relationship between flexural and compression strength.

Depending on the expression used, the ratio of flexural strength to compressive strength ranges from 0.11 to 0.23 (Mindess et al., 2003). A group of researchers used Long Term Pavement Performance (LTPP) data to investigate the relationship of existing compressive-flexural strength correlation equations and measured flexural and compressive strengths (Mallela et al., 2001). Many existing correlation equations have the form

$$MR = K\sqrt{f_c'} \qquad (2.1)$$

with MR = Modulus of Rupture (flexural strength) in psi

K = a constant varying between 8 and 10, and

f_c' = the compressive strength of concrete (psi).

What the study found was that the correlation equations under-predict the concrete's flexural strength by approximately 25-200 psi. The study also considered the variability in concrete compressive and flexural strengths. The within-project flexural strength variability was approximately 160 psi, and the within-project compressive strength variability was 2045 psi (Mallela et al., 2001).

2.2.5 JPCP Loads

Truck axle loads and configurations, moisture gradients, and temperature gradients are the primary sources of flexural stresses that cause damage in JPCPs.

2.2.5.1 Truck Axle Load Characterization for JPCP

Truck loads are predicted based on axle load spectrum and distribution (Kim et al., 1999). In addition to axle weight, the following items are considered when characterizing traffic loads (ARA, Inc., 2004c):

- Base year truck-traffic volume (design year)
- Vehicle (truck) operation speed
- Truck-traffic directional and lane distribution factors
- Vehicle (truck) class distribution
- Load distribution factors
- Axle and wheel base configurations
- Tire characteristic and inflation pressure
- Truck lateral distribution factor
- Truck growth factors.

2.2.5.2 Temperature and Moisture Gradients through JPCPs

Temperature and moisture gradients through the concrete layer cause flexural stresses in the concrete slabs due to curling and warping (ARA, Inc., 2004c). Curling in a concrete slab is also caused by a built-in temperature gradient, differential drying shrinkage, and creep (Rao & Roesler, 2005; Yu et al., 1998; Khazanovich 1994; and Larson & Dempsey, 1997).

Moisture gradients in concrete slabs are typically caused when moisture content in the slab is higher at the bottom than the top. Moisture gradients are caused by changes in relative humidity (ARA, Inc., 2004c) and are influenced by the coefficient of thermal expansion, a property of the concrete, which by itself, can change according to relative humidity (Jeong et al., 2012).

2.2.6 JPCP Distresses

There are many JPCP distresses, but the most common distresses are transverse cracking (Yu & Darter, 2003) and unevenness at the joints referred to as joint faulting (Khazanovich, 2003). Transverse cracking is the primary JPCP structural fatigue distress type (ARA, Inc., 2003a and Khazanovich et al., 2000) and will be the JPCP distress focused on in this dissertation. Transverse cracking is illustrated in Figure 2.6.

Figure 2.6 Example of a JPCP transverse crack

Transverse cracks originate either at the bottom of the slab and propagate upward (bottom-up cracking) or at the top of the slab and propagate downward (top-down cracking). Bottom up cracking occurs when trucks near the longitudinal edge cause a critical tensile stress in the middle of the slab. This stress is greatly increased when a positive temperature gradient exists in the slab (top of the slab is warmer than the bottom of the slab). Repeated truck axle loads under these conditions contribute to fatigue damage at the bottom of the slab and, eventually, cracks form due to the fatigue damage.

Top-down cracking is caused when critical stresses occur on the pavement surface near the longitudinal edge of the pavement. The causes of critical stresses on the slab surface include truck axles that are spaced such that they simultaneously load both ends of the slab, a negative temperature gradient (the surface is cooler than the bottom), and a moisture gradient. The fatigue damage caused by these stresses eventually causes cracks to form on the surface of the concrete (ARA, Inc., 2003a). Two primary factors in JPCP transverse cracking are concrete layer thickness and flexural strength.

2.3 Mechanistic-Empirical Pavement Design Guide

The Mechanistic-Empirical Pavement Design Guide (MEPDG), recently adopted by the American Association of State Highway and Transportation Officials (AASHTO), is a procedure for the design of new and reconstructed jointed plain concrete pavements (JPCP) (Darter et al., 2005). The MEPDG uses performance prediction models to evaluate the adequateness of design by comparing predicted distresses with acceptable levels of distress. Reliability analysis is an important part of the MEPDG (Khazanovich et al., 1998), and it is used to consider uncertainty and variation in design and construction so pavements perform to a desired level of reliability. The MEPDG distress prediction equations predict distresses with 50% reliability and the MEPDG reliability equations are used to adjust distress predictions to a desired level of reliability i.e. 90%.

2.3.1 MEPDG Design

The MEDPG approach to design requires an iterative process. A trial design is proposed and analyzed to determine if the design meets the performance requirements specified by the designer. If the pavement does not meet the criteria, the design is

adjusted and re-analyzed until it meets the performance requirements. The following steps are used for JPCP design (ARA, Inc., 2004a):

1. Define site specific conditions such as axle loads, climate, and soil conditions; define layers and layer thicknesses, specify subgrade, base, and concrete properties
2. Establish the criteria for acceptable design performance at the end of the pavement's design period (i.e. 15% of slabs cracked)
3. Select the level of reliability required for performance indicators (i.e. 90%)
4. Use the MEPDG to process inputs to obtain monthly values of axle load, material property evolution, and climatic conditions needed for design evaluations for the entire design period.
5. The MEPDG computes the structural response, including stresses and deflections, using finite-element based models for each axle type and load and for each damage-calculation increment throughout the design period.
6. The MEPDG calculates accumulated damage for each month of the design period.
7. The MEPDG predicts distresses (i.e. transverse cracking) on a month-by-month basis throughout the design period using the calibrated mechanistic-empirical performance models integrated into the MEPDG.
8. The MEPDG reliability equations evaluate the expected performance of the trial design at the designated reliability.
9. Modify the design and repeat the MEPDG evaluation until the design meets the established criteria.

The mechanistic-empirical prediction for fatigue cracking involves an incremental damage accumulation algorithm. Damage is accumulated on a monthly basis and the damage is correlated with cracking observed in JPCPs across North America. The correlation produces a calibrated model that predicts JPCP transverse cracking (ARA, Inc., 2003a). The MEPDG JPCP transverse cracking model is represented by Equation 2.3. Equations 2.4 and 2.5 represent the general fatigue damage accumulation considering all critical factors for transverse cracking.

$$CRK = \frac{100}{1 + FD^{-1.68}} \tag{2.3}$$

$$FD = \sum \frac{n_{t,j,k,l,m,p}}{N_{t,j,k,l,m,p}} \tag{2.4}$$

$$\log\left(N_{i,j,k,l,m,n}\right) = C_1 \times \left(\frac{MR_i}{\sigma_{i,j,k,l,m,n}}\right)^{C_2} \tag{2.5}$$

where,

$n_{i,j,k,l,m,n}$ = applied number of load applications at conditions i, j, k, l, m, and n

$N_{i,j,k,l,m,n}$ = allowable number of load applications at conditions i, j, k, l, m, and n

MR_i = PCC modulus of rupture at age i, psi

$\sigma_{i,j,k,l,m,n}$ = applied stress at conditions i, j, k, l, m, and n

i = age

j = month

k = axle type

l = load level (incremental load for each axle type)

m = temperature difference

n = traffic path

C_1 = calibration constant = 2.0

C_2 = calibration constant = 1.22

2.3.2 MEPDG Reliability

Because of the uncertainty associated with predicting pavement distresses, Figure 2.7 (Darter et al., 2005) illustrates that the actual distress could be higher or lower than the expected value.

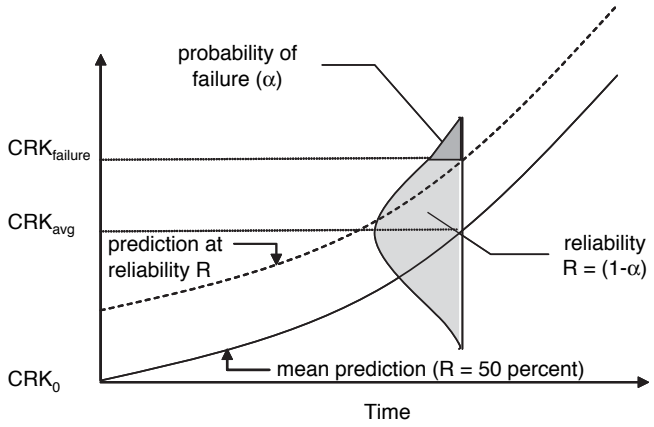

Figure 2.7 MEPDG design reliability concept

The sources of uncertainty that cause the distribution of the error about the mean expected prediction are caused by errors in estimated axle loads, fluctuations in climate over many years, variations in layer thicknesses, material properties, and subgrade characteristics, differences between mean as-designed and as-built materials and other layer properties, and prediction of model limitations and errors (Darter et al., 2005).

In the MEPDG, reliability of a given design is defined as the probability that the predicted performance of the pavement for a given design will be satisfactory over the time period under consideration. "The distress predicted on the basis of the calibrated MEPDG mechanistic-empirical models and mean values for all inputs can be though of

as being at a 50% reliability estimate i.e. there is a 50% chance that the predicted number of cracked slabs will be greater than or less than the mean prediction assuming that the distribution is symmetrical" (Darter et al., 2005).

The MEPDG transverse cracking prediction reliability analysis is based on the assumption that the error in the prediction of mean slab cracking is normally distributed. Because of the normal distribution assumption, the variation of cracking around the mean distress prediction can be defined as the mean predicted distress and a standard deviation. The MEPDG transverse cracking reliability equation is stated in Equation 2.6.

$$CRACK_p = CRACK_{mean} + STD_h * Z_p \quad (2.6)$$

Where:

$CRACK_p$ = Cracking level corresponding to the reliability level, P

$CRACK_{mean}$ = the percentage of cracked slabs corresponding to 50% of the slabs for the distribution of measured pavement thicknesses.

Z_p = Standard normal deviate (mean 0, STD 1) corresponding to reliability level, P.

STD_h = The standard deviation term, which is a function of the error associated with the data used to calibrate the cracking model and is calibrated with a procedure that correlates predicted cracking to measured cracking. This concept is illustrated in Figure 2.8 (ARA, Inc., 2003b), which shows measured cracking on the y-axis and predicted cracking on the x-axis.

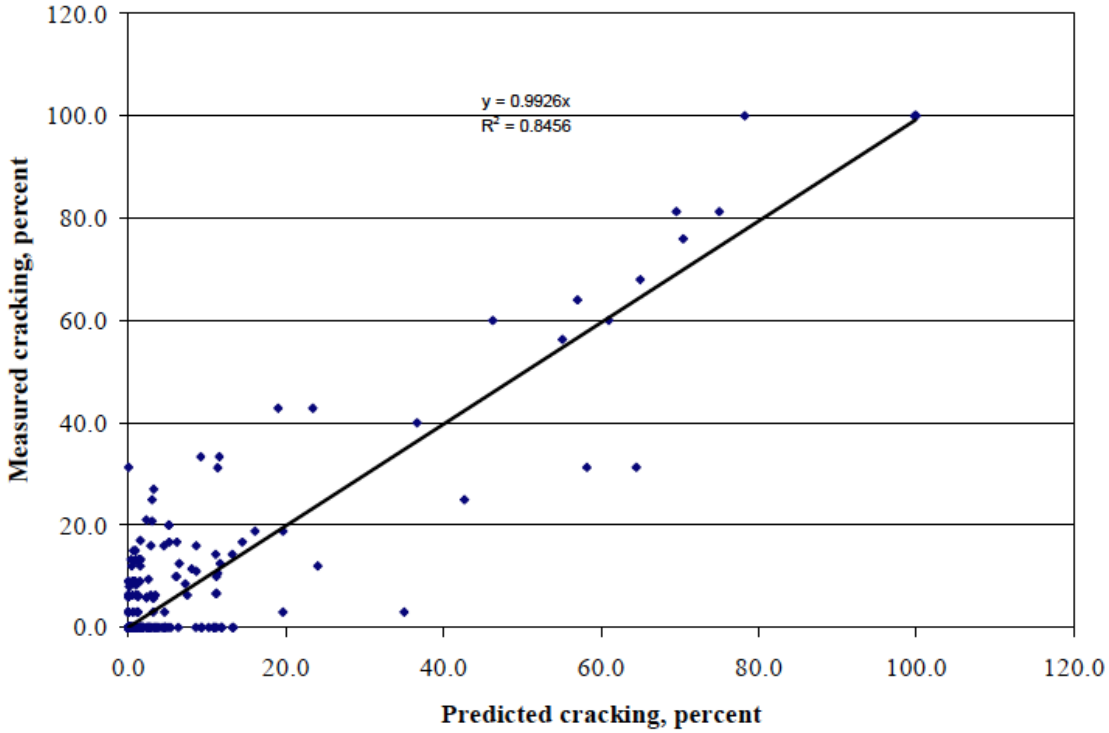

Figure 2.8 Correlation of predicted and measured cracking to calibrate standard deviation term that is included in the MEPDG transverse cracking reliability equation

Equation 2.7 is the calibrated standard deviation term used in the MEPDG transverse cracking reliability analysis.

$$STD_h = -0.00198 * CRACK_{mean}^2 + 0.56875 * CRACK_{mean} + 2.76825 \quad (2.7)$$

The calculation for standard deviation (STD_h) is a function of mean cracking ($CRACK_{mean}$) and is calibrated to represent all uncertainty of transverse cracking distress predictions due to all possible sources. The research in the subsequent chapters aims to address this limitation.

2.4 Non-Destructive Testing Methods for Concrete Pavement

In conjunction with the review of concrete thickness testing for rigid pavements, this section of the literature review investigates non-destructive testing methods and technologies used to measure concrete layer thicknesses in rigid pavements. Non-

destructive concrete pavement testing methods have been evolving since the 1970s but not until recently has the technology been economical, user friendly, and accurate enough for some concrete property assessment.

The most utilized non-destructive testing technologies for pavement testing are ground penetrating radar (GPR), ultrasonic techniques, impact echo (IE), and seismic methods. Most of these non-destructive testing technologies have been used to evaluate both asphalt and concrete thickness, presence of internal distresses or voids, compression and flexural strength, or modulus (Nazarian et al., 2006). The following sections briefly review some of the most-used NDT technologies used for analyzing pavement properties.

2.4.1 Probing Method

A few states, in particular, Wisconsin and Minnesota, have been using the probing method for concrete layer thickness quality control in rigid pavements since 1988. Plates are randomly placed on the base surface before final layer paving. Probes rely on contact with these plates to verify that the probe tip has reached the bottom of the concrete layer. In Wisconsin, for example, probes are taken 2 times per unit, which is defined as 250 ft. long and one lane width wide (Allison et al., 2010). Probing was found to be almost 600% faster than taking cores, especially once a construction crew developed a process for taking the probing measurements (Nasief et al., 2011).

The drawbacks of this NDT method are that it is limited in terms of collecting thickness information in terms of location and timing. The probe can only be applied before the concrete hardens and is limited to locations were metal plates were pre-placed on the aggregate base prior to paving with concrete.

2.4.2 Ground Penetrating Radar

Ground Penetrating Radar (GPR) is a technology used to explore the subsurface condition of pavement layers including the asphalt and concrete surface layers and base layers. This non-destructive pavement evaluation method sends an electromagnetic pulse through the pavement layers via an antenna. The electromagnetic pulse is either ground or air coupled into the pavement (Edwards & Mason, 2011), but for large-scale pavement evaluation, air coupled GPR is most commonly used. Electromagnetic pulses reflect off of internal layer interfaces where a material's dielectric constant changes, such as at the interface with the base and subbase layers, reinforcement, areas with trapped moisture, and large air voids (Al-Qadi et al., 2005). A receiving antenna reads the reflected electromagnetic waves. Amplitudes and arrival times of the reflected electromagnetic waves are used to estimate inclusion location and layer thickness (Holzschuher et al., 2007).

The speed of the initial electromagnetic pulse affects the performance and output of the GPR analysis. GPR devices used for exploring pavements typically operate in the range of 1 to 2 GHz (Edwards & Mason, 2011), although research efforts are going towards the development of 3 GHz devices (Lee et al., 2002) because higher operational frequencies are needed to detect features of thinner pavements. Lower frequencies achieve deeper penetration but decrease the vertical resolution. The effective depth of electromagnetic wave penetration is a function of the dielectric constant of the layer materials, the frequency of the wave, and the power output and receiver sensitivity of the GPR (Holzschuher et al., 2007).

The strengths of GPR systems are that they collect pavement layer thickness data quickly, unobtrusively, and inexpensively, and the data are accurate enough for management consideration (FHWA, 2000). For example, GPR was used to preview the condition of a concrete pavement (JPCP) before an asphalt overlay to identify areas of voids and moisture (Nam et al., 2011). However, if the goal if accurate concrete thickness assessment, GPR may not be the best NDT device for the job because of the reasons previously described.

2.4.3 Impact Echo

Impact Echo (IE) is a technology created specifically to explore the subsurface condition of concrete (Sansalone, 1997). This non-destructive concrete evaluation method requires a short duration mechanical impact with a small steel ball against the concrete surface, which generates low frequency stress waves. A receiver within centimeters of the impact point measures the sound waves that are reflected back to the surface by discontinuities within the concrete (Carino, 2001 and Sansalone, 1997). The large wavelengths resulting from low frequency waves (1-60 kHz) do not reflect off of aggregates, small cracks, and pores, which is a problem for higher frequency waves (Schubert et al., 2004).

Impact Echo has been used to identify structural geometry, detect flaws such as cracks, voids, shallow delaminations, honeycombing, and surface opening cracks, and can detect acoustic behavior of interfaces between materials i.e. for layered structures, repaired structures, and reinforced/pre-stressed structures (Sansalone, 1997). The primary flaws of IE are its lack of redundancy and sensitivity to geometrical boundaries.

Practical experience has shown that a single point measurement is not reliable and is sensitive to small shifts of source and sensor positions (Schubert et al., 2004).

2.4.4 MIT-Scan T2

Magnetic imaging tomography, given the nickname MIT-Scan T2, uses electromagnetic sensors to measure the intensity of a magnetic field caused by an eddy current in a pre-placed metal reflector. Most concrete properties have little effect on magnetic fields, which eliminates the sensitivity of the device to the heterogeneous nature of concrete (FHWA, 2009). The MIT-Scan T2 measures the depth of concrete to an accuracy of 0.5% of the measured depth plus 0.04 in. MIT-Scan T2's strengths are that it is portable, quick, and accurate. The major drawback is that it requires the placement of a metal plate on the pavement's base surface before either the asphalt or concrete layer is placed (FHWA, 2009), and testing can only be performed in locations containing a plate.

2.4.5 PSPA

The Portable Seismic Pavement Analyzer (PSPA) is a hand-held, portable device that uses free-free resonant column seismic technology to measure transverse and shear resonant frequencies of a concrete specimen. The free-free resonant column technology is capable of determining concrete's dynamic Young's modulus and dynamic Poisson's ratio. Through a correlation of longitudinal and shear resonant frequencies, the Poisson's ratio of the concrete along with a theoretical field Young's modulus can be determined. Furthermore, resonant frequencies can be associated with the concrete's compressive and flexural strengths if those values are measured on concrete cylinders or cores (Nazarian et al., 2003).

A limitation of PSPA is that resonance frequency depends on aggregate type. This requires that compressive and flexural strengths be correlated with PSPA readings for each concrete mixture and site condition (i.e. humidity and temperature). As a result, it is difficult to make meaningful comparisons of concrete properties measured with PSPA at different sites. Furthermore, an involved setup and measurement process make implementing PSPA testing difficult on a routine basis.

2.4.6 Ultrasonic Tomography

Ultrasonic tomography uses elastic shear wave impulse time-histories to reconstruct two-dimensional scans of a concrete plane. Two types of ultrasonic tomography devices are reviewed here—one with an air-coupled transducer and another with a dry-point contact transducer array.

2.4.6.1 Air-Coupled Ultrasonic Pulse Velocity

Air-Coupled Ultrasonic Pulse Velocity (UPV) is a non-destructive technology that uses air-coupled ultrasonic transducers to send sound waves through concrete. The transducers should be located 0.8 to 1.6 in. off of the concrete surface (Zhu & Popovics, 2005 and Centrangolo & Popovics, 2010). This technology is still in development, but it promises an effective method for measuring concrete structures accessible from two sides. It eliminates the need for the coupling agent typically required of ground-coupled ultrasonic transducers. While this method has the potential to improve the productivity of the measurement process, the loss of energy at the air-concrete interface limits the observation depth of concrete that can be analyzed with this technology.

2.4.6.2 MIRA

MIRA is an ultrasonic tomography device that uses dry point contacts, which do not require a coupling agent to transfer low-frequency shear waves into the test short length scale. Figure 2.9 shows the ultrasonic tomography device, MIRA, with 10 channels (columns) and 4 rows of transducers that each send and receive shear waves. In total, each MIRA test collects measurements from 45 sending and receiving transducer pairs as illustrated by Figure 2.10.

Figure 2.9 MIRA (Acoustic Control Systems)

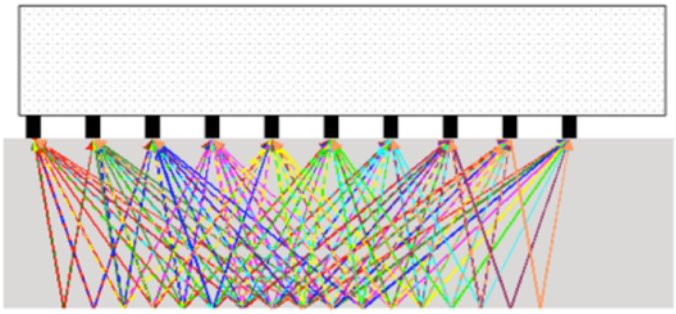

Figure 2.10 The pattern of MIRA's 45 sending and receiving pairs (Acoustic Control Systems, 2010)

MIRA's typical operating frequency is 50 kHz in concrete and 30kHz in asphalt, which allows wave penetration depth through highly heterogeneous materials. Compared

to the frequency of medical or industrial ultrasonic tomography applications, which operate on the MHz scale, these frequencies are low. The shear waves are reflected at changes in acoustic impedance, which is defined as the product of density and velocity of the material (Graff, 1991 and Achenbach, 1973).

A MIRA measurement is taken by ensuring full contact of the transducers with the concrete surface, giving 45 sending and receiving shear wave impulses and a corresponding reconstruction. There are two components to a MIRA measurement—a shear surface velocity and a Synthetic Aperture Focusing Technique (SAFT) B-scan. The surface velocity measurement establishes the velocity of sound wave travel through the concrete and is indicative of material stiffness, which can be correlated to maturity and strength. During a surface velocity measurement, sound waves travel horizontally through the concrete, just below the surface. MIRA's output for the shear velocity is calculated using the direct arrival times from various transducers with set spacing and this velocity is used when reconstructing the second type of MIRA output, the SAFT B-scan.

During a SAFT B-scan, shear waves are emitted into the material and changes in acoustic impedance cause reflections back to the surface (Hoegh & Khazanovich, 2012). A SAFT B-scan is used to interpret the acoustic signals and produces a two-dimensional, true-to-size tomogram that displays a picture of the tested concrete area (Figure 2.11). The center of a high reflectivity location is associated with the highest changes in acoustic impedance indicated by the lighter shades on the tomogram. Figure 2.11 shows a typical output signal where a reflection between concrete and a material of different

acoustical impedance can be observed. The thickness measurement corresponds to the center of the interface reflection (Hoegh & Khazanovich, 2012).

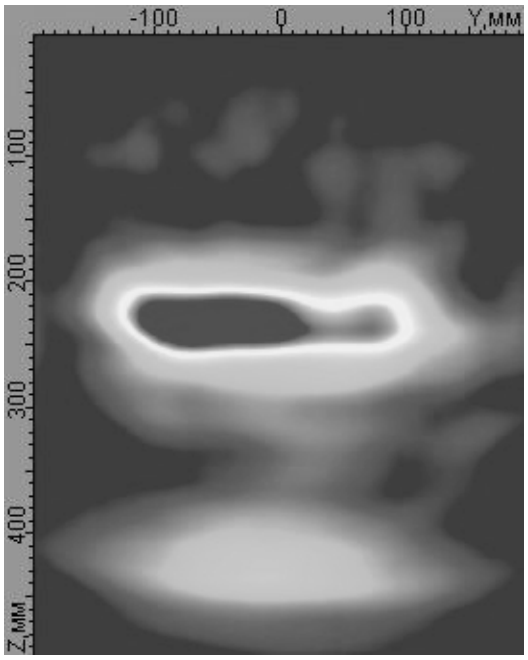

Figure 2.11 SAFT B-scan tomogram

Considering pavement thickness measurements, flaw detection, and rebar location, MIRA has two significant limitations. First, it is limited in ability to measure asphalt, especially in warm conditions due to asphalt's modulus variation with depth and significant shear wave absorption. Secondly, it can only measure one layer (Edwards & Mason, 2011) for typical slab on grade pavement designs. MIRA's strengths are that it can accurately give positional information about any changes in acoustic impedance such as subsurface defects or inclusions such as rebar within concrete. Next, it has built-in redundancy and self-calibrates, allowing for pavement thickness and rebar depth measurements to within 0.25 in. (Hoegh et al., 2011). Finally, it is lightweight, portable, and does not require significant user expertise to collect measurements.

2.5 Measuring Concrete Properties with Ultrasonic and Seismic NDT Devices

Non-destructive concrete testing device technology has advanced enough to measure concrete thickness, identify rebar location, and capture large voids and cracks. Many ultrasonic and some seismic NDT devices have also been employed to measure concrete flexural and compressive strength and the concrete properties of modulus of elasticity, Poisson's ratio, and density. Ultrasonic and seismic technologies have the potential to identify concrete properties because the speed of wave propagation is contingent on the concrete's modulus, PR, and density. In turn, these properties predict the strength of concrete.

When a disturbance (stress or displacement) is applied at a point on a surface—the disturbance propagates through the solid as three types of waves (Carino, 2001):

- P-wave—propagation of normal stress, spherical wavefront
- S-wave—propagation associated with shear stress, spherical wavefront
- R-wave—travels away from disturbance along the surface

In an infinite, isotropic, elastic solid, P-wave speed (C_p) is related to Young's modulus of elasticity, E, Poisson's ratio, v, and the density, p, as seen in Equation 2.9. S-waves propagate at a slower speed (C_s), but are dependent on the same material properties (Equation 2.10) (Liang & Wu, 2002 and Krautkramer & Krautkramer, 1990):

$$C_p = \sqrt{\frac{E(1-\nu)}{\rho(1+\nu)(1-2\nu)}} \qquad (2.9)$$

and

$$C_s = \sqrt{\frac{G}{\rho}} = \sqrt{\frac{E}{2\rho(1+\nu)}} \qquad (2.10)$$

Given C_p or C_s, E, ρ, and ν, when three of the four are known, the fourth value can be theoretically calculated.

If the concrete modulus of elasticity is predicted with Equations 2.9 or 2.10, existing equations can be used to correlate modulus of elasticity with concrete compressive strength and concrete flexural strength with compressive strength (Mallela et al., 2001). Using these correlation equations, both f'c and the flexural strength of concrete could be predicted with the predicted modulus of elasticity. More appealing, though is a non-destructive testing device, which could measure the compressive or flexural strength of concrete directly, and many researchers have attempted to show that NDT devices can accurately predict the compressive and/or flexural strength of concrete

In one study, ultrasonic pulse velocity (UPV) was used to estimate concrete strength by measuring dynamic modulus, static modulus, and secant modulus. Starting with a concrete mixture comprised of a baseline aggregate gradation, aggregate type, maximum aggregate size, water-to-cement ratio, cement type, and ambient air temperature, the study's authors varied these parameters one at a time, made concrete samples, measured the samples with a UPV device, and correlated the measured velocity with compressive strength, static modulus, dynamic modulus, and secant modulus. Least squares regression was used to find coefficients for best-fit equations of velocity versus each concrete parameter. The velocity was most sensitive to aggregate type, aggregate gradation, and maximum aggregate size (Trtnik et al., 2009).

If each concrete mixture was considered independently, there was little scatter in the velocity vs. compressive strength plot. However, if all concrete mixtures were

considered together, the range of compressive strengths for one velocity measurement was near 30 MPa (4,371 psi), which is an unacceptable range because 4,000 psi is a typical compressive strength of a non-high performance concrete. The velocity vs. modulus data plot showed a range of 4 GPa (580,150 psi) for one velocity. A typical modulus of elasticity for concrete is 25 GPa (3.6×10^6 psi) so that range could produce 16% error in prediction of a modulus. This experiment showed that there was not a universal velocity that corresponded to a particular modulus or compressive strength. Rather, ultrasonic wave velocities were highly sensitive to aggregate type, gradation, and maximum size.

In another study, authors combined the NDT technologies of ultrasonic velocity and rebound hammer to estimate concrete compressive strength considering concrete properties such as aggregate type, cement content, and water-to-cement ratio. Through a series of statistical analyses of over 1000 data sets obtained from the literature, authors developed a regression equation that predicted the compressive strength of concrete based on UPV, rebound hammer number, concrete water-to-cement ratio, and concrete age. While the analysis to achieve the regression equation was rigorous, the regression equation was not validated for practical use (Huang et al., 2011).

In a third study, free-free resonant column technology in the form of a portable seismic pavement analyzer (PSPA) was used along with concrete maturity to develop a correlation between the time-temperature factor of concrete and concrete flexural and compressive strength (Nazarian et al., 2003). The study showed a strong correlation between the time temperature factor for concrete maturity and concrete compressive and flexural strength, but there were significant drawbacks to the methodology. First,

extensive calibration of both the portable seismic testing device (PSPA) and the maturity method were conducted in a laboratory setting before this technology could be used to estimate a pavement's strength and modulus of elasticity in the field. Secondly, assumptions were made regarding the concrete's density. Third, the relationship between the modulus of elasticity in the lab and in the field was empirically determined and may or may not apply to all concrete types. Finally, when the authors investigated the correlation between the time-temperature factor and compressive and flexural strength for one concrete mixture, regression analysis showed a controlled relationship. When multiple concrete mixtures were investigated, the correlation error became large, even though the same type of aggregate was used in all of the mixtures. This method was highly dependent on specific concrete mixtures and the methodology was not transferrable to a generalized study of the relationship between seismic analysis, concrete maturity, and strength of all concrete mixtures.

These studies show that when ultrasonic and seismic NDT technology were used to predict concrete properties including compressive and flexural strength and modulus of elasticity, the results were highly dependent on the concrete mixture. This suggests that either the technology is not adequate for strength or modulus characterization and/or the correlation equations (Equations 2.9 and 2.10), which convert velocity to modulus or strength, are so dependent on other variable concrete properties such as Poisson's ratio and concrete density (which are rarely known) that they do not adequately predict concrete strength or modulus.

2.6 Summary

A recently introduced Mechanistic-Empirical Pavement Design Guide (MEPDG) for the design of new and reconstructed jointed plain concrete pavement (JPCP) (Darter et al., 2005) recognizes uncertainty and variation in pavement design and construction. The reliability analysis used by the MEPDG considers uncertainty from all sources as one value that is a function of mean cracking and calibration constants instead of considering uncertainty from each source individually. Because of this limitation, there is little incentive to diminish variability of individual pavement characteristics.

Recent advancements in NDT technology allow for the characterization of concrete thickness variation in JPCPs. NDT devices can measure concrete layer thickness as often as desired but it is still desirable to establish standard sample spacing to avoid cost. When core samples are used to measured JPCP concrete layer thickness, sample spacing is limited by cost and damage to the pavement, and the measurements do not quantify the effect of variability of the design inputs on predicted pavement performance.

3 ULTRASONIC TOMOGRAPHY ACCURACY AND VARIABILITY

3.1 Introduction

The concept of using NDT devices to measure concrete thickness is not a new idea. What has changed is that the NDT technology finally has the accuracy and robustness to consider integrating it into mainstream use. The ultrasonic tomography device, MIRA, was used throughout this dissertation to measure the concrete layer thickness of Jointed Plain Concrete Pavement (JPCP). Although there are many NDT devices that measure concrete thickness, MIRA was selected for collection of concrete thickness data for this dissertation because of its many strengths. MIRA's redundant linear array allowed for reliable measurements, while the lightweight and portable nature of the device permitted several full-scale testing opportunities. The spatial diversity of the measurement process also allowed for self-calibration at each measurement location, which enabled reliable measurements over large areas of pavement. In future chapters of this dissertation, MIRA concrete thickness measurements will be used to characterize the thickness variability of the concrete layer in rigid pavements. Thus, it was important to document MIRA's measurement sensitivities and legitimize its ability to accurately measure concrete layer thickness. This chapter presents MIRA's sensitivity, repeatability, and accuracy for the measurement of concrete thickness.

MIRA's SAFT B-scan sensitivities were determined using MIRA measurement data from multiple concrete pavements (for more information on SAFT B-scans, refer to the literature review). The first section of this chapter will explore the variation in SAFT B-scan measurements (using concrete thickness determination variability) when thickness scans are taken repeatedly at one spot without moving MIRA between measurements.

The second part of this chapter will compare hand-measured concrete core thickness to MIRA-determined concrete thickness at the same location.

3.2 MIRA Thickness Measurement Sensitivity

3.2.1 Methodology

Three concrete pavements were used to determine the sensitivity of MIRA's surface velocity and thickness measurements. These pavements were located in the State of Minnesota and the concrete layer ranged in thickness from 5 in. to 10 in. In order to determine the MIRA's thickness measurement sensitivity, SAFT B-scans were taken multiple times in one location without moving MIRA between measurements.

To expedite the analysis, an automated, highest reflectivity thickness procedure developed at the University of Minnesota was used to extract the concrete thickness measurements from the MIRA outputs. This procedure allowed for consistent analysis of sound concrete pavement thickness. However, if any subsurface damage within the concrete layer was present, the automated procedure was no longer applicable, and the thickness measurements that resulted in very shallow values (i.e. 2-3 in.) were not counted in this analysis.

3.2.2 Repeatability of MIRA Thickness Measurements

The thickness measurements produced by taking 2 SAFT B-scans at the same location without moving MIRA, were compared. Table 3.1 displays 60 SAFT B-scan thickness measurements. The columns labeled T1 and T2 represent the first and second SAFT B-scan measurements, respectively, and the column labeled T1-T2 represents the difference between them. Only 4 of the 60 differences were not equal to zero and these

instances are highlighted in Table 3.1. The maximum reported concrete thickness difference was 0.092 in., and the minimum measured concrete thickness difference was 0 in.

Table 3.1 SAFT B-scan thickness measurements recorded without disturbing MIRA between measurements

Trial Number	T1	T2	T1-T2	Trial Number	T1	T2	T1-T2
1	9.781	9.781	0.000	31	5.471	5.471	0.000
2	10.056	10.087	-0.031	32	5.563	5.563	0.000
3	10.362	10.362	0.000	33	5.502	5.502	0.000
4	10.148	10.148	0.000	34	5.257	5.257	0.000
5	9.445	9.445	0.000	35	5.044	5.044	0.000
6	9.659	9.659	0.000	36	5.257	5.257	0.000
7	5.135	5.135	0.000	37	5.471	5.471	0.000
8	5.013	5.013	0.000	38	5.288	5.288	0.000
9	5.227	5.227	0.000	39	5.319	5.349	-0.031
10	5.441	5.441	0.000	40	5.471	5.471	0.000
11	5.196	5.196	0.000	41	5.533	5.533	0.000
12	5.227	5.257	-0.031	42	5.533	5.533	0.000
13	5.441	5.441	0.000	43	5.227	5.319	-0.092
14	5.594	5.594	0.000	44	5.257	5.257	0.000
15	5.471	5.471	0.000	45	5.319	5.319	0.000
16	5.135	5.135	0.000	46	5.441	5.441	0.000
17	5.074	5.074	0.000	47	5.288	5.288	0.000
18	5.257	5.257	0.000	48	5.319	5.319	0.000
19	5.441	5.441	0.000	49	5.471	5.471	0.000
20	5.227	5.227	0.000	50	5.563	5.563	0.000
21	5.288	5.288	0.000	51	5.471	5.471	0.000
22	5.441	5.441	0.000	52	5.257	5.257	0.000
23	5.563	5.563	0.000	53	5.288	5.288	0.000
24	5.471	5.471	0.000	54	5.257	5.257	0.000
25	5.227	5.227	0.000	55	5.502	5.502	0.000
26	5.074	5.074	0.000	56	5.288	5.288	0.000
27	5.288	5.288	0.000	57	5.349	5.349	0.000
28	5.441	5.441	0.000	58	5.471	5.471	0.000
29	5.288	5.288	0.000	59	5.563	5.563	0.000
30	5.319	5.319	0.000	60	5.471	5.471	0.000

The data presented in Table 3.1 shows that MIRA rarely contributed to variation in concrete thickness measurements, and when it did, the variation was less than 0.1 in. For comparison, MN/DOT measures the length of concrete cores with a 9-probe hydraulic device. Measurements are taken to the nearest 0.05 in. and averaged. According to ASTM C 1542 Standard Test Method of Measuring Length of Concrete

Cores, a single operator coefficient of variation was found to be 1.94%. The document goes on to say that two measures of the same core should not differ by more than 5.43% of the mean core length. Finally, the ASTM document reports that the between laboratory coefficient of variation for core length measurements was found to be 4.35% so two measures of the same core by two different individuals should not differ by more than 12.18% of the mean length of the core.

3.3 Comparison of Concrete Thickness Determined by MIRA and Hand Measured Concrete Cores

3.3.1 Methodology

While MIRA technology was found to produce repeatable concrete thickness measurements, the next part of this analysis entailed comparing concrete core thickness measurements with MIRA concrete thickness measurements that were taken at the same location. The concrete pavements used for this study were located in the States of Minnesota, Virginia, Mississippi, and Georgia. To collect the pavement thickness measurements, a location was marked on the pavement, MIRA was used to take a self-calibrated SAFT B-scan, the location was cored with a concrete coring machine, the thickness of the resulting concrete core sample was measured multiple times with a tape measure, and the thicknesses measurements were compared.

3.3.2 Results

Table 3.2 displays data comparing core-measured and MIRA-measured concrete pavement thicknesses from a single location. The first column indicates the core-measured thickness. The second column indicates the MIRA determined concrete

thickness. The third column shows the difference between the core and MIRA measured concrete thicknesses. The number of data points represented in Table 3.2 is 27.

Table 3.2 Comparison of core measured and MIRA measured concrete thicknesses

Sample Number	Core Thickness Avg. (in)	MIRA Thickness Avg. (in)	Core - MIRA (in)
1	7.93	7.98	-0.05
2	7.99	8.04	-0.05
3	8.09	8.25	-0.16
4	8.40	8.71	-0.31
5	7.48	7.79	-0.31
6	7.84	7.95	-0.10
7	9.70	9.67	0.02
8	8.46	8.50	-0.04
9	8.21	8.04	0.17
10	7.52	7.73	-0.22
11	8.42	8.27	0.15
12	24.96	25	-0.04
13	24.92	24.21	0.71
14	24.63	24.8	-0.17
15	14.92	14.37	0.55
16	14.96	15.16	-0.20
17	15.5	15.04	0.46
18	7.54	7.2	0.34
19	8	7.56	0.44
20	8.33	8.46	-0.13
21	12.75	12.68	0.07
22	11.17	10.93	0.24
23	12.75	12.14	0.61
24	13	12.66	0.34
25	12.625	12.33	0.30
26	12.25	11.65	0.60
27	14.75	14.37	0.38

The absolute maximum measured concrete thickness discrepancy was 0.7 in. (measured in a section of concrete that was 24 in. thick) and the absolute minimum measured concrete thickness discrepancy was 0.02 in. To put these results in the perspective of the ASTM concrete core measurement standards for an 8 in. thick core, the thickness measurement could vary by as much as 0.44 in. depending on the person making the measurement. For a 24 in. thick core, the thickness measurement could vary by as much as 1.4 in. This suggests that the cause of any discrepancy between core and

MIRA measured thicknesses is likely somewhere in the middle because of the variability in concrete thickness measurements introduced by the concrete core thickness measurement process. It is important to remember that the difference between the core and MIRA thicknesses cannot be attributed only to MIRA.

Figure 3.1 is a scatter plot comparing the core and MIRA concrete thicknesses along with a line with a slope of 1 and a best-fit line through the data points. Figure 3.2 shows the difference between core and MIRA thickness measurements compared to design concrete thickness.

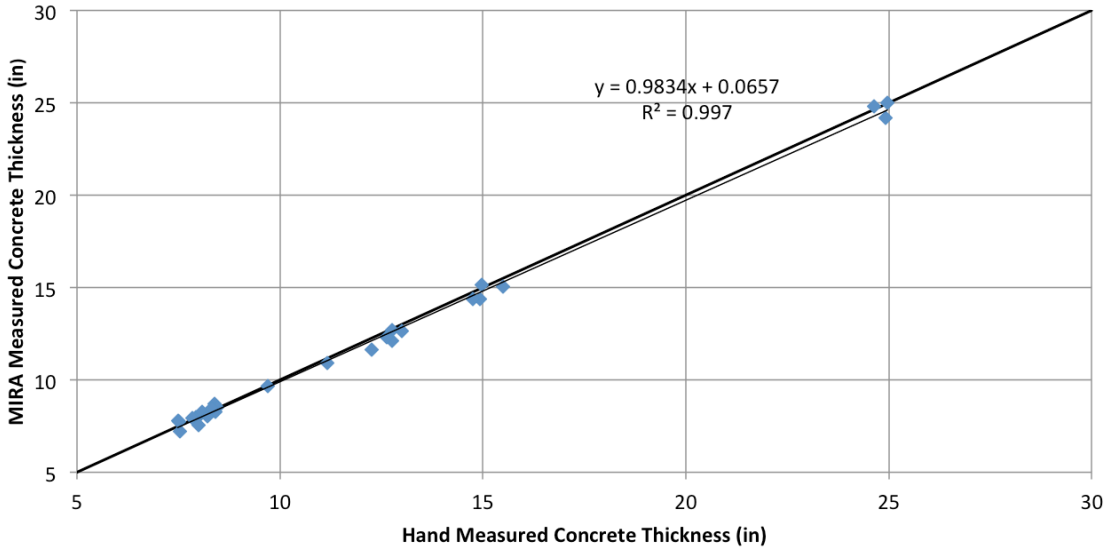

Figure 3.1 Scatter plot of hand measured vs. MIRA measured concrete thicknesses

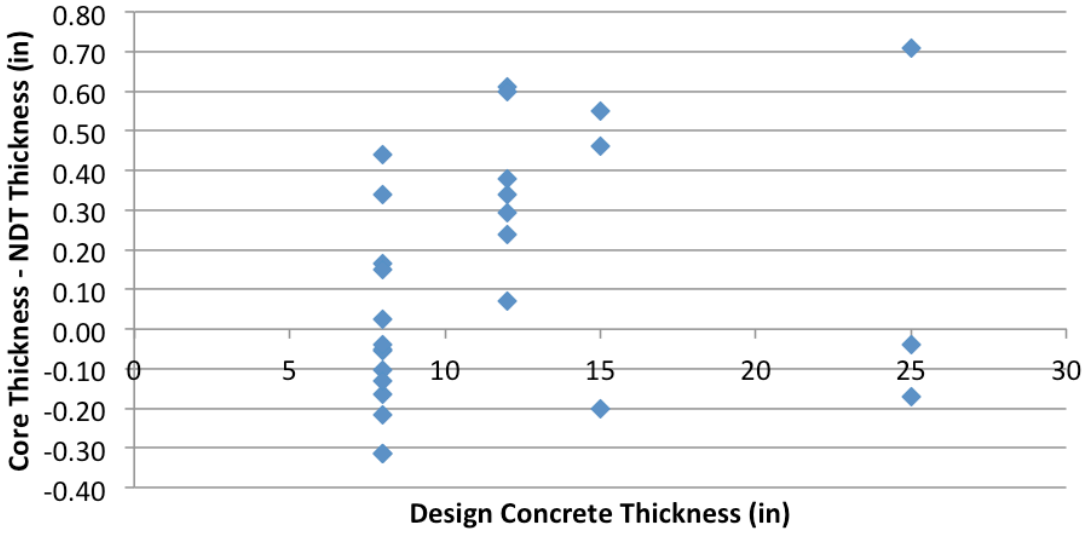

Figure 3.2 Design concrete thickness plotted versus core thickness minus MIRA (non-destructive testing device) thickness

3.3.3 Discussion

Figure 3.1 demonstrates that the difference between core-measured and MIRA-measured concrete thickness is small. Figure 3.2 illustrates that for this data set, core thickness exceeded MIRA thickness more than half of the time. Figure 3.2 also illustrates that the design concrete thickness does not influence the difference between core and MIRA measurements.

Figure 3.1 shows that the core and MIRA measured concrete thicknesses were 98% similar with a 99% correlation level, which suggests a confident correlation between core and MIRA concrete thickness measurements. Figure 3.2 shows that all of the differences in core and MIRA thickness measurements were within ¾ in. and generally skewed slightly higher than the core measurements. As discussed earlier, the core thickness measurement could vary by as much as 0.44 in. suggesting that the discrepancies are within the variation of both measurement techniques.

3.4 Conclusion

The accuracy of NDT devices is often questioned. MIRA is a relatively new NDT device to users in the United States, so the purpose of this chapter was to assess the accuracy of MIRA thickness measurements. The experiments presented in this chapter showed that

- MIRA produced negligible thickness measurement error.
- Compared to concrete core measurements, MIRA was accurate for measuring concrete thickness.
- Comparing MIRA thickness to core-measured thickness was not a prudent way of evaluating the accuracy of MIRA thickness measurements because the potential for core measurement error was often greater than then difference between the core and MIRA thickness. A better way of determining the accuracy of MIRA would be to evaluate a specimen with a known and calibrated thickness.

With the measurement sensitivity of MIRA known, MIRA was used to collect JPCP concrete layer thickness data from three concrete pavements. The next chapter evaluates the concrete thickness variation of these concrete pavements.

4 RIGID PAVEMENT THICKNESS VARIABILITY

4.1 Introduction

The thickness of the concrete layer in rigid pavements is traditionally measured by drilling and measuring the length of a concrete core sample. This procedure is destructive so the number of samples is limited. For example, the Minnesota Department of Transportation (MN/DOT) requires a concrete thickness sample every 1000 ft. Until recently, this was the most accurate method for measuring concrete thickness. Non-destructive testing (NDT) device technology has recently improved to the extent that they could be considered as an alternative to measuring concrete thickness by core length, but they are not yet used extensively outside of research settings. The advantage of using the NDT device to measure concrete thickness is that the destructive process of coring does not limit the number of thickness samples or the location of thickness samples collected. This chapter evaluates concrete layer thickness in jointed plain concrete pavements (JPCPs) with the non-destructive testing device, MIRA, and with concrete cores in order to compare concrete layer thickness variation measured by both methods.

4.2 JPCP Concrete Layer Thickness Measurement

The JPCPs selected for concrete layer thickness evaluation were located in southern Minnesota and were designated Highway 1 (Hwy 1), Highway 2 (Hwy 2), and Highway 3 (Hwy 3). Table 4.1 summarizes design features of each of the JPCPs.

Table 4.1 Summary of JPCP design features

JPCP ID	Concrete Layer Design Thickness (in.)	Number of Lanes	Shoulder Condition	Pavement Classification (MN)
Hwy 1	9	4	Widened	Minnesota State Highway
Hwy 2	8	4	Widened	Minnesota State Highway
Hwy 3	8	2	Widened	County State Aid Highway (CSAH)

These JPCPs were chosen for thickness evaluation because they were newly constructed rigid pavements that had not been opened to traffic when the thickness data was acquired.

Without prior knowledge of how often to measure the JPCP concrete layer thickness to capture both longitudinal and transverse concrete layer thickness variation using NDT technology, two sample protocols were selected to measure concrete thickness. These sampling protocols and the core sampling protocol are described below.

4.2.1 Sample Protocol 1

Sample Protocol 1 entailed using MIRA to measure rigid pavement concrete layer thickness every 15 ft. in the same location of each slab in the truck lane. The concrete layer thickness was measured approximately 2 ft. north and 3 ft. west of the lower east corner (facing the direction of traffic) of the slab. The objective of the first sampling protocol was to rapidly and consistently measure concrete thickness over thousands of feet of pavement. Figure 4.1 shows a schematic of the measurement location for Sample Protocol 1. The total length of pavement evaluated was not equal for all highways but depended on safety and/or the length of the construction project.

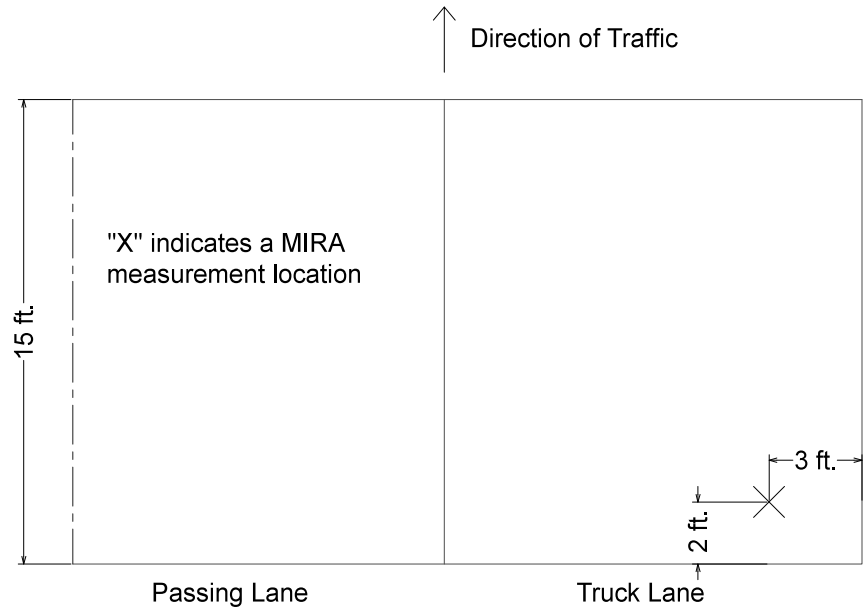

Figure 4.1 Sample Protocol 1 thickness measurement location for Hwys 1, 2, and 3.

4.2.2 Sample Protocol 2

The objectives of the second sampling protocol were twofold. First, it was not known if a measurement every 15 ft. was enough to adequately measure concrete thickness variation within the rigid pavements. Secondly, this sampling protocol considered transverse thickness variation. Sample Protocol 2 entailed taking six equally spaced thickness measurements per slab along the longitudinal paths coinciding with 2 ft. and 11 ft. to the west of the right lane edge along 500 ft. of pavement. The 2 ft. and 11 ft. measurement locations were as close to the slab edge and/or joints as possible while avoiding the edge effect of ultrasound measurements. 500 ft. was selected as the measurement length because many pavement test sections, which are used to study long-term pavement behavior throughout the United States, are 500 ft. long. The thickness measurements taken 2 ft. from the lane edge and 11 ft. from the lane edge will be referred to as the edge and center locations, respectively, throughout the remainder of this

document. The MIRA thickness measurements taken at 2 ft. from the right lane edge were desirable because the right lane edge is where critical stresses form in JPCPs and transverse cracking is typically initiated. A schematic of Sample Protocol 2 thickness measurement locations is shown in Figure 4.2.

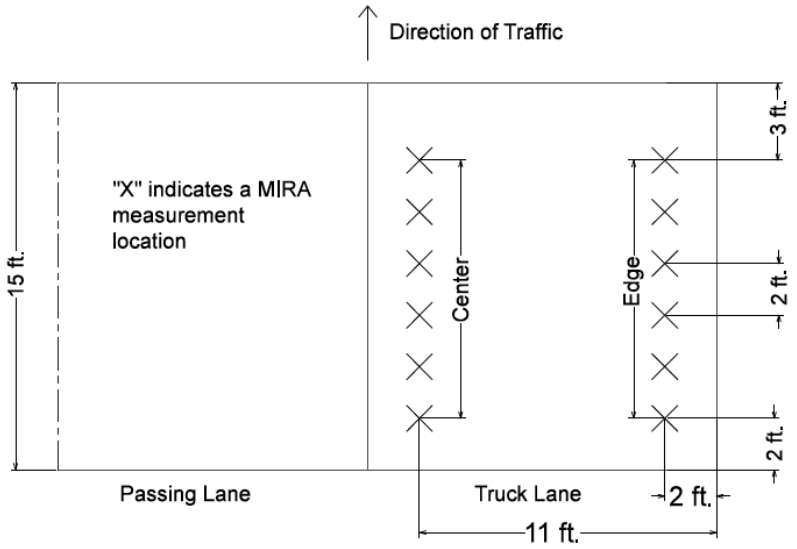

Figure 4.2 Sample Protocol 2 thickness measurement locations for Hwys 1, 2, and 3

4.2.3 Concrete Cores

JPCP concrete layer thickness was also evaluated by measuring the thickness of 4 in. drilled cores from Hwys 1 and 2. The cores were taken according to the MN/DOT QA/QC thickness measurement protocol detailed in the literature review, which required a core approximately every 1000 ft. These core thickness measurements were collected and measured by MN/DOT employees or contractors and obtained from MN/DOT. The concrete core thicknesses for Hwy 3 were not available.

4.3 Concrete Layer Thickness Evaluation

The concrete layer thickness measurements from Hwy 1, Hwy 2, and Hwy 3 collected according to Sample Protocol 1, Sample Protocol 2, and by measuring cores

were plotted vs. longitudinal location. A descriptive statistical analysis was employed to compare the thickness mean, standard deviation, variance, and other statistics for each sample protocol from each site. Next, NDT and core thickness measurements were compared. Finally, concrete thickness measurements from Sample Protocol 1 and the concrete cores were analyzed through the Minnesota Department of Transportation's (MN/DOT) concrete thickness QA/QC protocol.

For each highway, a table and a series of figures depict the concrete layer thickness measurements according to each measurement protocol. For each highway, a table summarizes thickness statistics for Sample Protocol 1, Sample Protocol 2, and cores including length of pavement evaluated, number of samples evaluated, JPCP design concrete thickness, mean thickness, thickness standard deviation, maximum thickness, minimum thickness, and thickness range. The plots following the table are a series of plots and histograms, with each series representing a measurement protocol. For example, the first plot following the table shows concrete layer thickness measurements taken according to Sample Protocol 1 and from core samples. Following the plot is a histogram of thickness measurements taken according to Sample Protocol 1. The next plot shows the concrete layer thickness measurements taken according to Sample Protocol 2, and this plot is followed by histograms of thicknesses collected from the edge and center locations. The following table and figures were assigned to each highway:

- Highway 1: Table 4.2 and Figures 4.3 to 4.6
- Highway 2: Table 4.3 and Figures 4.7 to 4.10
- Highway 3: Table 4.4 and Figures 4.11 to 4.14

Table 4.2 Summary statistics for the Hwy 1 concrete layer thickness measured according to the Sample Protocol 1, Sample Protocol 2, and core measurements

Hwy 1	Sample Protocol 1	Sample Protocol 2		Cores
		Edge	Center	
Length of Pavement Evaluated (ft.)	6645	500	500	6551
Number of data points	444	204	204	7
Design Thickness (in.)	9			
Mean Thickness (in.)	9.15	8.12	9.02	9.24
Thickness Standard Deviation (in.)	0.45	0.31	0.21	0.43
Max Recorded Thickness (in.)	11.00	9.38	9.45	9.88
Min Recorded Thickness (in.)	8.01	8.01	8.44	8.69
Thickness Range (in.)	3.00	1.38	1.01	1.19

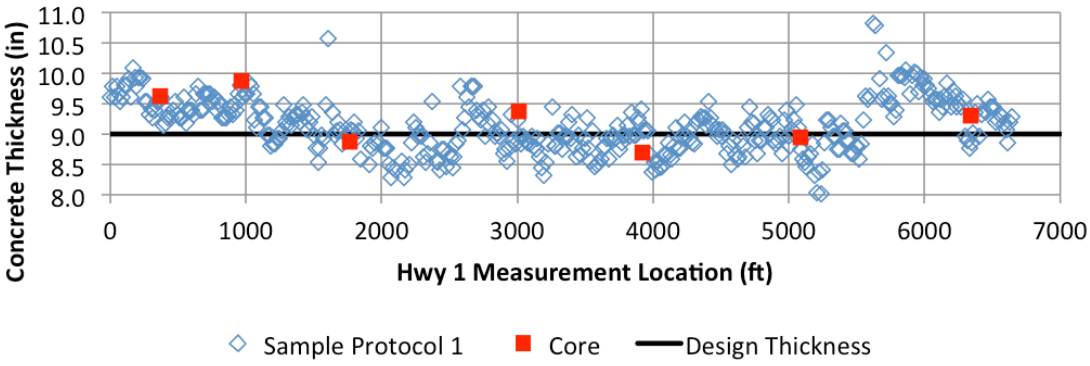

Figure 4.3 Hwy 1 concrete thicknesses measured according to Sample Protocol 1 and concrete cores

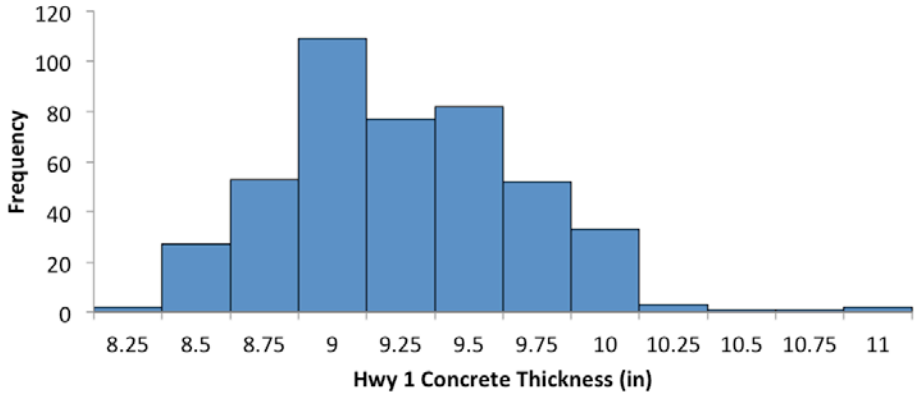

Figure 4.4 Histogram of Hwy 1 concrete layer thicknesses measured according to Sample Protocol 1

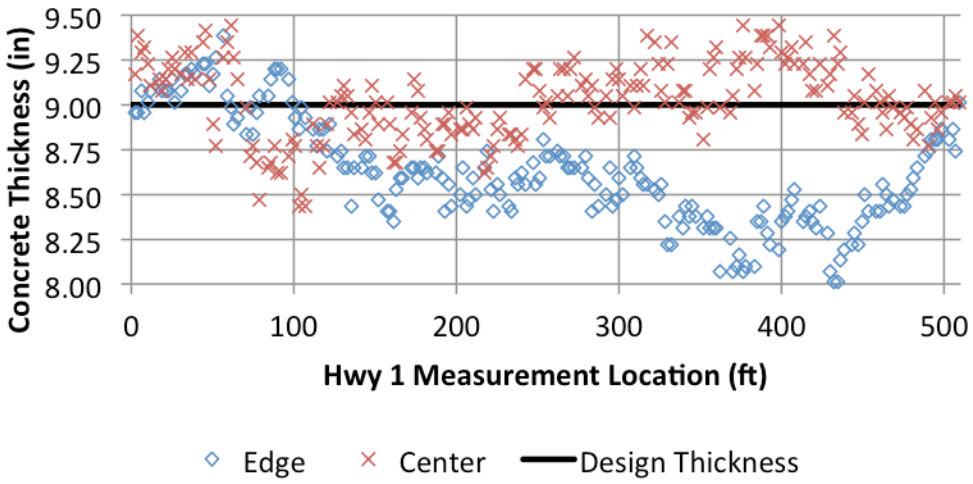

Figure 4.5 Hwy 1 concrete layer thicknesses measured according to Sample Protocol 2 near the edge and center

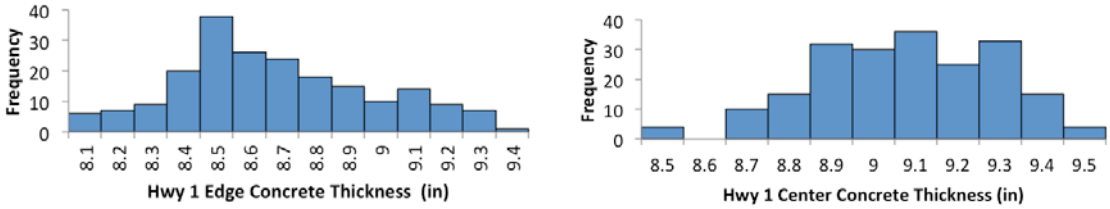

Figure 4.6 Histograms of Hwy 1 concrete layer thicknesses measured according Sample Protocol 2 at edge (left) and center (right)

Table 4.3 Summary statistics for the Hwy 2 concrete layer thicknesses measured according to the Sample Protocol 1, Sample Protocol 2, and core measurements

Hwy 2	Sample Protocol 1	Sample Protocol 2		Cores
		Edge	Center	
Length of Pavement Evaluated (ft.)	15985	500	500	15045
Number of data points	1032	204	196	16
Design Thickness (in.)	8			
Mean Thickness (in.)	8.27	8.19	8.25	8.39
Thickness Standard Deviation (in.)	0.34	0.16	0.16	0.29
Max Recorded Thickness (in.)	9.42	8.59	8.68	9
Min Recorded Thickness (in.)	7.34	7.83	7.89	8
Thickness Range (in.)	2.08	0.76	0.79	1

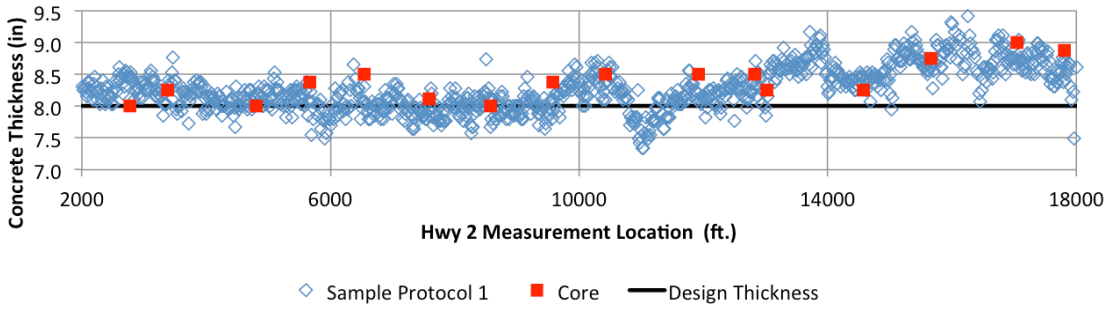

Figure 4.7 Hwy 2 concrete thicknesses measured according to Sample Protocol 1 and concrete cores

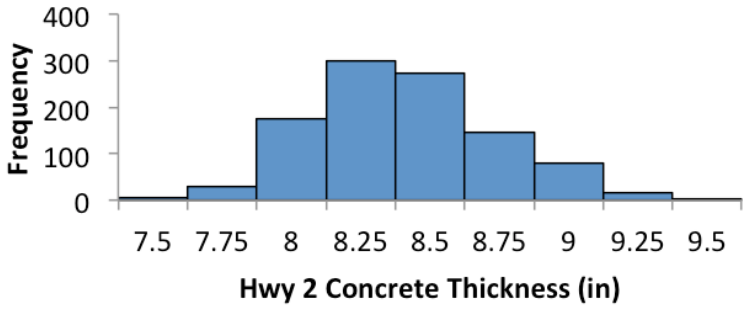

Figure 4.8 Histogram of Hwy 2 concrete layer thicknesses measured according to Sample Protocol 1

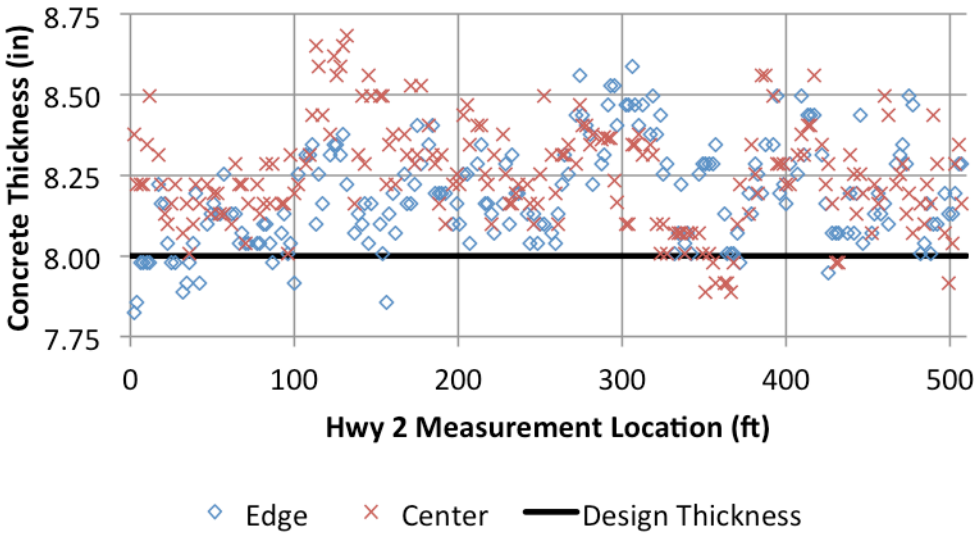

Figure 4.9 Hwy 2 concrete layer thicknesses measured according to Sample Protocol 2 near the edge and center

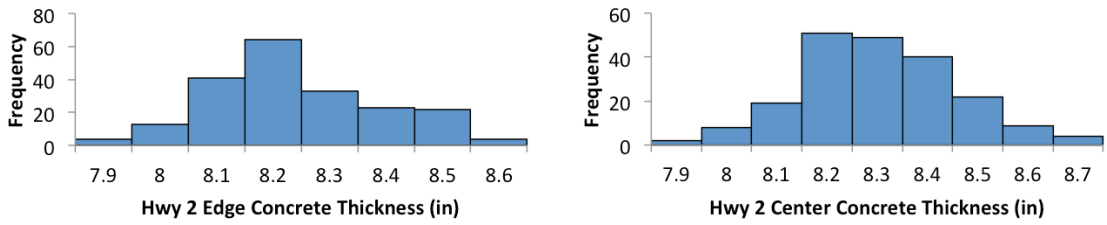

Figure 4.10 Histograms of Hwy 2 concrete layer thicknesses measured according Sample Protocol 2 at edge (left) and center (right)

Table 4.4 Summary statistics for the Hwy 3 concrete layer thicknesses measured according to the Sample Protocol 1, Sample Protocol 2, and core measurements

Hwy 3	Sample Protocol 1	Sample Protocol 2		Cores
		Edge	Center	
Length of Pavement Evaluated (ft.)	3000	500	500	Data Not Available
Number of data points	201	183	194	
Design Thickness (in.)	8			
Mean Thickness (in.)	7.75	7.84	7.83	
Thickness Standard Deviation (in.)	0.17	0.14	0.16	
Max Recorded Thickness (in.)	8.16	8.22	8.16	
Min Recorded Thickness (in.)	7.24	7.52	7.58	
Thickness Range (in.)	0.825	0.70	0.58	

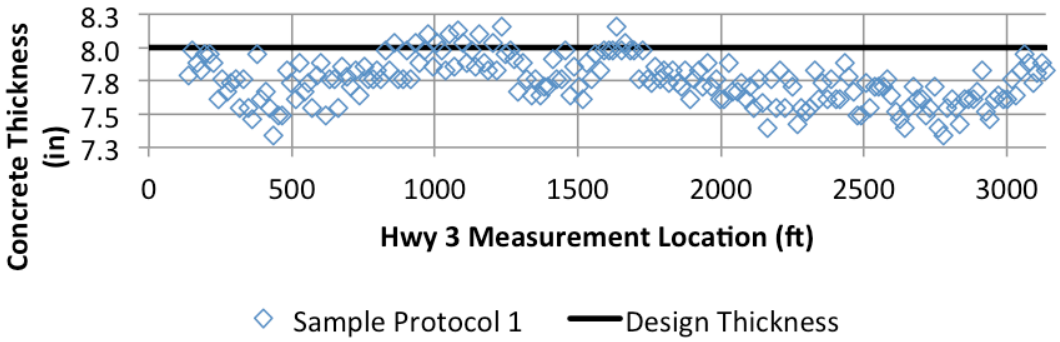

Figure 4.11 Hwy 3 concrete thicknesses measured according to Sample Protocol 1 (core thickness measurements were not available)

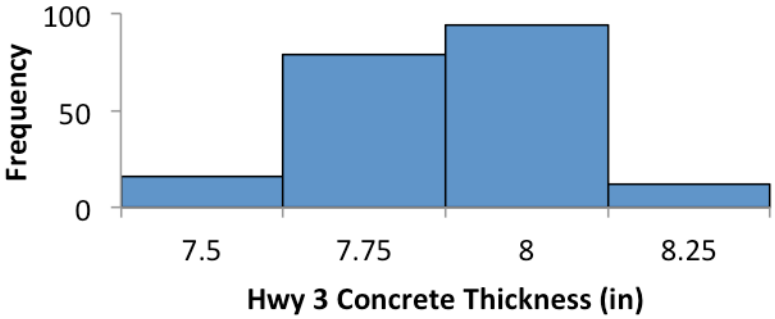

Figure 4.12 Histogram of Hwy 3 concrete layer thicknesses measured according to Sample Protocol 1

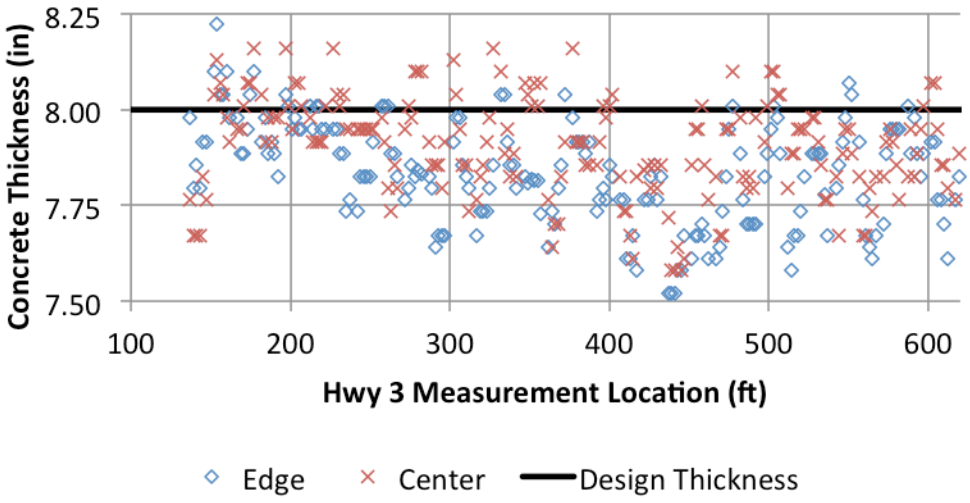

Figure 4.13 Hwy 3 concrete layer thicknesses measured according to Sample Protocol 2 near the edge and center

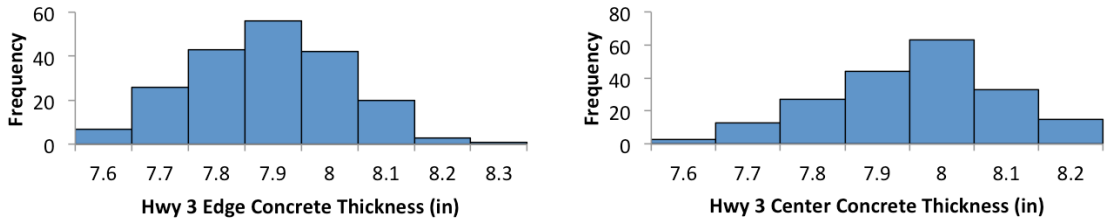

Figure 4.14 Histograms of Hwy 3 concrete layer thicknesses measured according Sample Protocol 2 at edge (left) and center (right)

4.4 JPCP Concrete Layer Thickness Analysis

4.4.1 JPCP Sample Protocol 1 Thickness Measurements Compared to Design Thickness

As can be observed from the non-destructive concrete layer thickness measurements collected on Hwys 1, 2, and 3 according to Sample Protocol 1 (1 measurement every 15 ft. over thousands of feet), the measurements on three pavements coincidently resulted in three thickness distributions. The average Hwy 1 concrete thickness measurements slightly exceeded the design thickness, and the Hwy 1 thickness measurements displayed the most variability around the design thickness. The range of the Hwy 1 concrete thickness was 3 in. across 6,500 ft. of pavement. The average Hwy 2 concrete thickness was 0.3 in. greater than the design thickness, and the Hwy 2 concrete thickness displayed less variability than the Hwy 1 concrete thickness. Over almost 16,000 ft. of pavement, the Hwy 2 thickness range was approximately 2 in. The Highway 3 concrete thickness measurements were the least variable with a range of less than 1 in., but thicknesses were consistently less than the design thickness. The average measured concrete thickness for Hwy 3 was 0.25 in. below the design thickness.

4.4.2 JPCP Sample Protocol 1 Thickness Compared to Core Thickness

The non-destructive concrete layer thickness measurements taken according to Sample Protocol 1 and the core thickness measurements were taken over approximately the same length of pavement on each highway. For concrete core thickness measurements from both the Hwy 1 and Hwy 2 pavements (Hwy 3 cores were not available), the mean thicknesses and thickness standard deviations were similar for the NDT and core measurements. The difference in the thickness measurements between the

NDT device and cores was most apparent by comparing the range of thickness measurements from the NDT device and the cores. For Hwy 1, NDT measurements indicated the range of thickness measurements was 3 in. and the core measurements indicated a thickness range of 1.2 in. Similarly, for Hwy 2, NDT measurements resulted in a thickness measurement range of 2 in., and the core measurements resulted in a thickness range of 1 in.

What these statistics suggest is that while the cores and NDT devices predict approximately the same average thickness, the core measurements fail to capture the full range of maximum and minimum thicknesses over a length of pavement. Figures 4.3 and 4.7 corroborate this observation. The solid squares, which represent the core thickness measurements, correlate well to the triangles, which represent the NDT thickness measurements. However, it is obvious from these plots that there is oscillation above and below the design thickness between the core measurements that would not be observed if cores were the only means used to measure the concrete layer thickness. Furthermore, the core thickness measurements miss the maximum and minimum concrete thicknesses.

4.4.3 Effect of Transverse Thickness Measurement Location on the Concrete Thickness Variation Profile as Measured by Sample Protocol 2

The Sample Protocol 2 thickness measurements considered more frequent thickness measurements over a shorter length of pavement than Sample Protocol 1. As was explained in Section 4.2.2 for Sample Protocol 2, six thickness measurements were taken between transverse joints at 2 ft. and 11 ft. from the right lane edge. This protocol was followed for 500 feet. Thickness measurements, taken from two different locations within a slab, allowed for the comparison of concrete layer thicknesses in the transverse

direction. Figure 4.5 shows the Hwy 1 thickness measurements taken according to Sample Protocol 2. The Hwy 1 data suggests that the transverse location of a concrete thickness measurement is an important consideration when measuring concrete thickness along the length of the project. Referring to Figure 4.5, at approximately 250 ft., the thickness measurements taken near the edge and the center begin diverging until they reach a peak divergence of approximately 1.5 in. around 400 ft., which is a significant divergence for concrete thickness located at transverse locations 9 feet apart in the same rigid pavement slab. It is interesting to note that the shallow concrete is occurring near the edge of the pavement, which is the location of critical stresses for JPCPs. The thicknesses converge near 500 ft.

The Hwy 2 Sample Protocol 2 edge and center thickness measurements displayed on Figure 4.9 appear to follow the same thickness measurement pattern except for a small divergence near 150 ft. At this divergence, the edge concrete thickness drops to the design thickness of 8 in. while the center concrete thickness rises to near 8.75 inches. This is not as dramatic as the difference between edge and center concrete thicknesses for the Hwy 1 example because the range was not as great and the edge thickness measurements did not fall below the design thickness. However, 0.75 in. is a still a significant difference in thickness for two locations that are only 9 feet apart and were paved with the same paver.

Finally, Figure 4.13 illustrates the Hwy 3 concrete thickness measurements taken according to Sample Protocol 2. These thickness measurements mirror those taken according to Sample Protocol 1: there is little variability in the measurements and the measurements are consistently less than the design thickness.

4.4.4 Effect of Section Length and Sample Spacing on Concrete Thickness Measurement Variation

The differences in concrete thickness variability between Sample Protocol 1 and Sample Protocol 2 were both the length of pavement over which samples were collected (thousands of ft. vs. 500 ft.) and sample spacing (15 ft. vs. 2 ft.). For Hwys 1, 2, and 3, the differences in the concrete thickness statistics between the Sample Protocol 1 and 2 data sets were most evident in the thickness standard deviation and the range. Both the thickness standard deviation and the thickness range were less for the Sample Protocol 2 data then the Sample Protocol 1 data. In fact, the Sample Protocol 2 ranges were closer to those measured by the core measurements. What this suggests is that greater frequency does not affect the measured ranges of concrete thickness variation, but less length does.

4.4.5 Comparing Sample Protocol 1 and Core Thickness Measurements Using MN/DOT's QA/QC Thickness Assessment Protocol

The current MN/DOT QA/QC thickness assessment protocol, outlined in the literature review, was applied to the Hwy 1 and Hwy 2 NDT thickness measurements collected according to Sample Protocol 1 and to the core thickness measurements. This was done to consider how more frequent thickness measurements could impact the workmanship of the contractor in order to avoid financial penalty. Because the concrete thickness QA/QC protocol traditionally relies on thickness measurements taken every 1000 ft., the protocol averages cores taken in 5000 ft. sections. If the average core thickness exceeds 0.1 in. less than the design thickness, the contractor is financially penalized according to Table 2.2. As the average core thickness decreases below the

design thickness, the penalties become more severe and exploratory coring is mandatory if any single core is more than 0.5 in. deficient. The protocol had to be slightly modified to accommodate a thickness measurement every 15 ft., and these modifications and results of the QA/QC protocol applied to the Hwy 1 and Hwy 2 Sample 1 Protocol and core thickness measurements are explained below.

The concrete thickness QA/QC analysis involved three steps.

1. Sample Protocol 1 and core thickness averages were re-calculated based on a prescribed thickness ceiling of design depth + 0.3 in. In other words, any thickness measurements that exceeded the design depth + 0.3 in. were re-assigned the thickness of design depth + 0.3 in.
2. The average concrete thickness per section of pavement was determined. Each "section" is 5,000 ft. of one traffic lane. For the purposes of this exercise, Hwy 1 was considered as 1-6,500 ft. pavement section. Hwy 2 was considered as 2-5,000 ft. sections and 1-6,000 ft. section. Hwy 3 was not considered because the core data was not available. Concrete thickness measurements obtained from both Sample Protocol 1 and core measurements were averaged for each section of pavement. These averages were then evaluated for deficiencies that would lead to contractor payment deductions. MN/DOT pay deductions are found on Table 2.2 in Chapter 2.
3. The final step of the MN/DOT QA/QC analysis required tabulating the number of NDT and core thickness measurements that were deficient by more than 0.5 in. The MN/DOT QA/QC specification requires exploratory coring when a concrete layer thickness deficiency is more than 0.5 in. less than the design depth in order

to determine the area of deficient thickness. The results of the MN/DOT concrete thickness QA/QC protocol applied to Sample Protocol 1 and core thickness measurements are summarized below.

The Hwys 1 and 2 Sample Protocol 1 and core concrete layer thickness measurements that exceeded the concrete layer design depth by more than 0.3 inches were reduced to the design depth + 0.3 in. With this ceiling applied, the average concrete thicknesses of each "section" decreased. In general, the MN/DOT thickness ceiling modification decreased the average concrete thickness between hundredths of an inch to 0.1 in. Table 4.5 shows the average NDT and core concrete layer thicknesses calculated with the full value of each thickness measurement and with the MN/DOT thickness ceiling applied.

Table 4.5 Comparison of measured concrete thickness averages to MN/DOT modified concrete thickness averages (SP1 = Sample Protocol 1).

	Hwy 1		Hwy 2					
	Section 1		Section 1		Section 2		Section 3	
	Cores	SP1	Cores	SP1	Cores	SP1	Cores	SP1
Average Thickness (in.)	9.24	9.15	8.61	8.63	8.35	8.09	8.21	8.12
MN/DOT Modified Average Thickness (in.)	9.1	9.03	8.28	8.29	8.23	8.06	8.16	8.10

The MN/DOT QA/QC assessment protocol penalizes average thickness deficiencies between 0.1 and 0.5 in. These penalties did not apply to any of the Hwy 1 or Hwy 2 sections that were evaluated because the penalties are based on the average thickness of a section, not on individual thickness measurements. As indicated in Table 4.5, all of the average modified Sample Protocol 1 and core thicknesses remained above the design concrete thickness.

As noted above, if a single concrete thickness measurement (core or NDT) exceeds a 0.5 in. thickness deficiency below the design thickness, the MN/DOT QA/QC thickness protocol requires exploratory thickness evaluation to determine the extent of the thickness deficiency. Table 4.6 shows the number of core and Sample Protocol 1 thickness measurements that exceeded a 0.5 in. deficiency. None of the core thicknesses required exploratory thickness evaluation, but some of the NDT thickness measurements would have triggered exploratory thickness measurements. For purposes of the NDT thickness measurements, it was assumed that the next "core" was 15 ft. away instead of MN/DOT's prescribed 10 ft. away. This coincided with the distance between the NDT thickness measurements collected according to Sample Protocol 1. To determine the deficient thickness area per pavement section, the number of concurrent NDT thickness measurements with thickness deficiencies exceeding 0 5 in. were multiplied by the distance between NDT measurements (15 ft.) and the assumed lane width (12 ft.). Although the lane widths of the truck lanes at Hwys 1 and 2 were widened lanes (13.5 ft.), for purposes of this exercise, lane widths were assumed to be 12 ft. Table 4.6 shows the pavement area calculated for payment penalty based on deficient concrete thicknesses.

Table 4.6 Summary of MN/DOT payment penalties for areas of concrete thickness deficiencies greater than design depth minus 0.5 in. (SP1 = Sample Protocol 1)

	Hwy 1		Hwy 2					
	Section 1		Section 1		Section 2		Section 3	
	Cores	SP1	Cores	SP1	Cores	SP1	Cores	SP1
# of thick. meas. < (design depth - 0.5 in.)	0	29	0	1	0	5	0	1
Area for payment penalty (yd^2)	0	580	0	20	0	100	0	20
Payment penalty at \$20/yd^2	\$0	\$11,600	\$0	\$400	\$0	\$2,000	\$0	\$400

As summarized in Table 4.6, at Hwy 1, 0 cores and 29 out of 444 or 6.5% of the NDT concrete thickness measurements resulted in a contractor payment penalty based on a concrete thickness deficiency of greater than 0.5 in. The total cost to the contractor would have been $11,600. At Hwy 2, zero cores and a total of 7 thickness measurements from 3 sections resulted in a contractor payment penalty based on a concrete thickness deficiency of greater than 0.5 in. The total cost to the contractor would have been $2,800.

The aim of assessing the concrete layer thicknesses with the MN/DOT QA/QC protocol was not to implicate contractors in wrongdoing, but to illustrate the inadequacy of core thickness measurements every 1000 ft. The analysis represented two specific examples, which happened to indicate that contractors would be penalized by more frequent thickness measurements made possible by NDT devices. It is equally likely that an analysis of concrete pavement thickness with an NDT device could reveal that the contractor is over-paving the concrete thickness in order to meet MN/DOT's requirements. With the knowledge of the concrete layer thickness variation afforded by more frequent thickness measurements, the contractor could potentially decrease material costs.

4.5 Conclusions

A significant body of data has been collected showing the potential for concrete layer thickness variation in jointed plain concrete pavements. The following conclusions were made from the analysis of JPCP concrete layer thickness. First, there is significant thickness variation across the length of concrete pavements. Next, the transverse sample location is important. Because the most important location in a JPCP is near the edge

where taking cores in not desirable, the ability of NDT devices to measure concrete thickness at almost any location is important. Finally, when cores are the only means to measure concrete layer thickness, sample spacing is controlled by cost and damage to the pavement. NDT devices allow for concrete thickness measurements as often as desired but it is still desirable to establish sample spacing to avoid unneeded costs. Chapter 5 proposes methodologies for recommending sample spacing so that concrete thickness variation is adequately characterized with the minimum number of measurements.

5 USING AUTOCORRELATION TO PREDICT SAMPLE SPACING FOR ADEQUATE CHARACTERIZATION OF CONCRETE LAYER THICKNESS

5.1 Introduction

Non-destructive concrete testing (NDT) devices have made it possible to take closely spaced and accurate concrete layer thickness measurements over large areas of rigid pavements. Nevertheless, it is still desirable to limit the number of measurements to what is needed. When considering repetitive sampling over some distance, a sampling interval that is too long results in a high probability of missing information about the characteristic being tested (i.e. missing a pavement thickness measurement that is lower than the desired thickness). If the sampling interval is too short, unnecessary resources are used to gather and process the measurements. The qualification of what is "too long" and "too short" is a function of cost, risk aversion, and historical experience. This chapter explores two methods to approximate the sample spacing for any repetitive sampling procedure by using concrete layer thickness variation as an example.

This chapter is split into three primary sections. First, concrete pavement thickness data, collected with the ultrasonic tomography non-destructive testing device, MIRA, was used as seed data to inform and validate the methods developed for approximating sample spacing. Information on the collection of rigid pavement thickness data will be briefly summarized. Next, because the sampling frequency approximation methods are rooted in autocorrelation concepts from the fields of geostatistics and time series analysis, the mathematical concepts of the variogram and the autocorrelation function are reviewed. Finally, the development and results of the two methodologies used to estimate appropriate sample spacing are presented and discussed.

5.2 Concrete Layer Thickness Measurement Protocol and Methodology

This section reviews the measurement protocols used to collect the concrete layer thickness data from the jointed plain concrete pavements (JPCPs) with an ultrasonic, tomographic NDT device. As discussed in Chapter 4, concrete layer thickness measurements were taken from Hwys 1, 2, and 3 according to two different measurement protocols: Sample Protocol 1 and Sample Protocol 2. With Sample Protocol 1, the concrete layer thickness was measured with the NDT device, every 15 ft. over thousands of feet. The thickness measurements were spaced at 15 ft. because the JPCP joints were cut at 15 ft. and it was convenient to use the joints as a guideline for the measurement location, which was located at the same spot on each pavement slab. Approximately, the distances across which thickness measurements were taken for each highway were 6,500 ft. for Hwy 1, 16,000 ft. for Hwy 2, and 3,000 ft. for Hwy 3. A schematic of this testing protocol can be found on Figure 4.1 in Chapter 4. For Sample Protocol 2, the NDT device was used to take 6 measurements between joints, spaced at 2 ft. intervals, in two locations on the slab: near the slab's edge and near the longitudinal/center joint (pavement dependent). This measurement protocol was followed for 500 ft. for each highway. A schematic of this testing protocol can be found on Figure 4.2 in Chapter 4.

5.3 Autocorrelation

Autocorrelation is a commonly used concept in geostatistics and time series analysis that depicts how measurements within the same data set are related to each other depending on the distance or time step separating the measurements (Chatfield, 2004). In this chapter, autocorrelation was used to show how concrete pavement thickness data were correlated depending on the distance between thickness measurements and to detect

other trends in the data such as periodicity. The non-destructively measured concrete pavement thickness data were well suited for this type of analysis because the measurements were collected at relatively equal spacing over some distance.

In addition to measurement data collected at equally spaced spatial or time intervals, data sets that are well suited for autocorrelation analysis have a property called stationarity. Stationarity implies that there is a constant mean and variance for the data taken at all times or locations. Stationarity-properties of series are unaffected by a change in the origin of time or location (Chatfield, 2004). In other words, the properties of a set of measurements or observations made over a period of time or over a distance will not change substantially if the observations are shifted in time or space.

Autocorrelation principles are the statistical building blocks used to define either the variogram or the autocorrelation function, which will be described further in the next sections. First, the autocovariance term will be derived from the equations used to estimate a data set's mean, variance, and covariance. Autocovariance is the term given to the measurement of data autocorrelation.

With a stationary, normal, finite, second-order data series $Z_i = \{Z_1, Z_2 \ldots, Z_N\}$, where N equals the number of data points collected, the mean (μ) of the data series is defined by:

$$E(Z_i) = \mu_z \qquad (5.1)$$

where $E(Z_i)$ represents the expected value of the mean of data series, Z_i, which is estimated by the sample mean, $\bar{Z}$, a unbiased estimator of μ (Chatfield, 2004):

$$\bar{Z} = \frac{1}{N}\sum_{i=1}^{N} Z_i \qquad (5.2)$$

The variance (σ^2) of data series Z_i is defined by:

$$Var(Z_i) = \sigma^2 \tag{5.3}$$

The variance is estimated by the sample variance, S^2 (Chatfield, 2004):

$$S^2 = \frac{1}{N-1}\sum_{i=1}^{N}(Z_i - \bar{Z})^2 \tag{5.4}$$

The covariance is a measure of how two random data series, Z_i and B_i, are related and is defined by (Chatfield, 2004):

$$Cov(Z, B) = E(Z_i - \mu_z)(B_i - \mu_b) \tag{5.5}$$

The covariance is estimated by the sample covariance, s_{zb}:

$$s_{zb} = \frac{1}{(N-1)}\sum_{i=1}^{N}(Z_i - \bar{Z})(B_i - \bar{B}) \tag{5.6}$$

If the covariance between two random variables is 0, then the variables are completely independent (Navidi, 2011).

When the covariance measures a relationship between variables within the same data series at some time or spatial lag $k = |t - i|$, it is called autocovariance ($C_{|t-i|}$):

$$Cov(Z_i, Z_t) = C_{|t-i|} \tag{5.7}$$

The autocovariance can be estimated by the sample autocovariance at lag k, $\hat{C}_k$:

$$\hat{C}_k = \frac{1}{N}\sum_{i=1}^{N-k}(Z_i - \bar{Z})(Z_{i+k} - \bar{Z}) \tag{5.8}$$

With the autocovariance equation established, the next steps entail finding the semi-variogram or the autocorrelation function of the data series, both of which are tools to identify the correlation of data points separated by distance or time, respectively.

5.3.1 Semi-Variogram

The semi-variogram is a statistically based, quantitative, description of a surface's roughness and is a function of the separation distance, k, between data points. The variogram shows the dissimilarity between data points within the same data series (Barnes, 2012b). The mathematical definition of the semi-variogram ($\gamma_z(k)$) is (Barnes, 2012b):

$$\gamma_z(k) = \frac{1}{2}E((Z_{i+k} - Z_i)^2) \qquad (5.9)$$

The semi-variogram can be approximated by the experimental semi-variogram ($\hat{\gamma}_z(k)$) (Barnes, 2012 and Chiles, 1999):

$$\hat{\gamma}_z(k) = \frac{1}{2N(k)}\sum_{i=1}^{N-k}\left((Z_{i+k} - \bar{Z}) - (Z_i - \bar{Z})\right)^2 \qquad (5.10)$$

Although not obvious from Equation 5.10, it can be shown that the semi-variogram is a function of a data series' variance and autocovariance (Barnes, 2012b):

$$\gamma_z(k) = Var(Z_i) + Cov(Z_i, Z_t) \qquad (5.11)$$

The semi-variogram is typically displayed as a plot of the semi-variance vs. lag distance. An idealized semi-variogram looks similar to Figure 5.1 (Bohling, 2005).

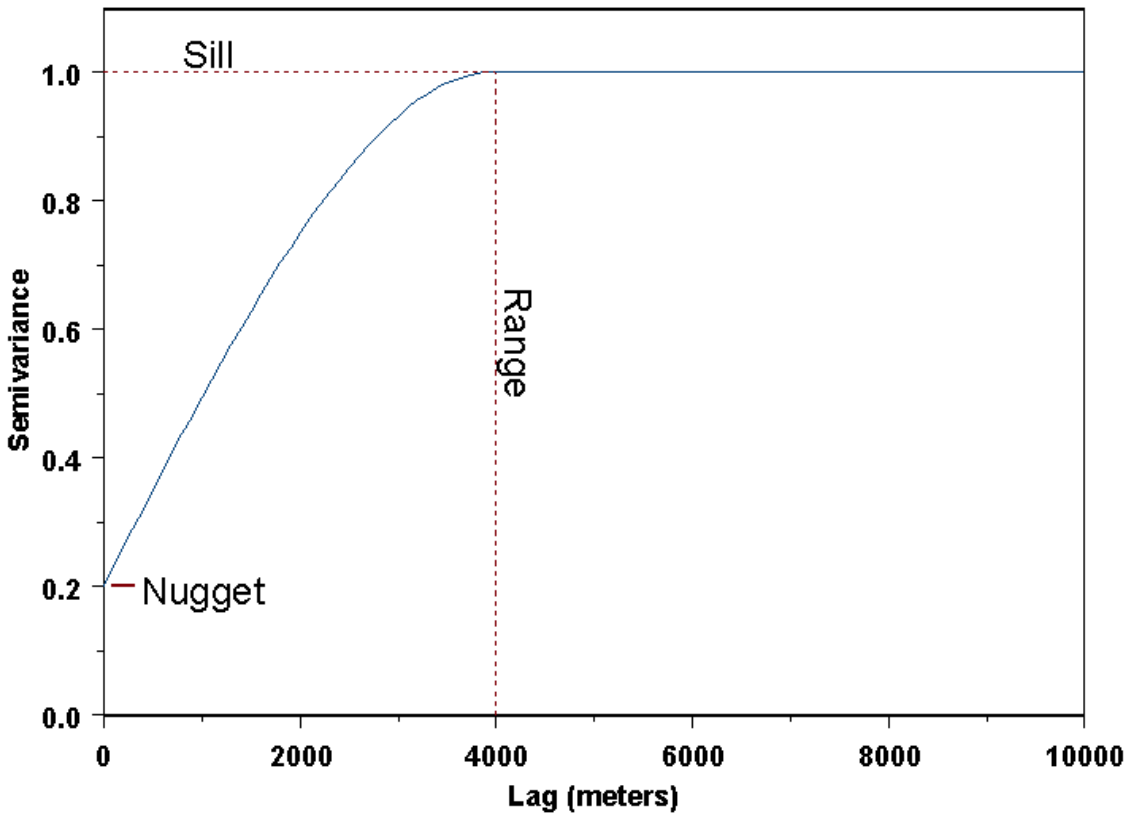

Figure 5.1 Idealized semi-variogram plot highlighting the nugget effect, the sill, and the range

Figure 5.1 is an idealized version of a semi-variogram plot that typically consists of discrete points at chosen data separation (lag) distances. The semi-variogram plot has three distinct features named the Nugget, the Range, and the Sill. These are illustrated in Figure 5.1. The Nugget is the vertical gap between 0 and the semi-variogram at zero separation distance. The Nugget Effect measures the variance of measurement error and the spatial variability that occurs at length scales less than the sample spacing. The covariance of the data points decreases as the lag distance increases until the covariance equals zero indicating that the data are no longer correlated. It is at this point where the plot level off, and this part of the semi-Variogram is called the Sill. The Sill often must be estimated as the semi-variogram plot rarely reaches a definite plateau as illustrated by

Figure 5.1. The lag distance at which the semi-variogram reaches its Sill is determined by the Range. The Range estimates the location at which the data points are no longer correlated.

If the semi-variogram plot displays non-monotonic behavior, it suggests that the data has an embedded structure, which must be removed from the data in order to use the semi-variogram. For example, periodic behavior indicates a non-monotonic semi-variogram and can be characterized as a hole effect semi-variogram (Pyrcz, 2004). "The hole effect is characterized by the presence of one or more bumps on the semi-variogram which correspond to an equivalent number of holes on the covariance" (Chiles, 1999). The hole effect is indicated by a high value on the semi-variogram surrounded by low values and vice versa. The hole effect is illustrated in Figure 5.2 (Pyrcz, 2004).

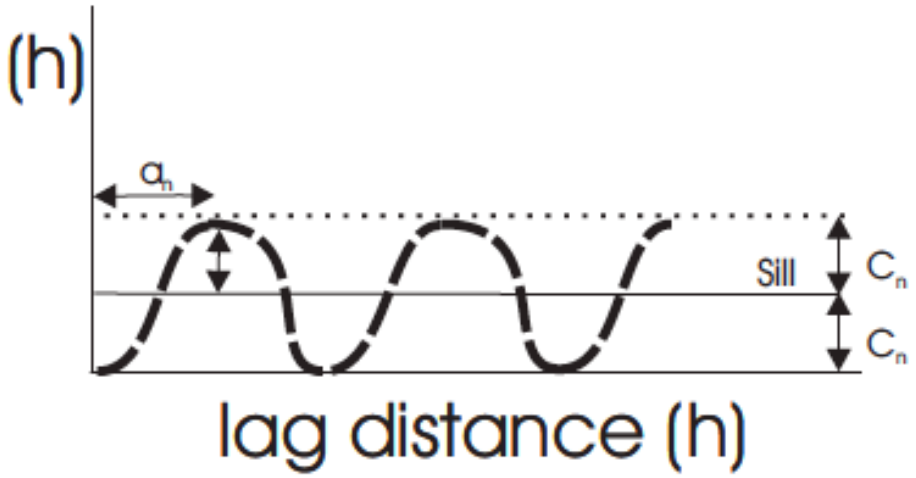

Figure 5.2 Example of a hole effect semi-variogram

With a set of concrete thickness data determined with the NDT, MIRA, the semi-variogram was used as a tool to estimate concrete layer thickness sample spacing. The

premise of using the semi-variogram for sample spacing prediction is that data collected from points close together are likely more similar than data collected from points far apart, so the distance at which samples are no longer correlated is an appropriate time to take a concrete layer thickness measurement.

5.3.2 Autocorrelation Function

The value of autocovariance is difficult to interpret because it is dependent on units. A typical way of standardizing the autocovariance requires dividing by the variation of Z (which is equal to the square of the standard deviation of Z). Standardizing the autocovariance results in a value termed the autocorrelation function, which is a number between ± 1 that measures the linear association (correlation) of the variables being compared.

The autocorrelation function, ρ_k, is defied by:

$$\rho_z = \frac{C_{|t-i|}}{\sigma^2} \tag{5.12}$$

The autocorrelation function is estimated by the sample autocorrelation function, $\hat{\rho}_z(k)$:

$$\hat{\rho}_z(k) = \frac{\hat{C}_z(k)}{\hat{C}_{k=0}} = \frac{\frac{1}{N}\sum_{i=1}^{N-k}(Z_i-\bar{Z})(Z_{i+k}-\bar{Z})}{\frac{1}{N-1}\sum_{i=1}^{N}(Z_i-\bar{Z})^2} \tag{5.13}$$

The autocorrelation function is simply the autocovariance at any lag distance divided by the autocovariance at a lag distance equal to zero.

The autocorrelation function is always 1 when the lag k = 0. When the autocorrelation function becomes zero at some lag, k, the data are no longer related—they are completely independent. In order to eliminate the possibility that autocorrelation in the data is not a random function of white noise, a 95% confidence interval

surrounding the 0 autocorrelation axis is typically shown on plots of autocorrelation function vs. lag and is calculated by

$$\pm \frac{z_{1-\alpha/2}}{\sqrt{N}} \qquad (5.14)$$

with z = value from the standard normal table for a confidence limit, α (Chatfield, 2004). An example of a plotted autocorrelation function is displayed in Figure 5.3

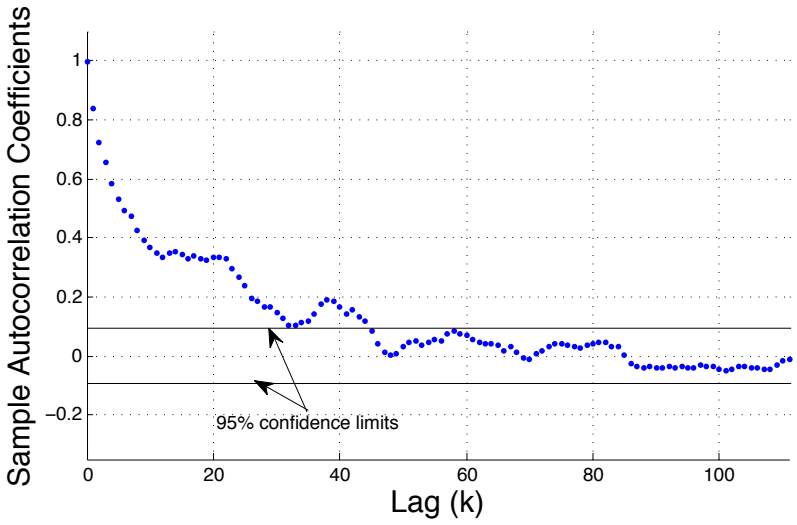

Figure 5.3 Example of a plotted autocorrelation function

The point where the autocorrelation function crosses into the 95% confidence limit range indicates the lag distance where the data series are no longer correlated. This point was used to identify where it was appropriate to take another sample measurement.

5.3.3 Comparison of the Semi-Variogram and the Autocorrelation Function

The basis for the semi-variogram and the autocorrelation function is autocovariance. A plot of the autocorrelation function is theoretically a mirror image of the semi-variogram. The semi-variogram is a measure of dissimilarity and can be thought of as a sum of the data's variance and autocovariance. When the autocovariance

is near zero, the data are no longer correlated. The autocorrelation function is a measure of data similarity. It shows the data's normalized autocovariance. When the autocorrelation function nears zero, the data cease to be correlated. In practice, the trend analysis associated with the semi-variograms was found to reveal non-monotonic behavior than was apparent from the autocorrelation function. It is more convenient to use the autocorrelation function as a correlation input into another model because it does not require the extra step of fitting a model to discrete data points.

5.4 Semi-variogram Range as an Indication of Repetitive Measurement Spacing

Because the semi-variogram is a measure of data correlation, the semi-variogram was used as a tool to evaluate the thickness data collected with the NDT device. It was thought that if many thickness data sets were analyzed with the semi-variogram (many more than were analyzed in this dissertation), users could begin to see a common range of Ranges for concrete pavements with similar characteristics and building climates that could be an indication of an approximate, even possibly universal, sample spacing for repetitive concrete pavement thickness measurements.

5.4.1 Semi-Variogram Assumptions

As noted earlier, for non-idealized semi-variograms, the Range where the semi-variogram reaches the Sill is typically estimated. In these analyses, the data separation lag distance (Range) that corresponded to approximately 95% of the semi-variogram Sill was used to identify the separation distance where the thickness measurements from Hwy 1, Hwy 2, and Hwy 3 were no longer correlated. With only three concrete thickness data sets to evaluate, the Range indicated by 95% of the semi-variogram sill was a reasonable staring point. As more data sets are analyzed, this assumption could change.

As will be demonstrated with the semi-variogram plots of concrete thickness data, actual semi-variogram plots are a series of discrete data points that correspond to lag distances. Typically, the semi-variogram is modeled as a continuous plot. In this chapter's analyses, an exponential model (Chiles, 1999, p. 84) was used to model the semi-variograms.

5.4.2 Semi-variogram Evaluation of the Concrete Layer Thickness Measurements Collected According to Sample Protocol 1 for Hwys 1, 2, and 3

Sample Protocol 1 concrete thickness measurements for Hwys 1, 2, and 3 were incorporated into semi-variogram plots in Figures 5.4, 5.5, and 5.6, respectively. Each semi-variogram plot shows thickness variance vs. separation distance (lag). Table 5.1 tabulates the approximate variance indicated by the semi-variogram Nugget effect, Sill, and Range indicated by Figures 5.4-5.6.

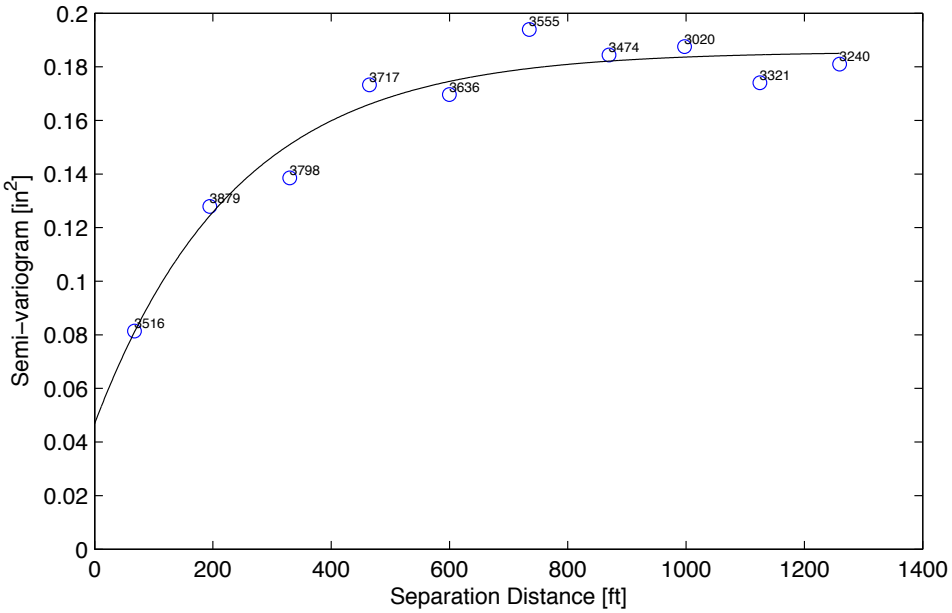

Figure 5.4 Semi-variogram of the Hwy 1 concrete layer thickness data obtained according to Sample Protocol 1. The circles show the experimental semi-variogram, with the associated number of pairs, and the line is the fitted exponential model

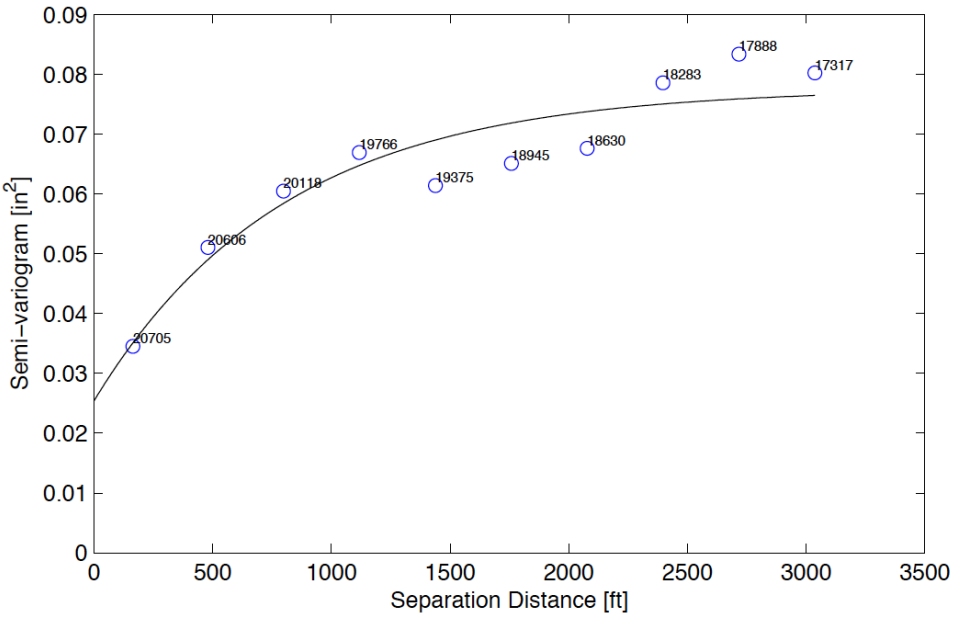

Figure 5.5 Semi-variogram of the Hwy 2 concrete layer thickness data obtained according to Sample Protocol 1. The circles show the experimental semi-variogram, with the associated number of pairs, and the line is the fitted exponential model

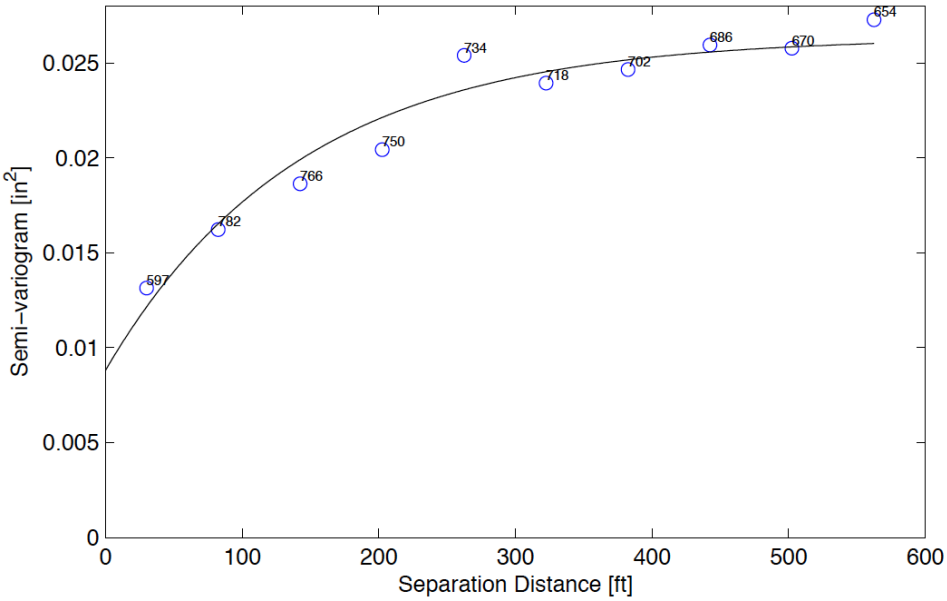

Figure 5.6 Semi-variogram of the Hwy 3 concrete layer thickness data obtained according to Sample Protocol 1. The circles show the experimental semi-variogram, with the associated number of pairs, and the line is the fitted exponential model

Table 5.1 Nugget effect, Sill, and Range indicated by semi-variograms representing concrete layer thickness data obtained according to Sample Protocol 1 from JPCP Hwys 1, 2, and 3

JPCP Hwy	Sample Protocol 1 Semi-variogram	Approximate Nugget (in^2)	Approximate Sill (in^2)	95% of Approximate Sill (in^2)	Range (ft)
1	Figure 5.4	0.05	0.183	0.174	575
2	Figure 5.5	0.026	0.076	0.072	1750
3	Figure 5.6	0.009	0.0252	0.024	250

As indicated by Table 5.1, the Ranges at which the concrete thickness measurements became uncorrelated varied between the three highways by approximately 1,500 feet, an unrealistically large spread, even though the concrete thickness variability was unique for each highway. The Hwy 2 Range was 1750 ft., which is longer than the 1000 ft. maximum thickness sample spacing specified by MN/DOT. The Hwy 3 Range showed the data become uncorrelated in the smallest distance (250 ft.) despite the fact that the Hwy 3 thickness data was the least variable of the three highways. The Nugget effects for the Hwy 2 and Hwy 3 thickness measurements were approximately 1/3 the quantity of the 95% Sill, indicating a large variance of measurement error and spatial variability occurring at length scales less than the sample spacing. These unrealistic results could be an indication that 15 ft. sample spacing was too large, or it could mean that the semi-variogram analysis of these data sets was inconclusive. It is important to note that only three data sets were analyzed, which may or may not be indicative of the semi-variograms of other concrete thickness data that were collected at 15 ft. spacing. Ideally, the semi-variogram would be used to model hundreds of concrete thickness data sets in order to determine if there is a universal (or a few) repetitive measurement spacing that could be used in most situations to measure concrete pavement thickness.

5.4.3 Semi-variograms Representing the Concrete Layer Thickness Measurements Collected According Sample Protocol 2 for Hwys 1, 2, and 3

Sample Protocol 2 concrete thickness measurements obtained from Hwys 1, 2, and 3 were evaluated by semi-variogram plots in Figures 5.7-5.12. There are two semi-variograms for each highway because thickness measurements were taken along two longitudinal locations of the right lane for each pavement. The first semi-variogram for each particular highway evaluates concrete thickness measurements taken 2 ft. from the right lane slab edge, referred to as the edge location, and the second semi-variogram evaluates thicknesses taken 11 ft. from the right lane slab edge, referred to as the center location. Table 5.2 tabulates the approximate variance indicated by the Nugget effect, Sill, and Range illustrated in Figures 5.7-5.12.

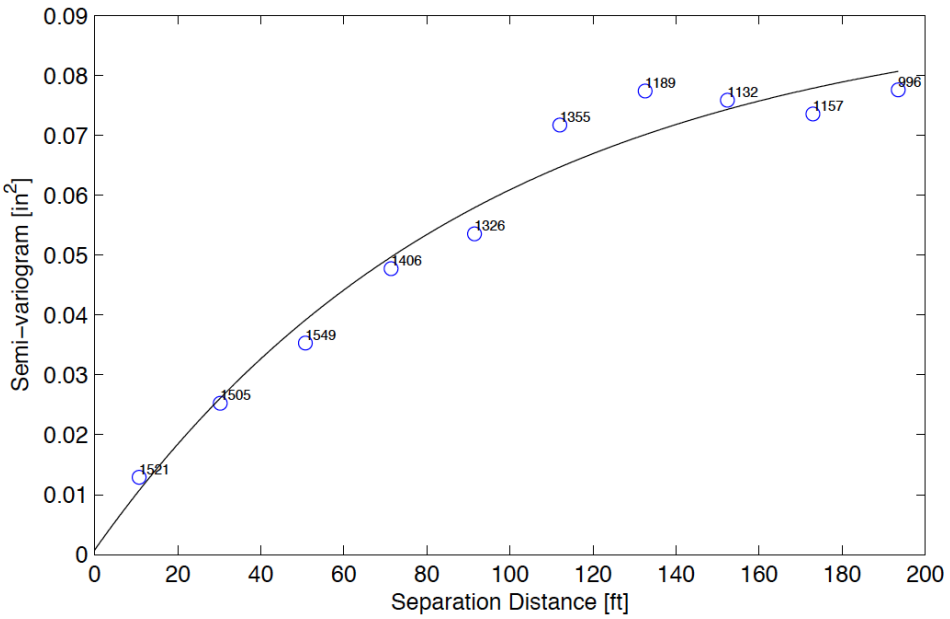

Figure 5.7 Semi-variogram of the Hwy 1 thickness measurements obtained according to Sample Protocol 2 at the edge location. The circles show the experimental semi-variogram, with the associated number of pairs, and the line is the fitted exponential model

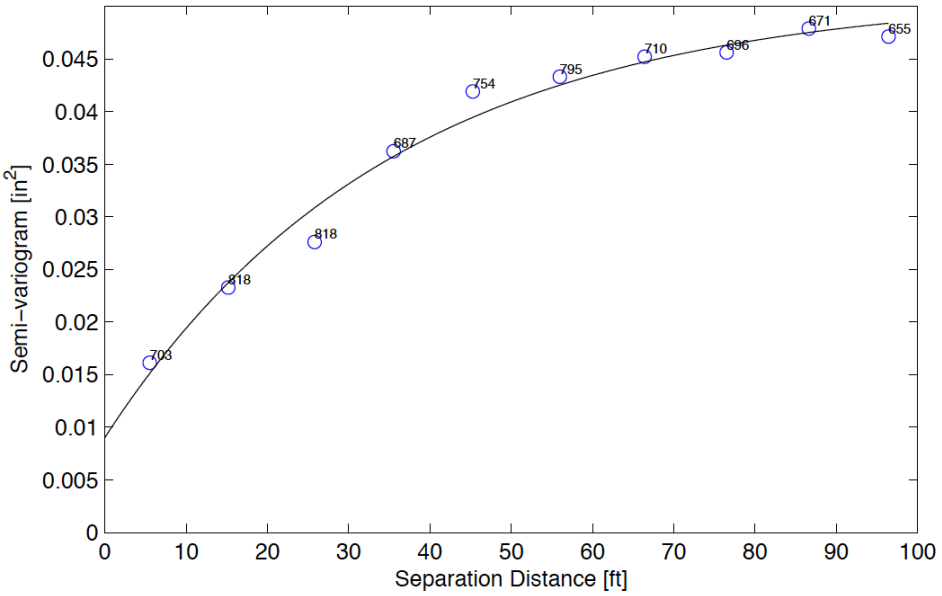

Figure 5.8 Semi-variogram of the Hwy 1 thickness measurements obtained according to Sample Protocol 2 at the center location. The circles show the experimental semi-variogram, with the associated number of pairs, and the line is the fitted exponential model

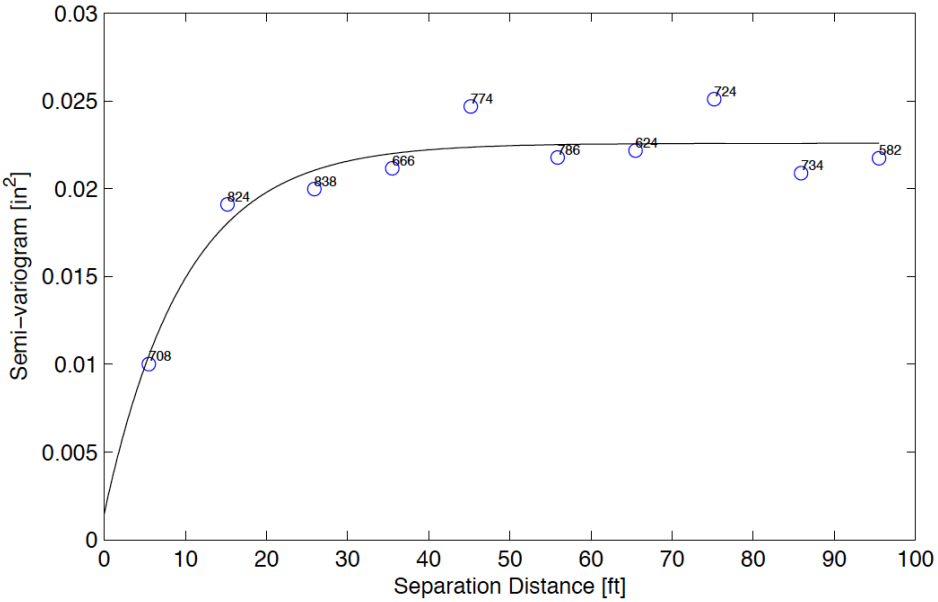

Figure 5.9 Semi-variogram of the Hwy 2 thickness measurements obtained according to Sample Protocol 2 at the edge location. The circles show the experimental semi-variogram, with the associated number of pairs, and the line is the fitted exponential model

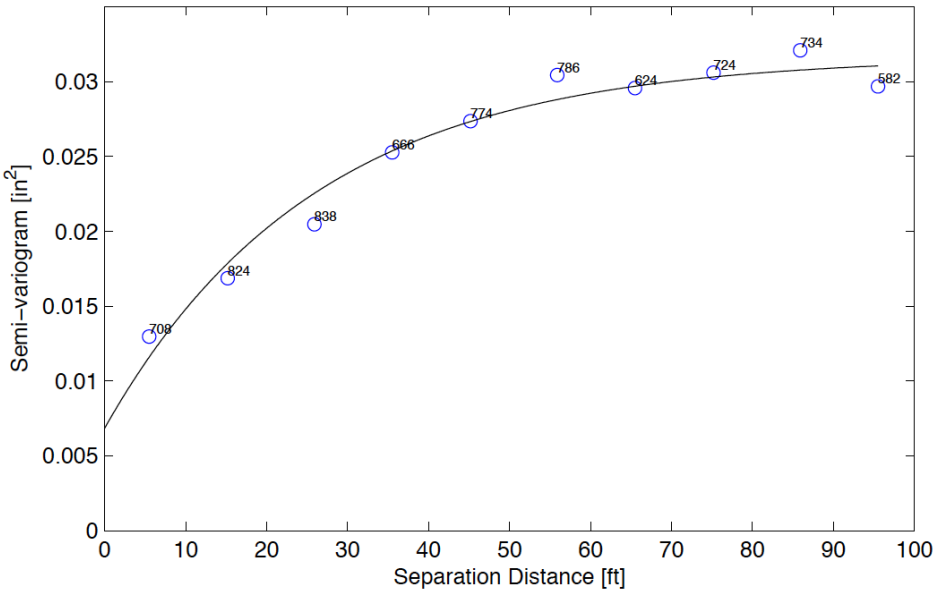

Figure 5.10 Semi-variogram of the Hwy 2 thickness measurements obtained according to Sample Protocol 2 at the center location. The circles show the experimental semi-variogram, with the associated number of pairs, and the line is the fitted exponential model

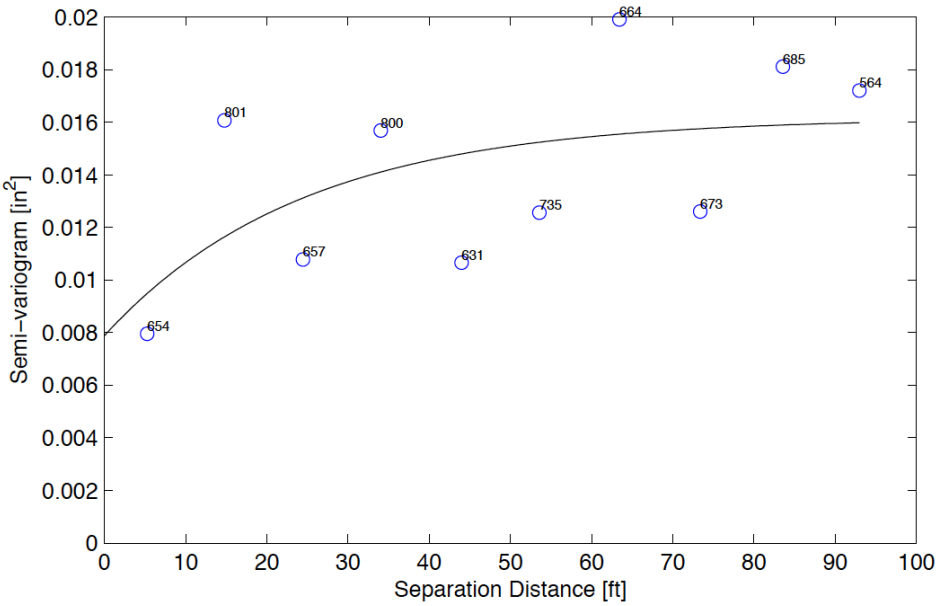

Figure 5.11 Semi-variogram of the Hwy 3 thickness measurements obtained according to Sample Protocol 2 at the edge location. The circles show the experimental semi-variogram, with the associated number of pairs, and the line is the fitted exponential model

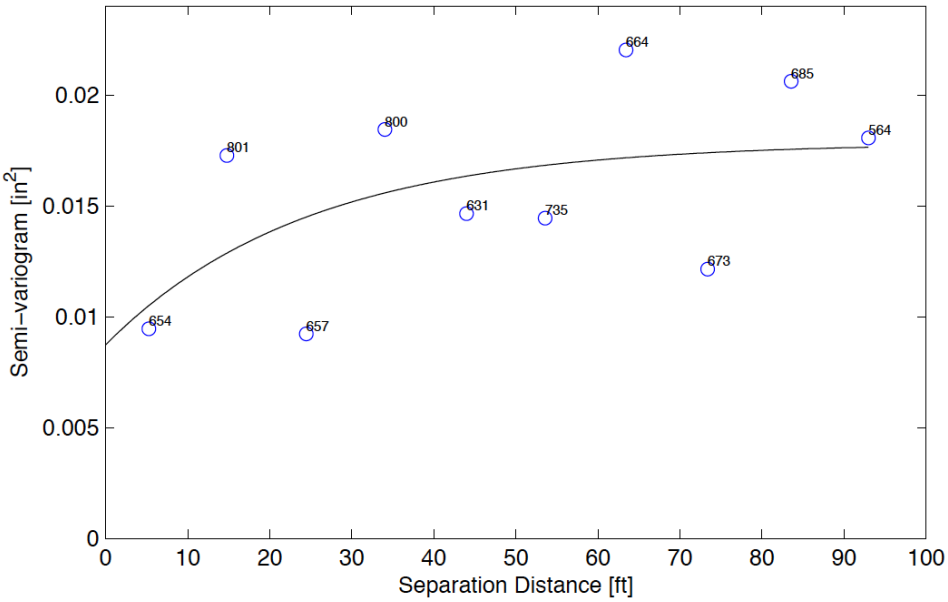

Figure 5.12 Semi-variogram of the Hwy 3 thickness measurements obtained according to Sample Protocol 2 at the edge location. The circles show the experimental semi-variogram, with the associated number of pairs, and the line is the fitted exponential model

Table 5.2 Nugget effect, Sill, and Range indicated by semi-variograms representing concrete layer thickness data obtained according to Sample Protocol 2 in the edge and center locations of Hwys 1, 2, and 3

JPCP Hwy	Sample Protocol 2 Semi-variogram	Location	Approximate Nugget (in^2)	Approximate Sill (in^2)	95% of Approximate Sill (in^2)	Range (ft)
1	Figures 5.7 and 5.8	Center	0.009	0.048	0.046	72
		Edge	0	0.081	0.077	165
2	Figures 5.9 and 5.10	Center	0.007	0.032	0.03	70
		Edge	0.002	0.028	0.027	35
3	Figures 5.11 and 5.12	Center	periodicity			
		Edge	periodicity			

The lengths at which the Sample Protocol 2 thickness measurements became uncorrelated were on the order of tens to hundreds of feet, which is more prudent than hundreds to thousands of feet. The approximate Nugget effects were near zero and not a significant percentage of the 95% Sill. The Ranges indicated by the 95% Sills for the Hwys 1 and 2 thickness measurements near the edge and center of the same lane showed

that the thickness measurements became uncorrelated at different separation lengths. The differences between the lengths when the edge and center measurements became uncorrelated were 90 ft. and 35 ft. for Hwys 1 and 2, respectively even though the edge and center measurements were separated by only 9 ft. This observation reinforces the earlier observation from Chapter 4 that the transverse location of thickness measurements may show very different thickness variation profiles.

Again, with only three data sets to work with, it is unclear from these results if the semi-variogram is a viable tool for determining universal repetitive measurement spacing for concrete pavement thickness measurements. However, with thickness data sets generated with measurements every 2 feet, the semi-variograms indicate realistic lengths at which the data become uncorrelated. To qualify, the semi-variogram Ranges were "realistic" in the sense that repetitive thickness measurements could be taken at tens to hundreds of feet.

It also must be noted that the semi-variograms created for the Hwy 3 thickness measurements at the edge and center locations indicated periodically varying patterns. Periodicity in a semi-variogram is sometimes referred to as the hole effect model (Pyrcz, 2004), which means that the semi-variogram plot displays peaks and valleys in the sill (Figure 5.2). The semi-variogram was not meant to model periodically varying data so an attempt was made to model the Hwy 3 thickness measurements with other models.

5.4.4 Modeling Periodically Varying Concrete Thickness Measurements

The semi-variogram is only meant to model monotonically varying data. Because the Hwy 3 concrete thickness measurements displayed periodicity, other data modeling methods, besides the semi-variogram, were considered for the Hwy 3 concrete thickness measurements. With the semi-variogram model unusable, the end result of modeling the thickness data was modeling the periodicity rather than determining the correlation length. The Fast Fourier Transform and the Autoregression Model of order 1 were the two models considered.

As a first step, a periodic fit of the Hwy 3 thickness measurements was attempted using a Fast Fourier Transform (FFT). Figure 5.13 shows the FFT model and the Hwy 3 thicknesses measured at the center location. Each circle in Figure 5.13 represents a concrete thickness measurement and the solid line represents the FFT model, excluding outliers. It can be seen from Figure 5.13 that the FFT was an ill-fitting model for the Hwy 3 thicknesses measured at the center locations. A similar ill fit was observed for the edge location thickness data. The ill fits suggest that the thickness measurement periodicity was not uniform along the length of the pavement.

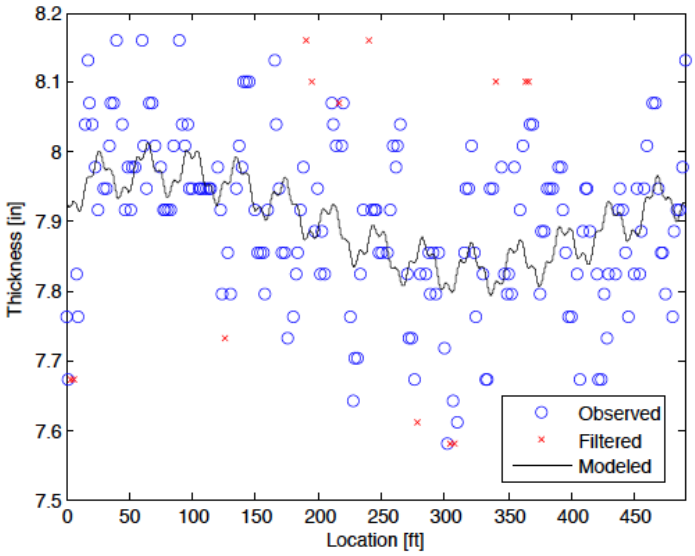

Figure 5.13 Fast Fourier Transform used to model the Hwy 3 concrete thickness data obtained according Sample Protocol 2 near the slab center

Because the FFT could not model the Hwy 3 concrete thickness measurements, an attempt was made to use the autoregressive model of order 1 to model the data. Briefly, the autoregressive model of order 1, AR(1), models the current value of thickness as a linear combination of the preceding value plus a regression residual, which is often referred to as a random shock (Barnes, 2012a). The AR(1) model is defined by:

$$z_t = \phi_1 z_{t-1} + \varepsilon_t \qquad (5.15)$$

where:

z_t = the predicted value of concrete thickness at time or distance, t,

ϕ = the model parameter, and

ε_t = residual term at time or distance, t, called random shocks, which are normally distributed with mean 0 and variance σ_ε^2.

The AR(1) model uses information from right now to predict what is happening in the future and implements the same concepts of autocovariance as the semi-variogram and the auto correlation function. The model parameter, ϕ, is a value less than 1. Smaller

values of ϕ mean that previously predicted values of concrete thickness have less influence on the current values of concrete thickness. Larger values of ϕ mean that previously predicted values of concrete thickness have greater influence on the current values of concrete thickness. Phi is determined by solving Equation 5.15 for ε_t and applying a least-squares objective function and minimizing the function with respect to ϕ.

Figure 5.14 shows an example of an AR(1) fit to the Hwy 3 thickness measurements taken at the center location. In Figure 5.14, "normalized data" refers to the concrete thickness data with the mean subtracted, "model" refers to the AR(1) model, and "random shock" refers to the residual thickness calculated by subtracting the AR(1) thickness from the normalized thickness. The AR(1) model was able to model the Hwy 3 thicknesses measured at both 2 ft. and 11 ft.

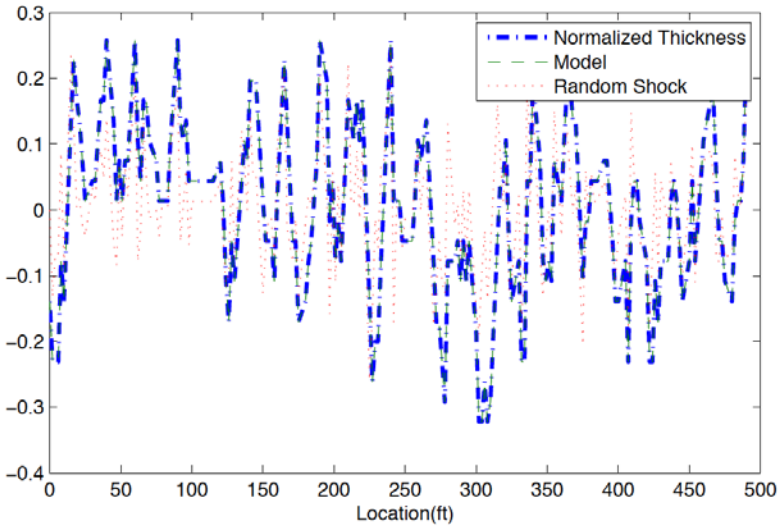

Figure 5.14 Autoregressive model fit of order 1 to the Hwy 3 concrete thickness measurements obtained according to Sample Protocol 2 at the center location

When an AR(1) model successfully models a data set, the random shocks (residuals) will be random with a zero mean. To verify this, the random shocks were

analyzed with a semi-variogram. As an example, Figure 5.15 shows a semi-variogram of the Hwy 3 center location AR(1) residuals. As shown on the semi-variogram, the AR(1) random shocks were horizontal or nearly horizontal which meant that the residuals were not autocorrelated but random and confirmed that the AR(1) model could model the Hwy 3 thickness data.

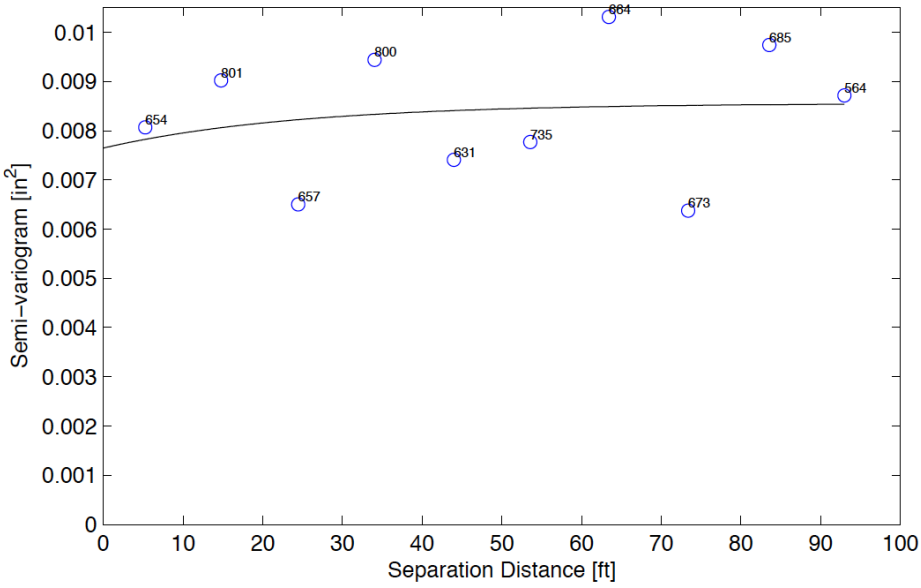

Figure 5.15 Semi-variogram of the Hwy 3, 11 ft. (center) concrete thickness random shocks (residuals) from an AR(1) fit. The circles show the experimental semi-variogram and are accompanied by the associated number of pairs. The line is the fitted exponential model

5.4.5 Summary of Using Semi-variograms to Estimate Sample Spacing

Concrete layer thickness measurements taken at 15 ft. or 2 ft. spacing from three JPCP highways were analyzed with the semi-variogram in order to identify when the data sets became uncorrelated. The semi-variogram Range, the measurement separation distance where the data become uncorrelated, was used as an estimation of repetitive sample spacing. The correlation distances indicated by the semi-variograms for Hwys 1, 2, and 3 thickness measurements collected according to Sample Protocol 1 were not

realistic. The semi-variogram method produced reasonable correlation lengths, and, therefore, sample spacing estimations when applied to the Hwy 1 and 2 thickness measurements collected according to Sample Protocol 2. The discrepancy between the Sample Protocol 1 and Sample Protocol 2 data of when the data series' became uncorrelated suggests that either the semi-variograms are not good predictors of repetitive sample spacing or that there were multiple autocorrelation scales within the thickness variation and that the scale of interest was captured by Sample Protocol 2—which was characterized by more frequent measurements over a shorter length of pavement compared to Sample Protocol 1.

The semi-variogram revealed that the Hwy 3 thickness measurements obtained according to Sample Protocol 2 displayed a periodically varying trend, which required the data to be modeled with a method other than the semi-variogram. When the semi-variogram was deemed unusable, the focus of the modeling switched from determining correlation length to modeling the data. Because of the periodicity, a Fast Fourier Transform was used to model the thickness measurements. This was also unsuccessful because the periodicity was not uniform across the distance measured. The Hwy 3 thickness measurements were successfully modeled with an autoregressive model of order 1.

Using the semi-variogram to estimate concrete thickness measurement spacing was a quick method to use correlation length to roughly estimate sample spacing, but original sample spacing and length of measurement were found to influence the estimated sample spacing so a better sample spacing prediction method is needed. Before a second method of estimating appropriate sample spacing for repetitive measurements is

presented, the next section presents another benefit of plotting a semi-variogram: the semi-variogram can be used to distinguish between reducible and irreducible variance.

5.5 Using the Semi-Variogram to Evaluate Thickness Variance

In addition to showing data correlation, the semi-variogram is a tool to evaluate the reducible and irreducible variance associated with measurement variation. The variance represented by the semi-variogram is made up of two parts:

- Irreducible variance between 0 and the Nugget effect that is due to measurement error and spatial variability that occurs at length scales less than sample spacing variogram
- Variance between the Nugget effect and the Sill, reducible by changing the processes and materials that cause the variance.

The distribution of the semi-variogram variance is depicted on the semi-variogram in Figure 5.16, a copy of Figure 5.4, which shows a semi-variogram of the Hwy 1 concrete layer thickness data obtained according to Sample Protocol 1. Arrows on Figure 5.16 indicate the ranges of the reducible and irreducible variance.

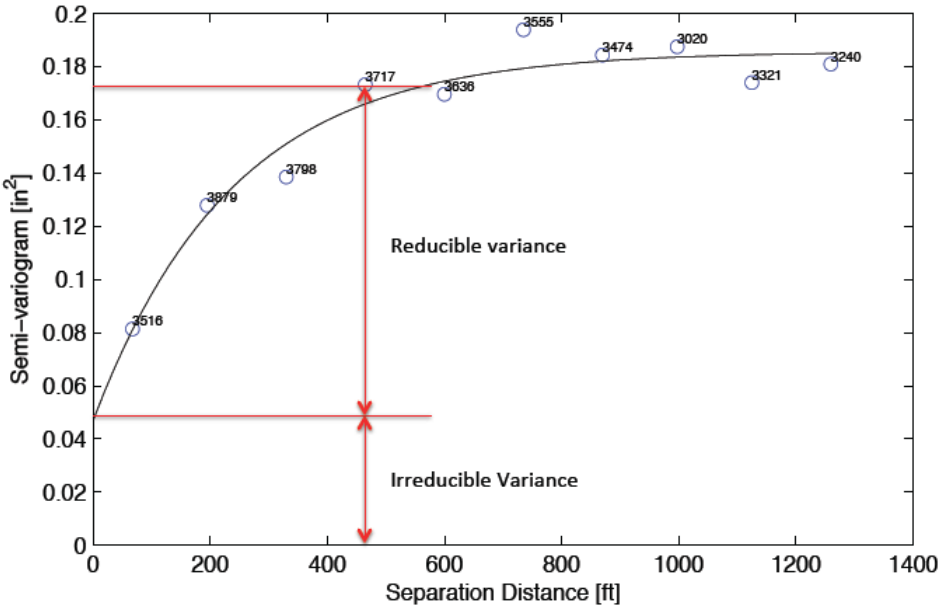

Figure 5.16 semi-variogram of the Hwy 1 concrete layer thickness data obtained according to Sample Protocol 1illustrating the components of reducible and irreducible variance

Identifying the portion of reducible data variance is important because it identifies the potential for decreasing variability. Without this information, the extent of possible variability reduction is unknown. The following example shows how identifying the reducible variance predicts potential cost savings for a pavement contractor or owner.

To begin, assume that the project specifications required 95% of the concrete thickness measurements to be greater than the concrete design depth minus 0.1 in. For a pavement with a designed concrete layer thickness of 9 in., this would require 95% of the thickness measurements to exceed 8.9 in. In order to fulfill this specification, the target in-situ thickness of the concrete layer would have to be greater than the design thickness and would depend on the thickness standard deviation.

The following calculations illustrate how to determine cost savings from reducing thickness measurement variability, assuming that something (i.e. paver technology or construction process) is improved to reduce the reducible variability:

Start with the standard normal z-score equation

$$z = \frac{x-\mu}{\sigma} \qquad (5.16)$$

and rearrange to solve for μ.

$$\mu = x - z\sigma \qquad (5.17)$$

x = minimum allowable thickness target without financial penalty (Design thickness – 0.1 in.)

z = the z-score obtained from the standard normal chart for 95% of the standard normal curve to be above the minimum thickness, x.

σ = square root of 95% sill variance for Sample Protocol 1 thickness measurements (Table 5.1)

μ = target pavement thickness

For this example,

x = 8.9 in.

z = -1.65

σ = 0.42 in.

Given these parameters, the target concrete thickness given the measured thickness variance would be:

$$\mu = 8.9\ in. — (-1.65) * 0.42\ in. = \mathbf{9.59\ in.}$$

Now, consider that the quantity of reducible variance, indicated in Figure 5.16, was halved by improving the paving equipment's performance, and a new target thickness was calculated. The reducible variance was re-calculated by:

1. subtracting the irreducible variance from the 95% Sill variance,

$$0.174\ in^2 - 0.05\ in^2 = \mathbf{0.124\ in^2}$$

2. halving the reducible variance,

$$½ * 0.124\ in^2 = \mathbf{0.062\ in^2}$$

3. adding the irreducible variance to the halved reducible variance to determine the reduced variance

$$0.062\ in^2 + 0.05\ in^2 = \mathbf{0.112\ in^2}.$$

The new standard deviation, σ_{new}, was calculated from the reduced variance

$$\sigma_{new} = \sqrt{0.112\ in^2} = \mathbf{0.33\ in}.$$

The revised target concrete thickness to ensure that 95% of the thickness measurements were above 8.9 in. is

$$\mu_{new} = 8.9\ in. - (-1.65) * 0.33\ in. = \mathbf{9.44\ in}.$$

The difference between the target thickness, determined with the original reducible variance, μ, and the reduced variance, μ_{new}, is

$$\mu - \mu_{new} = 9.59\ in. - 9.44\ in. = \mathbf{0.15\ in}.$$

The monetary savings resulting from decreasing the thickness variance by 0.062 in^2, which resulted in decreasing the target concrete thickness by 0.15 in. is represented by Equation 5.18 and is based on the following assumptions:

- 1 mile of highway was rebuilt with jointed plain concrete pavement.
- 1 yd^3 of concrete cost $45.

- Lane width = 12 ft.

$$5280\ \frac{ft}{mile} * 12\ \frac{ft}{lane} * 0.15\ in. * \frac{1\ ft}{12\ in} * \frac{\$45}{yd^3} * \frac{1\ yd^3}{27\ ft^3} = \frac{\mathbf{\$1{,}340}}{\boldsymbol{lane * mile}} \qquad (5.18)$$

This example illustrates that when the concrete thickness variance was reduced, the target concrete layer thickness required so that 95% of the thickness measurements exceeded 8.9 in. was reduced. This resulted in approximate cost savings of $1,340 per lane per mile in concrete costs.

This concludes analysis of examining concrete thickness data with the semi-variogram. The next section presents a more involved model than the semi-variogram for predicting an universally accepted sample spacing for concrete thickness measurements.

5.6 A Model for Estimating Concrete Thickness Sample Spacing

This section of Chapter 5 presents a model that simulates thousands of concrete thickness data sets using inputs calculated from previously measured thickness data in order to predict the probability that a selected measurement spacing will not result in missing an area of shallow concrete in concrete pavement. The model requires the inputs of mean thickness, standard deviation, and correlation length (determined from the autocorrelation function) that are calculated from concrete thickness measurements similar to those gathered with a NDT device according to Sample Protocol 1 or Sample Protocol 2.

5.6.1 Model Description

The conceptual model is described below. Consider a set of uniformly spaced thickness measurements:

$$(Z_1, Z_2, \cdots Z_n)$$

taken at locations:

$$(x_1, x_2, \cdots x_3).$$

The distance between two adjacent measurements is described by Equation 5.19 and is illustrated in Figure 5.17:

$$S = x_{i+1} - x_i \qquad (5.19)$$

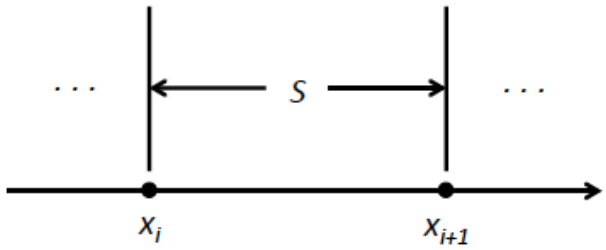

Figure 5.17 S equals the distance between two adjacent measurements

The model calculates the probability of missing an excursion as a function of the sample spacing, S. An excursion is defined as a thickness measurement below a user-specified thickness threshold (τ). If the sample spacing, S, is small, the likelihood of missing an excursion is small. As sample spacing increases, the likelihood of missing an excursion increases.

The statement presented in Equation 5.20 summarizes the function of the model. Consider two adjacent concrete thickness measurements, Z_i and Z_{i+1}, that are both above the thickness threshold, τ. Compute the probability that a thickness measurement taken somewhere between Z_i and Z_{i+1} falls below τ:

$$\Pr\left(min\,[Z(x)] < \tau\right) \mid Z(0) > \tau \; and \; Z(s) > \tau \qquad (5.20)$$

The sample spacing is chosen so that the probability of finding an excursion between sampling points is acceptably small. "Acceptably small" is defined by the user and reflects the risk of finding shallow concrete that the owner is willing to accept.

5.6.2 Model Computations

The model accepts the following arguments:

- Sample spacing, S
- Thickness threshold, τ
- Mean thickness, μ
- Standard deviation, σ
- Correlation length, λ

and returns the probability of finding an excursion between thickness measurements separated by sample spacing, S.

The model, programmed in MATLAB, generates concrete thickness measurements Z(x) with a second-order stationary multivariate random number generator with spatially correlated random variables. The model calls the MATLAB function *mvnrnd* that is assigned an exponential autocorrelation function (Equation 5.21) of the form:

$$Corr\left(Z(x_i), Z(x_j)\right) = \sigma^2 e^{\frac{-|x_i - x_j|}{\lambda}} \qquad (5.21)$$

Each simulated data set must satisfy the condition that the first and the last thickness measurements are above the thickness threshold, τ. When the data set satisfies this condition, it is considered a success and the intermediate points are scanned to determine if an excursion is present. If the data set does not satisfy the end point condition, the data set is discarded. The model simulates data sets until the number of data sets with an excursion reaches a user-defined number (on the order of thousands).

The model returns two outputs. One is the probability of finding an excursion between points that are separated by the sample spacing, S, and is displayed in Equation 5.22.

$$Probability\ of\ finding\ an\ excursion = \hat{p} = \frac{\#\ of\ excursions}{\#\ of\ data\ sets\ (N)} \tag{5.22}$$

The other is the approximate standard error on the probability and displayed in Equation 5.23.

$$stdp = \sqrt{\frac{\hat{p} * (1 - \hat{p})}{N}} \tag{5.23}$$

The MATLAB code language used to program the model can be found in Appendix A.

5.6.3 Using the Model to Evaluate The Probability of Missing a Hidden Excursion Given the Thickness Measurement Parameters from Hwys 1, 2, and 3

This section presents examples of how the model assessed the measurement spacing of Hwy 1, 2, and 3 thickness data sets given the correlation length, average thickness, and thickness standard deviation gleaned from those data sets.

5.6.3.1 Defining Model Input Parameters

In the following examples, concrete thickness measurements from Hwys 1, 2, and 3 taken according to Sample Protocol 1 were used to define the inputs into the model. Table 5.3 summarizes the concrete layer design thickness, threshold value (τ), mean thickness (μ), thickness standard deviation (σ), and autocorrelation length (λ) for use in modeling concrete thickness data with the model. The threshold thicknesses (τ) were

assigned based on the MN/DOT QA/QC contractor compensation table shown again for convenience in Table 5.4 (this table is also located and discussed in the literature review).

Table 5.3 Model inputs aggregated from Hwy 1, 2, and 3 concrete thickness data obtained according to Sample Protocol 1

	Model Input Parameters				
	Design (in)	**τ (in)**	**μ (in)**	**σ (in)**	**λ (ft)**
Hwy 1	9	8.9, 8.8, 8.7, 8.6, 8.5, 8	9.15	0.45	35
Hwy 2	8	7.9, 7.8, 7.7, 7.6, 7.5	8.27	0.34	260
Hwy 3			7.75	0.17	20

Table 5.4 MN/DOT contractor compensation deductions for thickness deficiencies in a section (or fractional section) of concrete pavement

Table 2301-14 Deductions for Thickness Deficiencies	
Thickness Deficiency Exceeding Permissible Deviations, *in [mm]*	**Adjusted contract unit price per sq. yd [sq. m] of Payment**
0.00 – ≤ 0.10 [≤ 3]	None (tolerance)
0.10 – ≤ 0.20 [3 – ≤ 5]	$0.20 [$0.25]
0.20 – ≤ 0.30 [5 – ≤ 8]	$0.40 [$0.50]
0.30 – ≤ 0.40 [8 – ≤ 10]	$0.70 [$0.90]
0.40 – ≤ 0.50 [10 – ≤ 13]	$1.00 [$1.25]
0.50 – ≤ 1.00 [13 – ≤ 25]*	$20.00 [$25.00]
* Perform exploratory coring as required by the Engineer.	

5.6.3.2 Model Results

The model was used to generate probability curves for missing an excursion (thickness deficiency) between sampling points given a range of τ values. Figures 5.18, 5.19, and 5.20 show the probability of finding an excursion in the concrete layer of rigid pavement given the parameters calculated with the Hwy 1, 2, and 3 thickness data, respectively. For sample spacing (S) between 1 ft. and 1000 ft., each plot shows a series of curves that represent the probability of finding a hidden excursion below the thickness thresholds of 0.1, 0.2, 0.3, 0.4, 0.5, and 1 in. below design thickness. Tables 5.5, 5.6, and

5.7 glean the probability of measuring an excursion from plots 5.18, 5.19, and 5.20, respectively, for sampling intervals of 1000, 500, 100, and 15 ft.

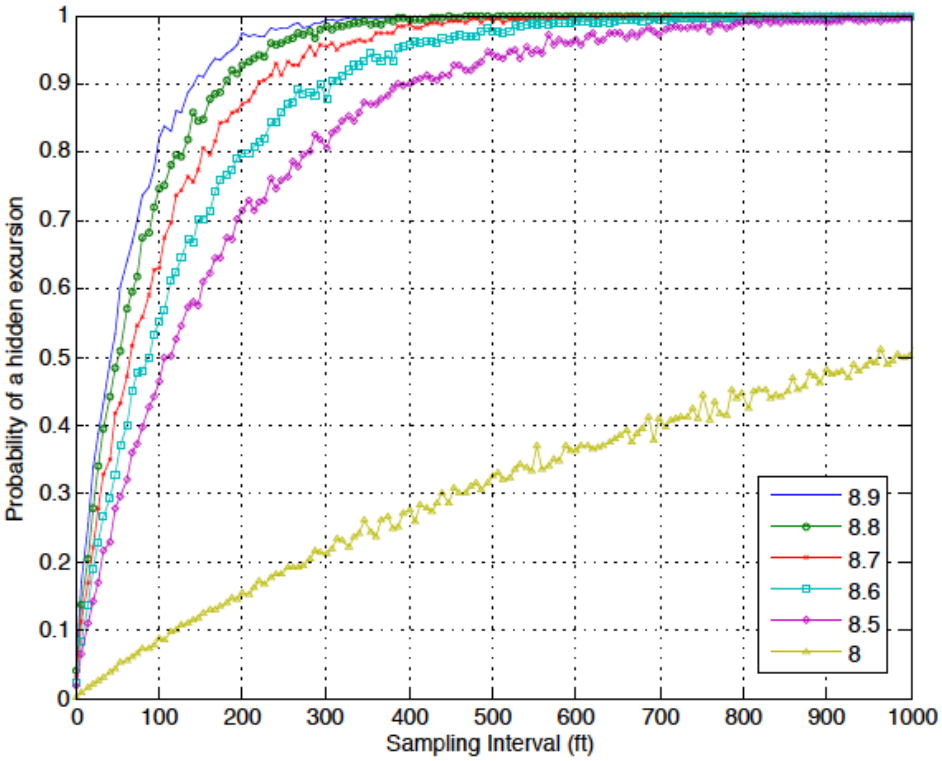

Figure 5.18 Probability of finding a hidden excursion based on the Hwy 1 thickness measurements obtained according to Sample Protocol 1

Table 5.5 Probability of finding a hidden excursion within the Hwy 1 concrete layer for sample spacing of 1000, 500, 100, and 15 ft.

MN/DOT Thickness Deficiency Categories (in)	Thickness Threshold, τ (in.)	Probability of Missing a Hidden Excursion Between Sampling Intervals			
		s=1000 ft	s=500 ft	s=100 ft	s=15 ft
0.00 to ≤ 0.10	8.9	100%	100%	82%	26%
0.10 to ≤ 0.20	8.8	100%	100%	73%	22%
0.20 to ≤ 0.30	8.7	100%	100%	62%	18%
0.30 to ≤ 0.40	8.6	100%	97%	54%	14%
0.40 to ≤ 0.50	8.5	100%	94%	46%	11%
0.50 to ≤ 1.00	8.0	50%	37%	8%	2%

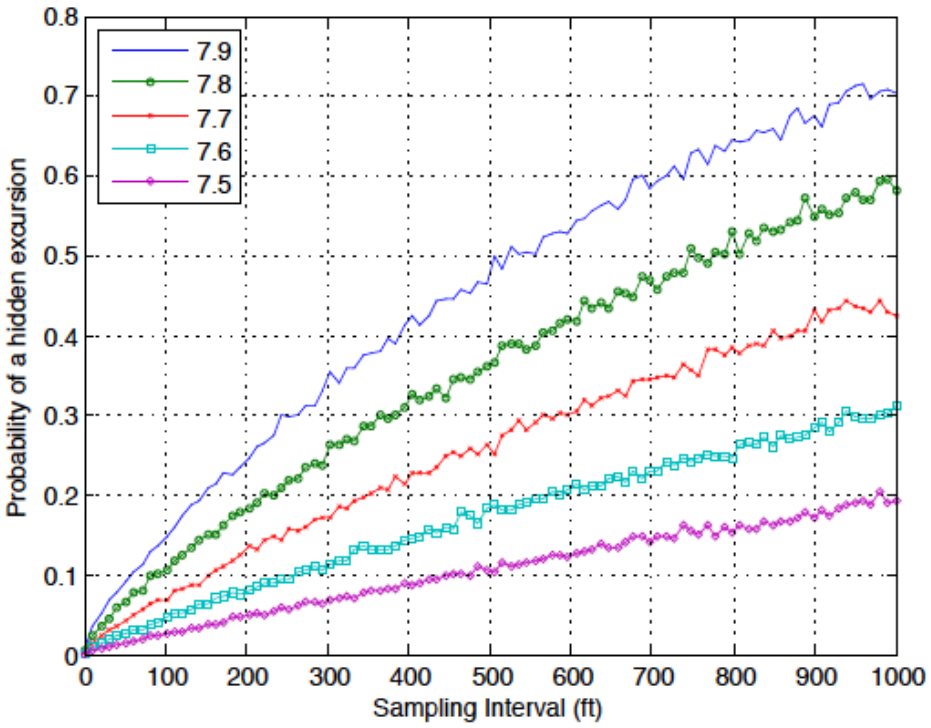

Figure 5.19 Probability of finding a hidden excursion based on the Hwy 2 thickness measurements obtained according to Sample Protocol 1

Table 5.6 Probability of finding a hidden excursion within the Hwy 2 concrete layer for sample spacing of 1000, 500, 100, and 15 ft.

MN/DOT Thickness Deficiency Categories (in)	Thickness Threshold, τ (in.)	Probability of Missing a Hidden Excursion Between Sampling Intervals			
		s=1000 ft	s=500 ft	s=100 ft	s=15 ft
0.00 to ≤ 0.10	7.9	70%	59%	15%	4%
0.10 to ≤ 0.20	7.8	58%	35%	11%	3%
0.20 to ≤ 0.30	7.7	44%	25%	7.3%	2%
0.30 to ≤ 0.40	7.6	30%	20%	4.4%	1.2%
0.40 to ≤ 0.50	7.5	20%	10%	2.6%	0.8%
0.50 to ≤ 1.00	7.0	≈ 0%	≈ 0%	≈ 0%	≈ 0%

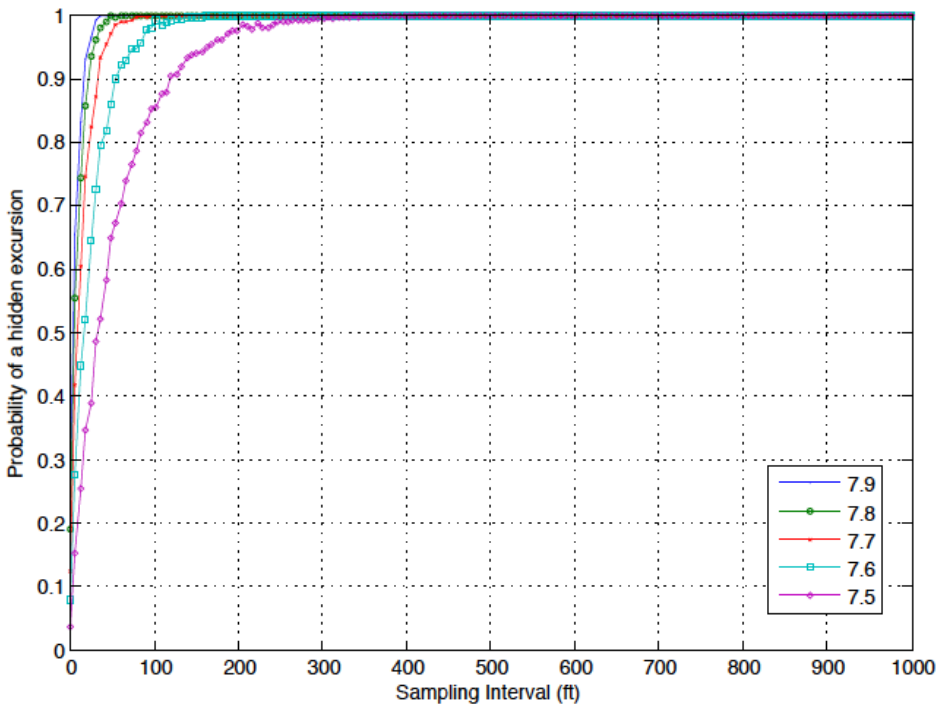

Figure 5.20 Probability of finding a hidden excursion based on the Hwy 3 thickness measurements obtained according to Sample Protocol 1

Table 5.7 Probability of finding a hidden excursion within the Hwy 3 concrete layer for sample spacing of 1000, 500, 100, and 15 ft.

MN/DOT Thickness Deficiency Categories (in)	Thickness Threshold, τ (in.)	Probability of Missing a Hidden Excursion Between Sampling Intervals			
		s=1000 ft	s=500 ft	s=100 ft	s=15 ft
0.00 to ≤ 0.10	7.9	100%	100%	100%	85%
0.10 to ≤ 0.20	7.8	100%	100%	100%	78%
0.20 to ≤ 0.30	7.7	100%	100%	100%	64%
0.30 to ≤ 0.40	7.6	100%	100%	98%	46%
0.40 to ≤ 0.50	7.5	100%	100%	85%	25%
0.50 to ≤ 1.00	7.0	≈ 0%	≈ 0%	≈ 0%	≈ 0%

In general, the following observations are true of each of the plots in Figures 5.18, 5.19, and 5.20. As the thickness threshold (τ) increases (i.e. from 8.9 to 8.8 in.), the probability of missing an excursion decreases. Also, as the sample spacing (S) increases, the probability of missing an excursion increases. It is important to note that Figures 5.19 and 5.20 do not show a curve for a threshold value of 1 in. below the design

thickness because the probability of an excursion less than or equal to 1 in. below the design thickness was almost zero.

Considering 1000 ft. sample spacing (the typical measurement spacing when cores are drilled in concrete pavements to verify thickness) and considering the Hwy 1 concrete thickness data inputs into the model, Table 5.5 indicates that there was a 100% chance of missing an excursion less than 8.9 through 8.5 in. and a 50% chance of missing an excursion less than 8.0 in. Considering the Hwy 2 concrete thickness data statistics, Table 5.6 indicates that at 1000 ft. sample spacing the probability of missing an excursion less than 7.9 in. was 70% and less than 0.5 in. was 20%. At 1000 ft. sample spacing and considering the Hwy 3 concrete thickness data statistics, Table 5.7 indicates that, there was a 100% chance of missing an excursion less than 7.9 through 7.5 in.

Considering a 500 ft. sample spacing, the probability of measuring an excursion using the Hwys 1 and 3 concrete thickness data statistics did not significantly improve from the 1000 ft. sample spacing. Considering 100 ft. sample spacing and Hwys 1 and 3 concrete thickness data statistics, there was a 46% probability of missing an excursion less than 8.5 in. and an 85% chance of missing an excursion of less than 7.5 in., respectively. Even at 15 ft. sample spacing, the probability of missing an excursion greater than 0.5 in. below the design thickness did not fall below 11% and 25% for Hwys 1 and 3, respectively.

For a sampling interval of 500 ft. and given the Hwy 2 concrete thickness data statistics, there was a 59% probability of missing an excursion less than 7.9 in. and a 10% chance of missing an excursion less than 7.5 in. At a sample spacing of 100 ft. and given the Hwy 2 data statistics, the probability of missing an excursion less than 7.9 in. was

15%. At a sample spacing of 15 ft., the probability of missing an excursion less than 7.9 in. was 4%.

5.6.4 Model Summary

A model was presented that simulates concrete thickness measurements between sampling points to determine the probability of measuring concrete thickness below some thickness threshold between sampling points. If the probability of missing shallow concrete between the sampling points is sufficiently low, then the sample spacing is adequate. If the probability of missing shallow concrete between sampling points is high, then the sample spacing is reduced and more data sets are generated. The user chooses the probability of missing shallow concrete that is commensurate with the risk they are willing to accept of having shallow concrete.

Statistics gleaned from three highway thickness data sets were used as inputs into the model to explore the model's output, but it is expected that hundreds of thickness data sets would be used to find a measurement spacing that would be either universally acceptable or a measurement spacing(s) that takes into account local design and construction variability and risk tolerance. Potentially, the model would be able to identify sample spacing requirements based on construction and environmental circumstances such as base material, contractor, or paver manufacturer.

Comparing the probabilities of missing a hidden excursion below any threshold, four factors contributed to lower probabilities: smaller sample spacing, a lower thickness standard deviation, a higher mean thickness, and a longer correlation length.

The model clearly shows that 1000 ft. and 500 ft. sample spacing are too broad to adequately capture concrete thickness variation within concrete pavements. Tying this

into MN/DOT's QA/QC protocol, if a core measurement at 1000 ft. sample spacing did measure a thickness deficiency, there would be a 100% chance that an equal or greater thickness deficiency would occur between the current core and the next core. As the sample spacing decreases from 500 ft., the chances of missing a thickness deficiency decrease, but not significantly until the sample spacing enters the 15 ft. range. With non-destructive testing equipment and software that automates the processing of the NDT measurements, this sort of sample spacing is realistic from a cost standpoint and it would not jeopardize the structure of the pavement because the measurement process is non-destructive.

5.7 Conclusion

This chapter presented two methods for estimating appropriate measurement spacing for repetitive measurements along a distance or for an amount of time. Concrete thickness measurements were the data used to introduce these methodologies. Non-destructive testing (NDT) devices that measure concrete thickness are able to take measurements at small sampling intervals for a relatively small cost and effort. The reason that measurement spacing was investigated is that it may not be necessary to take measurements at the smallest possible sampling interval to accurately characterize the variability of repetitive measurements.

The first method used semi-variograms of concrete layer thickness measurements to indicate when thickness data were no longer correlated. The measurement separation distance indicated at 95% of the semi-variogram Sill was assumed to approximate suitable concrete thickness sample spacing. The semi-variogram predicted reasonable concrete thickness sample spacing for thicknesses measured every 2 ft. (Sample Protocol

2) but produced unreasonable sample spacing estimates for thicknesses measured every 15 ft. (Sample Protocol 1). With only six data sets to study, the semi-variogram method appeared to be influenced by data correlations that can occur on more than one length scale, and may not be a consistent method for estimating repetitive sample spacing. The semi-variogram method also identified non-monotonic thickness data patterns that were not necessarily evident from looking at the plotted data. In this instance, an AR(1) model was found to model the periodicity of the Hwy 3 data. The semi-variogram was also used to distinguish between reducible and irreducible variance.

Secondly, a model was created to estimate the probability of finding a concrete thickness deficiency (excursion) below a thickness threshold within a sampling interval. The model was based on the premise that the probability of finding an excursion is less when measurements are taken closer together than when they are taken farther apart. The model simulated concrete thickness measurements given the mean, standard deviation, and autocorrelation length determined from previously measured concrete thickness data sets. The simulation assumed second order stationarity and an exponential autocorrelation function.

The model confirmed that the range of in-situ concrete thickness variability cannot be verified if sample spacing is once every 1000 ft., which is the standard measurement spacing used by the Minnesota Department of Transportation when core samples are drilled from the pavement to verify concrete thickness. Depending on the thickness data statistics used as inputs into the model, the model suggested that 15 ft. to 100 ft. would be appropriate concrete thickness measurement sample spacing. With NDT

devices that are commercially available, this measurement spacing is both feasible and cost effective.

This model only considered the statistics from three data sets as inputs into the model. Ideally, the mean, standard deviation, and autocorrelation lengths from hundreds of concrete pavements would be measured with a reliable NDT device and would be used with this model to explore the probabilities of missing shallow concrete given a particular set of construction circumstances.

6 RELIABILITY IN CONCRETE PAVEMENT DESIGN AND ANALYSIS

6.1 Introduction

The Mechanistic Empirical Pavement Design Guide (MEPDG) is used for the design of new and rehabilitated jointed plain concrete pavements (JPCP). One of the primary applications of the MEPDG is that it makes probabilistic predictions of transverse cracking distresses in JPCPs in order to evaluate the pavement's design characteristics. The MEPDG predicts distresses as probabilistic variables because there is uncertainty associated with the distress models, the inputs into the model, and the techniques used to calibrate the model, among other reasons (ARA, Inc., 2003b). The MEPDG's pavement design process, distress prediction models, and reliability analysis are explained in detail in Chapter 2.

The reliability analysis of MEPDG's distress predictions is limited because the reliability analysis cannot account for individual sources of uncertainty such as traffic load, climatic conditions, concrete material properties, JPCP layer thickness, and expected pavement life. Rather, the MEPDG characterizes predicted distress uncertainty as a lump sum. This is problematic because even when the cause of the uncertainty can be measured and reduced, the benefit of reducing the uncertainty cannot be accounted for in the MEPDG's analysis or design of pavement. This chapter presents a methodology that demonstrates how individual sources of uncertainty can be accounted for in the MEPDG cracking distress reliability analysis using concrete pavement thickness and modulus of rupture variation as examples. These properties were considered because thickness and MR are measureable quantities and because thickness is one of the primary properties that affects transverse cracking in JPCP.

6.2 Concrete Thickness and MR Data

The concrete layer thickness and flexural strength distributions considered in this study were collected from Hwy 2 according to sample Protocol 1. The concrete layer thickness data and thickness data collection methods are presented in Chapter 4. The Minnesota Department of Transportation (MN/DOT) supplied the results of 49 flexural stress beam tests, known as modulus of rupture (MR) tests, for this study. MR was measured by testing 6 in. x 6 in. x 20 in. concrete beams according to the three point bending procedure at one of MN/DOT's material testing labs. The mean MR was 640 psi and the MR standard deviation was 63 psi. Figure 6.1 displays the cumulative distribution of the measured MR values. The MR measurements were collected on a JPCP that was constructed at the same time and in the same part of the state and with the same materials and concrete mixture design as Hwy 2.

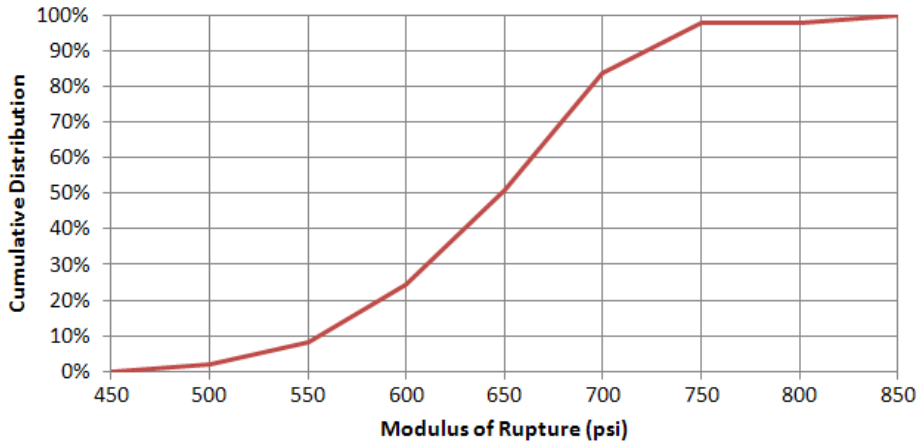

Figure 6.1 Cumulative distribution of the measured MR used to characterize the MR variability of the Hwy 2 pavement.

6.3 MEPDG Predicted Transverse Cracking Distress and Cracking Reliability Equations

The JPCP predicted distress investigated in this study was transverse cracking. The MEPDG transverse cracking prediction equations (Equations 2.3-2.5 in the literature review) predict the mean percent of slabs with transverse cracks for a given pavement. The MEPDG assumes that the predicted mean percent of slabs with transverse cracks is predicted with 50% reliability (p = 0.50). The MEPDG reliability equations (Equation 2.6 and 2.7 reproduced here for clarity as Equations 6.1 and 6.2) adjust the predicted transverse cracking percentage ($CRACK_p$) to the desired level of reliability.

The MEPDG reliability equation is a function of the percent of transverse cracking at 50% reliability ($CRACK_{mean}$) and a standard deviation term (STD_{all}). The Equation for standard deviation (Equation 6.2) is calibrated with field data that represents uncertainty in cracking prediction due to all causes.

$$CRACK_p = CRACK_{mean} + STD_{all} * Z_p \quad (6.1)$$

$$STD_{all} = -0.00198 * CRACK_{mean}^2 + 0.56875 * CRACK_{mean} + 2.76825 \quad (6.2)$$

Cumulative distribution curves of cracking prediction reliability (reliability curves) are obtained using Equations 6.1 and 6.2 for multiple probabilities given a mean predicted cracking and plotting the predicted percentage of transverse cracked slabs vs. reliability of prediction.

6.4 Transverse Cracking Reliability Curves

Two types of transverse cracking cumulative distribution curves were considered in this study. The first type was obtained from the MEPDG analysis described in section 6.3. The second type was obtained from the distribution of the MEPDG mean cracking

prediction by varying MEPDG characteristics such as concrete thickness and flexural strength. Both types of transverse cracking curves were created considering Highway 2 characteristics in the analyses.

To develop Type 1 transverse cracking cumulative distribution curves, the first step is to determine the MEPDG predicted cracking at 50% reliability. The predicted transverse cracking at 50% reliability ($CRACK_{mean}$) will reflect the MEPDG inputs of the Hwy 2 design, traffic loads of 2500 and 7500 AADTT, measured mean Hwy 2 thickness, and measured mean MR. The mean Hwy 2 measured thickness was 8.3 in. and the mean measured MR was 640 psi. A list of all MPEDG inputs can be found in Appendix B. The resulting $CRACK_{mean}$ was 0.3% for 2500 AADTT and 3.6% for 7500 AADTT. Next, $CRACK_{mean}$ was used in Equations 6.1 and 6.2 to produce the predicted cracking reliability curves for between 50% and 99% reliability. The predicted cracking reliability curves representing all sources of uncertainty in transverse cracking predictions are shown in Figures 6.2 and 6.3 (long dashes) for traffic levels of 2500 and 7500 AADTT, respectively.

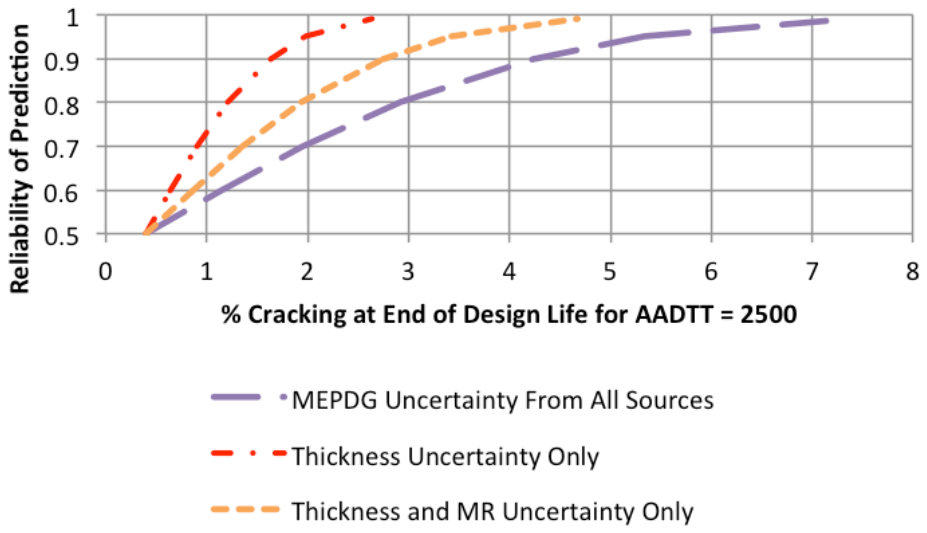

Figure 6.2 Predicted transverse cracking reliability curves for AADTT = 2500

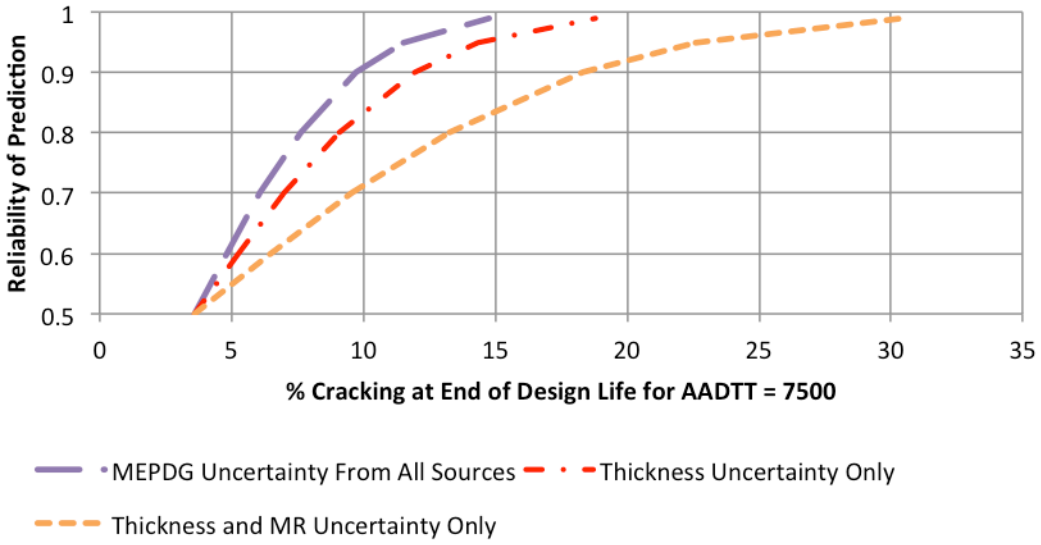

Figure 6.3 Predicted transverse cracking reliability curves for AADTT = 7500

Two-Type 2 transverse cracking cumulative distribution curves were created for each level of traffic (2500 and 7500 AADTT). The first Type 2 curve reflected the uncertainty caused only by measured thickness distribution, and the second Type 2 curve reflected the uncertainty caused by both measured thickness and MR distribution.

To analyze the effect of concrete thickness on predicted transverse cracking, MEPDG simulations for Hwy 2 pavements were conducted for concrete layer thicknesses from 6.3 in. to 9.5 in in 0.1 in increments. This range of thicknesses represents the range of thicknesses measured in the Hwy 2 pavement. The predicted transverse cracking response at 50% reliability was recorded for each concrete thickness. The resulting cracking predictions were assembled into a reliability distribution curve. A detailed procedure of converting the measured thickness variability into a predicted reliability curve is described in Appendix B. The predicted transverse cracking reliability curves that reflect only the uncertainty due to measured thickness variation are shown in Figures 6.2 and 6.3 (dash-dot) for AADTTs of 2500 and 7500, respectively.

Next, the effect of the measured variability of both thickness and modulus of rupture (MR) on the cracking reliability curve was analyzed. The MR measurements were assumed normally distributed and the normal distribution curve was divided into quintiles. The mean of each quintile was designated as a MR that was used as an input into the MEPDG. The mean MRs were 585, 624, 650, 676, and 714 psi. With these MR values, the process described to convert measured thickness variability into predicted cracking reliability curves was repeated with each MR value for AADTT = 2500 and AADTT = 7500. This procedure resulted in five cracking reliability curves for each level of truck traffic. The five individual reliability curves were combined into one reliability curve that reflected the uncertainty of transverse cracking prediction caused by the measured variation of both concrete thickness and MR. These curves are depicted in Figures 6.2 and 6.3 (short dashes) for traffic levels of 2500 and 7500 AADTT, respectively.

To create a reliability curve that allowed for known uncertainty, it was assumed that Equation 6.3 (Navidi, 2011) could be used to determine the standard deviation term, σ_R, that represented the distribution of concrete cracking prediction due to concrete thickness and MR distribution:

$$\sigma_R = \sqrt{\sigma_T^2 - \sigma_C^2} \quad (6.3)$$

Where

- σ_T is the value of STD calculated from Equation 6.2 that was used to calculate the reliability curve that represents all uncertainty
- σ_C is the value of STD used to calculate the reliability curve that represents uncertainty from concrete thickness and MR variation only
- σ_R is the value of STD used to calculate the transverse cracking reliability curve uncertainty due to remaining sources.

Once σ_R was determined, it was used as the STD term in Equation 6.1 along with the predicted percent of transverse cracking at 50% reliability ($CRACK_{mean}$), which was assumed to be the same as that predicted for the Type 1 transverse cracking reliability curve using mean thickness and mean MR, to create a new transverse cracking reliability curve. This reliability curve represents transverse cracking prediction uncertainty due to all sources except measured thickness and MR distribution. The curve is pictured in Figure 6.4 (individual small dots), which also includes the curves from Figure 6.2.

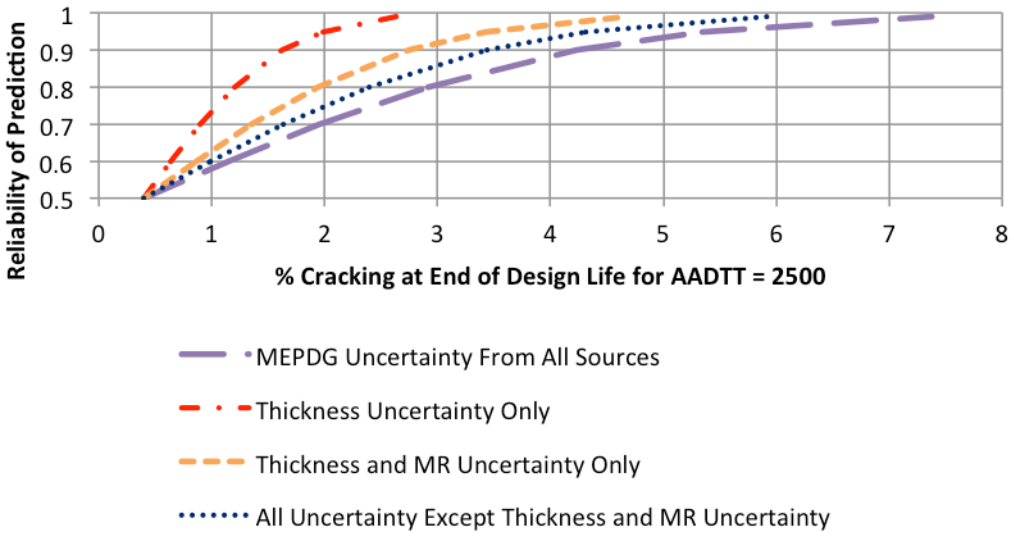

Figure 6.4 Predicted transverse cracking reliability curves for AADTT = 2500

An attempt to perform this same analysis for the traffic level of AADTT = 7500 was not successful because the curve indicated more cracking due to only concrete thickness and flexural strength distribution at a given reliability than was predicted due to all uncertainty. This is not a realistic scenario. The reasons for this scenario are not clear without further investigation, but there are some items to consider.

- Some of the highest truck traffic seen on Minnesota state highways is 2500 AADTT. 7500 AADTT far exceeds this level.
- When the MEPDG cracking equations were calibrated, it was assumed that the design concrete thickness and MR values (and all pavement properties used as inputs into the MPEDG) were the mean values. Given the extent of the thickness variation in the concrete layer of JPCPs highlighted by this dissertation, it is clear that the design concrete thickness is not often the mean thickness. This implies that the MEPDG transverse cracking equations, calibrated to produce the percent of cracked slabs with 50% certainty, may produce cracking levels that reflect a

certainty other than 50%. This means that the definition of MEPDG concrete thickness and stress inputs should be reconsidered.

6.5 Conclusion

It is important to quantify how variability in pavement properties contributes to predicted distress uncertainties in JPCPs because, currently, there lacks incentive to decrease variability of pavement properties. In this chapter, a methodology was presented to account for uncertainty in the MEPDG transverse cracking reliability curve due to measureable thickness and MR variation. This was facilitated by developments in non-destructive testing technology that allow the accurate, rapid, and low-cost measurement of concrete thickness variation. This methodology could be expanded to other pavement characteristics once technology advances and more physical and material concrete properties can be non-destructively and/or more accurately determined. Knowing the variability of rigid pavement components, understanding how that variability affects the long-term performance of pavements, and accounting for that variability in pavement analysis will lead to solutions for decreasing the variability, which will increase the quality of rigid pavements.

CHAPTER 7: SUMMARY AND CONCLUSIONS

Pavement performance prediction must account for uncertainties in pavement characteristics, future climate, traffic loading, etc. Past research identified that two pavement characteristics significantly affected cracking in Jointed Plain Concrete Pavements (JPCP), and these characteristics—concrete thickness and flexural strength—significantly vary along the pavement. This dissertation concentrated on quantifying the effect of concrete thickness and, to a lesser extent, flexural strength variability on JPCP performance.

The possibility of using non-destructive testing to assess thickness was evaluated, and it was found that ultrasound tomography is a reliable method for measuring concrete thickness with a high level of productivity and accuracy. A comparison of the non-destructive testing (NDT) device data and core data showed good agreement between thickness measurements. A significant body of thickness data was collected from three recently constructed typical JPCPs. It was found that JPCP concrete layer thickness can significantly vary (up to 3 in.) along a pavement that was several miles in length. It was also shown that concrete layer thickness sample spacing on the order of 1000 ft., which is a typical spacing used by state highway departments for core spacing, does not capture the extent of concrete layer thickness variability.

It was found that thickness varies significantly in the direction perpendicular to traffic (transverse direction). Considering that critical concrete stresses occur at the slab edge or right wheel path, it is desirable to measure thickness near the slab edge or wheel path, which is a highly undesirable location for core samples. These findings imply that with current pavement construction techniques and quality control methods, in some

locations, the deficiency of concrete thickness may cause premature pavement failure. At the same time, an excess of concrete thickness over design thickness in other locations causes unnecessary material consumption. Therefore, an improvement of quantification of concrete layer thickness variability as well as its effect on future performance is an important task.

Significant efforts in this study were dedicated to quantification of the variability of constructed pavement thickness and determination of requirements for thickness sampling spacing. A semi-variogram approach was used to find the minimum distance between thickness measurements that could define concrete thickness distribution in any pavement based on data correlation. This distance can be used in some cases as recommended sample spacing for thickness variability assessments in the future. In addition, a model was created to estimate the probability of finding a concrete layer thickness deficiency within a sampling interval. The model simulated thickness measurement sets that assumed second order stationarity and an exponential autocorrelation function. Application of this model to thickness measurements for pavements evaluated in this study demonstrated that compliance with thickness requirements cannot be ensured with high confidence if sample spacing is 1000 ft., a sample spacing used by many state highway departments for measuring thickness of core samples. Thickness sample spacing on the order of 15 ft. to 100 ft. produced reasonable confidence in measuring thickness variability.

Finally, the reliability analysis of JPCP cracking prediction in the Mechanistic-Empirical Pavement Design Guide (MEPDG) has been reconsidered. The MEPDG recognizes uncertainty in the transverse cracking prediction models due to variability of

design inputs and model error. However, the MEPDG reliability analysis cannot account for the degree of variability of individual input parameters because it does not separate the sources of uncertainty. The current reliability analysis does not allow the MEPDG to quantify the effect of improved material characterization prior to design or the affect of quality control on pavement performance. In this study, the effect of variability of concrete thickness and flexural strength was separated from the overall uncertainty in cracking prediction. This will potentially lead to a reduction in design thickness if a more stringent quality control is ensured. At the same time, it was shown that the definition of some MEPDG design inputs may need to be reconsidered. Currently, the MEPDG recommends providing mean concrete thickness and flexural strength for performance prediction, but it might be appropriate to replace them with thickness and strength at a certain level of confidence.

REFERENCES

1. Achenbach, J. D. (1973). *Wave Propagation in Elastic Solids.* Amsterdam: Elsevier Science.
2. Acoustic Control Systems. (2010). *Acoustic Control Systems.* Retrieved 12 29, 2012, from Ultra Low-Frequency Tomograph A104 MIRA Operation Manual: http://downloads.acsys.ru/eng/Documents/
3. Acoustic Control Systems. (n.d.). *Tomographic Systems*. (Acoustic Control Systems) Retrieved 12 29a, 2012, from Acoustic Control Systems: http://acsys.ru/eng/production/?type_id=16&subtype_id=7&product_id=23
4. ACPA. (1997, June 13). *American Concrete Pavement Association.* Retrieved November 25, 2012, from ACPA Position Paper on Methods of Strength Testing for Concrete Pavement Acceptance: www.pavement.com/Downloads/strength_position.pdf
5. ACPA. (2008, January 1). *TS204.1P: Uniform Support in Concrete Pavement Structures.* Retrieved November 21, 2012, from ACPA Technical Series Downloads for Subgrades and Subbases for Concrete Pavements: http://www.pavement.com/Concrete_Pavement/Technical/Downloads/TSs.asp
6. Allison, G. W., Whited, G. C., Hanna, A. S., & Nasief, H. G. (2010). Evaluation of Probing Versus Coring for Determination of Portland Cement Concrete Pavement Thickness. *Transportation Research Record: Journal of the Transportation Research Board, No. 2152* , 3-10.

7. Al-Qadi, I. L., Lahouar, S., Jiang, K., McGhee, K. K., & Mokarem, D. (2005). Accuracy of Ground-Penetrating Radar for Estimatng Rigid and Flexible Pavement Layer Thicknesses. *Transportation Research Record , 1940*, 69-78.
8. ARA, Inc. ERES Consultant Division. (2004a). *Guide for Mechanistic-Empirical Design of New and Rehabilitated Pavement Structures Part 3 Design Analysis Chapter 4: design of New and Reconstructed Rigid Pavments.* Washington, D. C.: NCHRP.
9. ARA, Inc., ERES Consultants Division. (2004b). *Guide for Mechanistic-Empirical Design of New and Rehabilitated Pavement Structures Part 2 Design Inputs Chapter 2 Material Characterization.* Washington, D.C.: NCHRP.
10. ARA, Inc., ERES Division. (2003a). *Guide for Mechanistic-Empirical Design of New and Rehabilitated Pavement Structures Final Document Apendix KK: Transerse Cracking of JPCP.* Washington, D.C.: NCHRP.
11. ARA, Inc., ERES Division. (2003b). *Guide for Mechanistic-Empirical Design of New and Rehabilitated Pavement Structures Final Document Appendix BB: Design Reliability.* Washington, D.C: NCHRP.
12. ARA. Inc., ERES Consultant Division. (2004c). *Guide for Mechanistic-Empirical Design of New and Rehabilitated Pavmeent Structures Part 2. Design Inputs Chapter 4. Traffic.* Washington, D.C.: NCHRP.
13. Barnes, R. (2012a, April 3). "Autoregressive Models" class notes. Minneapolis, MN.
14. Barnes, R. (2012b, May 3). "Variogram" class notes. Minneapolis, MN.

15. Bohling, G. (2005, October 17). *Introduction to Geostatistics and Variogram Analysis.* Retrieved April 25, 2013, from people.ku.edu/~gbohling/cpe940/Variograms.pdf
16. Carino, N. J. (2001). The Impact-Echo Method: An Overview. In P. Chang (Ed.), *Proceedings of the 2001 Structures Congress & Exposition* (p. 18). Reston, Virginia: American Society of Civil Engineers.
17. Centrangolo, G., & Popovics, J. (2010). Inspection of Concrete Using Air-Coupled Ultrasonic Pulse Velocity. *ACI Materials Journal , 107* (2), 155-163.
18. Chatfield, C. (2004). *The Analysis of Time Series, An Introduction, 6th Ed.* Boca Raton, FL: Chapman & Hall/CRC.
19. Chiles, J.-P. a. (1999). *Geostatistics Modeling Spacial Uncertainty.* New York, NY: John Wiley & Sons, Inc.
20. Darter, M. I., Khazanovich, L., Yu, T., & Mallela, J. (2005). Reliability Analyais of Cracking and Faulting Prediction in the New Mechanistic-Empirical Pavement Design Procedure. *Transportation Research Record: Journal of the Trnasportation Research Board , 1936*, 150-160.
21. Edwards, L., & Mason, Q. (2011). *Evaluation of Nondestructive Methods for Determining Pavement Thickness.* US Army Corps of Engineers, Engineer Research and Development Center . Viksburg, MS: Geotechnical and Structures Laboratory.
22. FHWA. (2000). *Ground Penetrating Radar for Measuring Pavement Layer Thickness.* Federal Highway Administration, Office of Asset Management. FHWA.

23. FHWA. (2009, August). *TechBrief: Determination of Concrete Pavement Thickness Nondestructively Using the Magnetic Imaging Tomography Technique.* Retrieved December 23, 2012, from U.S. Department of Transportation Federal Highway Administration: http://www.fhwa.dot.gov/pavement/concrete/pubs/hif09023/index.cfm

24. Graff, K. F. (1991). *Wave Motion in Elastic Solids.* Mineola, NY: Dover.

25. Hoegh, K., & Khazanovich, L. (2012). Correlation Analysis of 2D Tomographic Images for Flaw Detection in Pavements. *Journal of Testing and Evaluation , 40* (2), 247-255.

26. Hoegh, K., Khazanovich, L., & Yu, T. (2011). Ultrasonic Tomography Technique for Evaluation of Concrete Pavements. *Transportation Research Board 90th Annual Meeting Compendium of Papers DVD. 11-1644.* Washington, D.C.: Transportation Research Board.

27. Holzschuher, C., Lee, H. S., & Greene, J. (2007). *Accuracy and Repeatability of Ground Penetrating Radar for Surface Layer Thickness Estimation of Florida Roadways.* State of Florida DOT, State Materials Office. FL/DOT.

28. Huang, Q., Gardoni, P., & Hurlebaus, S. (2011). Predicting Concrete Compressive Strength Using Ultrasonic Pulse Velocity and Rebound Number. *ACI Materials Journal , 108* (4), 403-412.

29. Jeong, J.-H., Zollinger, D. G., Lim, J.-S., & Park, J.-Y. (2012). Age and Moisture Effects on Thermal Expansion of Concrete Pavement Slabs. *Journal of Materials in Civil Engineering , 24* (1), 8-15.

30. Jiang, Y., Selezneva, O. I., & Mladenovic, G. (2002). *Researcher's Guide ot the Long-Term Pavement Performance Layer Thickness Data.* Applied Research Associates, Inc., ERES Division. McLean, VA: FHWA.

31. Jiang, Y., Selezneva, O., Mladenovic, G., Aref, S., & Darter, M. (2003). Estimation of Pavement Layer Thickness Variability for Reliabiltiy-Based Design. *Transportation Research Record 1849 , 03-2886*, 156-165.

32. Khazanovich, L. (2003). *Guide for Mechanisitic-Empirical Design of New and Rehabilitated Pavement Structures Appendix JJ: Transverse Joint Faulting Model.* National Cooperative Highway Research Program. Washington D.C.: NCHRP.

33. Khazanovich, L. (1994). *Structural Analysis of Multi-Layered Concrete Pavement Systems.* University of Illinois, Champaign-Urbana, Civil Engineering. University of Illinois, Champaign-Urbana.

34. Khazanovich, L., Darter, M. I., Bartlett, R., & McPeak, T. (1998). *Common Characteristics of Good and Poorly performing PCC Pavements.* ERES Consultants, Inc. McLean, VA: Federal Highway Administration Office of Engineering Research and Development.

35. Khazanovich, L., Yu, T. H., Rao, S., Galasova, K., Shats, E., & Jones, R. (2000). *ISLAB2000-Finite Elment Analysis Program for Rigid and Composite Pavements.* Champaign, IL: ERES Division of ARA, Inc.

36. Kim, J. R., Titus-Glover, L., Darter, M. I., & Kumapley, R. K. (1999). Axle Load Distribution Characterization for Mechanistic Pavement Design. *Transportation Research Record: Journal of the Transportation Research Board , 1629*, 13-23.

37. Kosmatka, S. H., & Wilson, M. L. (2011). *Design and Control of Concrete Mixtures 15th Ed.* Skokie, IL: Portland Cement Association.

38. Krautkramer, J., & Krautkramer, H. (1990). *Ultrasonic Testing of Materials, 4th ed.* (4th ed.). New York, NY: Springer-Verlag.

39. Larson, G., & Dempsey, B. J. (1997). *Enhanced Integrated Climatic Model Version 2.0.* Urbana, IL: University of Illinois at Urbana-Champaign.

40. Lee, J.-S., Nguyen, C., & Scullion, T. (2002). *Development of a Prototype High-Frequency Ground-Penetrating Radar System.* Texas Transportation Institute. Austin, TX: FHWA and TxDOT.

41. Liang, M. T., & Wu, J. (2002). Theoretical eludication on the empirical formulae for the ultrasonic testing method for concrete structures. *Cement and Concrete Research , 32*, 1763-1769.

42. Mallela, J., Titus-Glover, L., Ayers, M. E., & Wilson, T. P. (2001). Characterization of Mechanical Properties and Variability of PCC Materials for Rigid Pavement Design. *7th International Conference on Concrete Pavements.* Orlando, FL.

43. Mindess, S., Young, J. F., & Darwin, D. (2003). *Concrete 2nd Ed.* Upper Saddle River, NJ: Pearson Education, Inc.

44. Minnesota Department of Transportation. (2005). Standard Specifications for Construction, 2005 Ed. St. Paul, MN: Minnesota Department of Transportation.

45. Morian, D. A. (2010). *Precision Statement for ASTM C-78, Flexural Testing, Airfield Concrete.* Innovative Pavement Research Foundation , Programs Management Office. Skokie, IL: IPRF.

46. Nam, B. H., Scullion, T., Stokoe II, K. H., & Lee, J.-S. (2011). Rehabilitation Assessment of Jointed Concrete Pavement Using the Rolling Dynamic Deflectometer and Ground Penetrating Radar. *Journal of Testing and Evaluation , 39* (3), 1-12.

47. Nasief, H. G., Whited, G. C., & Loh, W.-Y. (2011). Wisconsin Method for Probing Portland Cement Concrete Pavement for Thickness. *Transportation Research Record: Journal of the Tranportation Research Board, No 2228* , 99-107.

48. Navidi, W. (2011). *Statistics for Engineers and Scientists, 3rd Ed.* New York, NY: McGraw Hill.

49. Nazarian, S., Yuan, D., & Medichetti, A. (2003). Optimizing Opening of Portland Cement Concrete Pavements Using Integrated Maturity and Nondestructive Tests. *Transportation Research Record , 1861*, 3-9.

50. Nazarian, S., Yuan, S., Smith, D., Ansari, K., & Gonzalez, C. (2006). *Acceptance Criteria of Airfield Concrete Pavement using Seismic and Maturity Concepts: Appendix A.* Innovative Pavement Research Foundation, Programs Management OFfice. Skokie, IL: IPRF.

51. Pavement Interactive. (2007a, August 15). *Jointed Plain Concrete Pavement*. Retrieved November 23, 2012, from Pavement Interactive: http://www.pavementinteractive.org/article/jointed-plain-concrete-pavement/

52. Pavement Interactive. (2007b, August 16). *Tie Bars*. Retrieved May 8, 2013, from Pavement Interactive: http://www.pavementinteractive.org/article/tie-bars/

53. Pyrcz, M. J. (2004). *Geostatistical Association of Austrailia.* Retrieved March 12, 2013, from http://www.gaa.org.au/

54. Rao, S., & Roesler, J. (2005). Characterizing Effective Built-In Curling from Pavement Field Measurements. *Journal of Transportation Engineering , 131* (4), 320-327.

55. Sansalone, M. (1997). Impact-Echo: The Complete Story. *ACI Structural Journal, 94* (6), 777-786.

56. Schubert, F., Wiggenhauser, H., & Lausch, R. (2004). On the accuracy of thickness measurements in impact-echo testing of finite concrete specimens--numerical and experimental results. *Ultrasonics , 42*, 897-901.

57. Trtnik, G., Kavcic, F., & Turk, G. (2009). Prediction of concrete strength using ultrasonic pulse velocity and neural networks. *Ultrasonics , 49*, 53-60.

58. Yu, H. T., Khazanovich, L., Darter, M., & Ardani, A. (1998). Analysis of concrete Pavement Responses to Temperature and Wheel Loads Measured from Instrumentd Slabs. *Transportation Research Record: Journal of the Transportation Research Board , 1639*, 94-101.

59. Yu, T., & Darter, M. I. (2003). *Guide for Mechanistic-Empirical Design of New and Rehabilitated Pavement Structures Appendix KK: Transverse Cracking of JPCP.* National Cooperative Highway Research Program. Washington, D.C.: NCHRP.

60. Zhu, J., & Popovics, J. (2005). Non-contact imaging for surface-opening cracks in concrete with air-coupled sensors. *Materials and Structures , 38*, 801-806.

Appendix A: MATLAB Code for Estimating Sample Spacing

```
function [phat, stdp] = gaazo( s, tau, mu, sigma, lambda )

%-------------------------------------------------------------------------
% usage: [phat, stdp] = gaazo( s, tau, mu, sigma, lambda )
%
%   Compute the approximate probability of at least one undiscovered excursion below the threshold (tau) over a
%   sampling interval of length (s).
%
% arguments:
%   s         sampling interval [ft].
%
%   tau       thickness threshold [in].
%
%   mu        thickness mean [in].
%
%   sigma     standard deviation [in].
%
%   lambda    correlation length [ft].
%
% returns:
%   phat      the estimated probability,
%
%                 Pr( min[T(x)] < tau | T(0) > tau AND T(S) > tau )
%
%             where the "min" is computed over the interval 0 < x < S.
%
%   stdp      the approximate standard error of the estimated probability.
%
% notes:
%   o   This code models the T(x) as a second-order stationary Gaussian random process, with mean mu, standard
%       deviation sigma, and correlation length lambda.
%
%   o   This code uses an exponential autocorrelation function of the form
%
%       Corr(T(x_i), T(x_j)) = sigma^2 * exp( -|x_i - x_j| / lambda )
%
%   o   We use a brute force stochastic simulation (Monte Carlo) approach to compute (estimate) the probability.  This
%       is a computationally intense process.
%
%   o   The simulation is repeated until at least M excursions are found.
%       Some sensitivity testing on M is needed.
%
%   o   The minimum over the sampling interval is approximated by checking at a finite number of points N. Some
%       sensitivity testing on N is needed.
%
%   o   This function can be reworked in a standardized form using the
%       -   scaled sampling interval [s/lambda], and the
%       -   normalized threshold [(tau-mu)/sigma].
%
%   o   The name "gaazo" is the Ojibwe word for the verb "to hide".  This seemed appropriate since we are looking for
%       hidden excursions.
%
% written by:
%   Dr. Randal J. Barnes
%   Mary Vancura
%   Department of Civil Engineering
%   University of Minnesota
%
% version:
%  14 December 2012 (made the units correct and consisent)
%   6 September 2012
%-------------------------------------------------------------------------
```

```
% Manifest constants.
M = 1000;   % minimum number of excursions to be found.
N = 100;    % number of points in the sampling interval.
C = 100;  % number cases per random number generation.

% Check the arguments.
if( s < eps )
    error( 'The sampling interval s must be positive.' );
end

if( sigma < eps )
    error( 'The standard deviation sigma must be positive.' );
end

if( lambda < eps )
    error( 'The correlation length must be positive.' );
end

% Initialize.
X = linspace(0,s,N);
Mu = mu * ones(1,N);              % mean vector for thickness [in]
Sigma = nan(N,N);                 % autocovariance matrix [in^2]

for i = 1:N
    for j = 1:N
        Sigma(i,j) = sigma^2 * exp( -abs( X(i)-X(j) ) / lambda );
    end
end

% Repeat the stochastic simulation until there are at least M excursions.  In the following computations there are
% three counts of importance.
%
% Trials: count of the number of simulated sampling intervals.
%
% Successes: count of the number of simulated sampling intervals that satisfy the end points condition:
%
% ( T(0) > tau AND T(S) > tau )
%
% Excursions: count of the number of simulated sampling intervals that contain a hidden excursion below tau.
% That is,
%
% ( min[T(x)] < tau AND T(0) > tau AND T(S) > tau )

Trials      = 0;
Successes   = 0;
Excursions = 0;

while( Excursions < M )
    T = mvnrnd(Mu, Sigma, C);    % Realization vector of thicknesses [in]
    Trials = Trials + C;

    for k = 1:C
        if( T(k,1)>tau && T(k,end)>tau )
            Successes = Successes + 1;

            if( min(T(k,:))<tau )
                Excursions = Excursions + 1;
            end

        end

    end
```

```
        if Trials > M*10000;
            warning('Too many trials.Terminating before finding %d excursions.', M);
            break;
        end

    end

    % Compute the approximate probability, and the approximate standard
    % error for the estimate.

    phat = Excursions / Successes;

    stdp = sqrt( phat * (1-phat) / Successes );

end
```

Appendix B: Steps for Determining a Transverse Cracking Reliability Curve That Represents the Cracking Uncertainty Caused by Measured Variations of Thickness and MR

Step 1: Determining % of Cracked Slabs for Each Possible Measured Concrete Thickness and MR Value for AADTT = 2500 and 7500.

The range of concrete thickness measurements for the Hwy 2 pavement was 7.2 to 9.0 in. The MEPDG was used to analyze the Hwy 2 pavement for a range of thicknesses from 7.2 to 9.0 in. in 0.1 in. increments for MR values 585, 624, 650, 676, and 714 psi, and traffic levels equal to 2500 and 7500 AADTT. The following list summarizes MEPDG inputs, which were based on the Hwy 2 rigid pavement design and measured quantities including the pavement layer thicknesses, concrete mixture design, and laboratory tests performed on samples of hardened concrete. If a particular input was not listed, it remained as the MEPDG default value.

- Jointed plain concrete pavement (JPCP)
- Design life = 20 years
- Minneapolis/St. Paul International Airport climate file
- Design Traffic = Variable (AADTT)
- Concrete Thickness = Variable (in.)
- Joint spacing = 15 ft.
- Widened slab = 13.5 ft.
- Subgrade = A-6 material
- Base = 8 in. crushed granular material
- Unit weight of concrete = 145 pcf

- Poisson Ratio of concrete = 0.20
- Cementitious material = 550 lb/yd^3
- Water-to-cement ratio = 0.35
- Aggregate type = limestone
- MR = Variable (psi)

The result of each MEPDG run was the percent of slabs cracked at the end of the pavement's design life at 50% reliability for a given thickness, MR, and traffic level. Tables B.1, B.2, B.3, B.4, and B.5 show these cracking levels for MR values equal to 585, 624, 650, 676, and 714 psi, respectively. Each of the following tables represents one MR value. In each of the tables, the first column shows the possible concrete layer thickness measurements for the Hwy 2 rigid pavement. The second column shows the percent of cracked slabs for 750 AADTT, the third column shows the percent of cracked slabs for 2500 AADTT, and the fourth column shows the percent of cracked slabs for 7500 AADTT.

Table B.1 Percent of slabs cracked with 50% reliability for the stated range of pavement thickness and traffic values with MR = 585 psi.

Concrete Thickness (in)	% Cracking at End of Design Life for MR = 585 psi	
	AADTT	
	2500	7500
7.2	23.4	73
7.3	18.7	67
7.4	15.1	61.8
7.5	11.8	54.1
7.6	9.4	47.7
7.7	7.2	40.8
7.8	5.4	33.5
7.9	5.3	33.3
8.0	4	27.1
8.1	2.9	21
8.2	2.1	16.3
8.3	1.5	12
8.4	1.1	9.1
8.5	0.8	6.8
8.6	0.6	4.9
8.7	0.4	3.7
8.8	0.4	3.4
8.9	0.3	2.5
9.0	0.2	1.8

Table B.2 Percent of slabs cracked with 50% reliability for the stated range of pavement thickness and traffic values with MR = 614 psi.

Concrete Thickness (in)	% Cracking at End of Design Life for MR = 614 psi	
	AADTT	
	2500	7500
7.2	12.6	55.9
7.3	9.6	48.4
7.4	7.5	41.5
7.5	5.7	34.7
7.6	4.4	29.8
7.7	3.3	23
7.8	2.4	17.7
7.9	2.4	17.5
8.0	1.7	13
8.1	1.2	9.5
8.2	0.8	7
8.3	0.6	5.2
8.4	0.4	3.8
8.5	0.3	2.7
8.6	0.2	1.9
8.7	0.2	1.4
8.8	0.1	1.3
8.9	0.1	0.9
9.0	0.1	0.7

Table B.3 Percent of slabs cracked with 50% reliability for the stated range of pavement thickness and traffic values with MR = 650 psi.

Concrete Thickness (in)	% Cracking at End of Design Life for MR = 650 psi	
	AADTT	
	2500	7500
7.2	8	43.5
7.3	6	36.1
7.4	4.6	29.8
7.5	3.4	23.8
7.6	2.6	19.3
7.7	1.9	14.8
7.8	1.4	11
7.9	1.3	10.4
8.0	0.9	7.8
8.1	0.7	5.5
8.2	0.5	4
8.3	0.3	2.9
8.4	0.2	2.1
8.5	0.2	1.5
8.6	0.1	1
8.7	0.1	0.7
8.8	0.1	0.7
8.9	0.1	0.5
9.0	0	0.3

Table B.4 Percent of slabs cracked with 50% reliability for the stated range of pavement thickness and traffic values with MR = 676 psi.

Concrete Thickness (in)	% Cracking at End of Design Life for MR = 676 psi	
	AADTT	
	2500	7500
7.2	5.1	32.1
7.3	3.7	25.5
7.4	2.8	20.3
7.5	2.1	15.7
7.6	1.6	12.4
7.7	1.1	9.2
7.8	0.8	6.7
7.9	0.8	6.5
8.0	0.6	4.8
8.1	0.4	3.2
8.2	0.3	2.3
8.3	0.2	1.6
8.4	0.1	1.1
8.5	0.1	0.8
8.6	0.1	0.6
8.7	0.1	0.4
8.8	0	0.3
8.9	0	0.3
9.0	0	0.2

Table B.5 Percent of slabs cracked with 50% reliability for the stated range of pavement thickness and traffic values with MR = 714 psi.

Concrete Thickness (in)	% Cracking at End of Design Life for MR = 714 psi	
	AADTT	
	2500	7500
7.2	17.4	18.8
7.3	1.9	14.9
7.4	1.4	10.9
7.5	1.1	8.6
7.6	0.8	6.2
7.7	0.6	4.6
7.8	0.4	3.2
7.9	0.4	3.1
8.0	0.3	2.2
8.1	0.2	1.4
8.2	0.1	1
8.3	0.1	0.7
8.4	0.1	0.5
8.5	0	0.3
8.6	0	0.2
8.7	0	0.2
8.8	0	0.1
8.9	0	0.1
9.0	0	0.1

Step 2: Mapping the Measured Thickness Values to % Cracking for Each MR and Traffic Input.

Using the tables established in Step 1, each Hwy 2 concrete layer thickness measurement was correlated to a percent of slabs cracked at 50% reliability for each MR and traffic input level. Table B.6 illustrates this process for 30 of the 1032 thickness measurements for AADTT = 2500 and 7500 and MR = 650 psi. Column 1 of Table B.6 shows the sample of 30 concrete thickness measurements obtained from the Hwy 2 rigid pavement. Column 2 shows the predicted transverse cracking percentage at 50% reliability for AADTT = 2500 for the concrete thickness listed in column 1. Column 3 shows the predicted transverse cracking percentage at 50% reliability for AADTT = 7500 for the concrete thickness listed in column 1.

Table B.6 Example of mapping concrete thickness to % of cracked slabs for each traffic level and MR = 650 psi.

Measured Concrete Thicknesses	% Cracking at End of Design Life for MR = 650 psi	
	AADTT	
	2500	7500
8.6	0.1	1
7.5	4.6	29.8
8.2	0.5	4
8.1	0.7	5.5
8.3	0.3	2.9
8.7	0.1	1
8.7	0.1	1
8.6	0.1	1
8.6	0.2	1.5
8.5	0.2	2.1
8.4	0.2	2.1
8.7	0.1	1
8.4	0.3	2.9
8.8	0.1	0.7
8.7	0.1	1
8.6	0.2	1.5
8.5	0.2	2.1
8.6	0.2	1.5
8.4	0.3	2.9
8.4	0.3	2.9
8.6	0.2	1.5
8.3	0.3	2.9
8.3	0.3	2.9
8.4	0.2	2.1
8.4	0.2	2.1
8.5	0.2	2.1
8.3	0.3	2.9
8.7	0.1	0.7
8.5	0.2	2.1
8.9	0.1	0.7

Step 3: Creating the Cumulative Distribution Curve

Each measured thickness was now assigned a percent of transverse cracking at the end of the pavement's design life for a given level of traffic and MR. For each traffic level, there were five data sets, each representing the cracking uncertainty for a specific MR (585, 624, 650, 676, and 714 psi). Each one of these data sets was turned into a cracking reliability curve. The data for each curve is listed in Tables B.7, B.8, B.9, B.10, and B.11 for a traffic level of 2500 AADTT. In all of the Tables, the first column shows

the percent cracking level, the second column indicates the number of thickness measurements out of 1032 that were mapped to this particular cracking level, and the third column shows the cumulative number of thickness-turned-percent-cracking values that were equal to or less than the cracking level in column 1. This procedure was repeated for each level of traffic.

Table B.7 Cracking reliability curve representing cracking uncertainty for AADTT = 2500 and MR = 585 psi

% Cracking Level	Frequency	Cumulative % Cracking
0	0	0.00
0.2	19	0.02
0.3	27	0.04
0.4	89	0.13
0.6	60	0.19
0.9	52	0.24
1.2	103	0.34
1.5	80	0.42
2.1	127	0.54
2.9	156	0.69
4	107	0.79
5.4	73	0.87
5.5	63	0.93
7.3	50	0.97
9.5	12	0.99
11.9	7	0.99
15.2	5	1.00

Table B.8 Cracking reliability curve representing cracking uncertainty for AADTT = 2500 and MR = 624 psi

% Cracking Bins	Frequency	Cumulative % Cracking
0	0	0.00
0.1	82	0.08
0.2	113	0.19
0.3	52	0.24
0.4	103	0.34
0.6	80	0.42
0.9	127	0.54
1.2	156	0.69
1.7	107	0.79
2.4	136	0.93
3.3	50	0.97
4.4	12	0.99
5.8	7	0.99
7.6	7	1.00

Table B.9 Cracking reliability curve representing cracking uncertainty for AADTT = 2500 and MR = 650 psi

% Cracking Bins	Frequency	Cumulative % Cracking
0	19	0.02
0.1	176	0.19
0.2	155	0.34
0.3	80	0.42
0.5	127	0.54
0.7	156	0.69
1	107	0.79
1.3	73	0.87
1.4	63	0.93
1.9	50	0.97
2.6	12	0.99
3.4	7	0.99
4.6	7	1.00

Table B.10 Cracking reliability curve representing cracking uncertainty for AADTT = 2500 and MR = 676 psi

% Cracking Bins	Frequency	Cumulative % Cracking
0	82	0.08
0.1	268	0.34
0.2	80	0.42
0.3	127	0.54
0.4	156	0.69
0.6	107	0.79
0.9	136	0.93
1.2	50	0.97
1.6	12	0.99
2.1	7	0.99
2.8	7	1.00

Table B.11 Cracking reliability curve representing cracking uncertainty for AADTT = 2500 and MR = 714 psi

% Cracking Bins	Frequency	Cumulative % Cracking
0	247	0.24
0.1	310	0.54
0.2	156	0.69
0.3	107	0.79
0.4	136	0.93
0.6	50	0.97
0.9	12	0.99
1.2	7	0.99
1.4	7	1.00

Step 4: Combining the Cumulative Distribution Curves for Each Level of Traffic

The next step in creating the transverse cracking reliability curves representing prediction uncertainty due to thickness and MR variation for the Hwy 2 rigid pavement was to combine the five cracking reliability curves created for each MR value into one cracking reliability curve that represented thickness and MR variation for one level of traffic. Table B.12 shows the cracking reliability curve data for a traffic level of AADTT = 2500. The first column shows the cracking level. The second column shows the number of data points that fit within each cracking level. Note that the number of data

points is equal to 1032 x 5 = 5160 points. The third column shows the percentage of data points that are equal to or less than the cracking level indicated by the first column.

Table B.12 Cumulative distribution curve of percent of cracked slabs at the end of a pavement's design life for 50% reliability representing a measured variation in concrete thickness and MR values for traffic level AADTT = 2500

% Cracking Level	Frequency	Cumulative % Cracking
0	2711	0.53
0.1	1436	0.80
0.2	429	0.89
0.3	230	0.93
0.4	126	0.96
0.5	136	0.98
0.6	9	0.98
0.7	55	0.99
0.8	0	0.99
0.9	0	0.99
1	28	1.00

Step 5: Fitting Transverse Cracking Reliability Curves

To aid in the comparison and manipulation of the cracking reliability curves, the transverse cracking reliability curve accounting for the uncertainty in concrete layer thickness and MR was plotted for each level of traffic and then a best fit curve was fitted to each reliability curve using the MEPDG transverse cracking reliability equations (See Equation 2.5 in the literature review) for values of P = 0.5, 0.6, 0.7, 0.8, 0.9, 0.95, and 0.99 and Z_p = 0, 0.25, 0.52, 0.84, 1.28, 1.65 and 2.33. The model's $CRACK_{mean}$ term was determined as the mean percentage of cracking indicated by the cracking reliability curve representing transverse cracking prediction uncertainty due to concrete thickness and MR variation. $CRACK_{mean}$ equaled 0.4% and 3.8% for traffic levels of 2500 and 7500 AADTT, respectively. The standard deviation of uncertainty due to thickness and MR variability was determined by finding the STD that minimized the error between the combined cumulative distribution curve and the modeled curve. The standard deviation

term (STD_{t+MR}) equaled 1.8 in. and 11.5 in. for traffic levels of 2500 and 7500 AADTT, respectively. Figure B.1 shows the cracking probability curves produced by a measured variation of concrete layer thickness and MR for traffic levels of 2500 and 7500 AADTT.

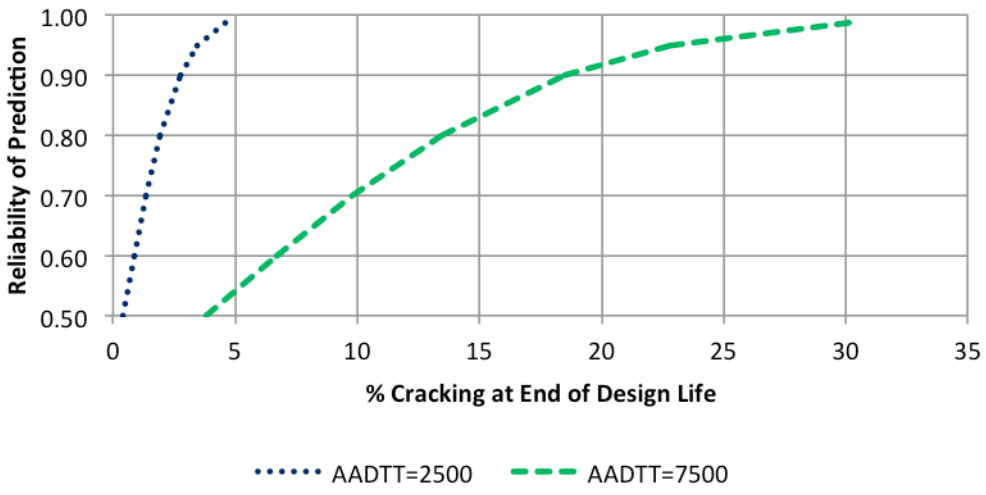

Figure B.1 Transverse cracking reliability curves representing cracking uncertainty for a measured variation in the pavement's thickness and MR for AADTT = 2500 and 7500